Bioprocessing with Bacteriophages Using Self-Cycling Fermentation

Zachary J. Storms

A thesis submitted to the Graduate and Post-doctoral Studies Office in partial fulfillment of the requirements for the degree of Doctor of Philosophy

Department of Chemical Engineering
McGill University
Montreal, Quebec, Canada

August 2012

ABSTRACT

A lack of innovation in production strategies of (bacterio)phages—viruses parasitic to bacteria—has limited recent developments in the applications. New phage-based industries need to develop efficient, large-scale bacteriophage production technologies. In this thesis, parameters affecting the phage infective process such as adsorption, host intracellular genetic material and host cell life cycle were studied; their influence on the production of virulent phages and recombinant proteins using a lysogenized phage as the expression vector is discussed.

Self-Cycling Fermentation (SCF), a cyclical, semi-continuous, automated process that maintains a bacterial culture in synchronized growth was incorporated into an industrially-relevant two-stage, recombinant protein production scheme using bacteriophages as the expression vector. By using SCF, productivity of the expressed gene product increased compared to a batch culture under similar conditions. Also, protein synthesis was influenced by the time at which the lytic phase was induced in the cell life cycle, suggesting protein production can be optimized with respect to the cell life cycle using SCF.

In addition, a new model for phage adsorption is proposed and the impact of phage adsorption efficiency on large-scale production was demonstrated. The proposed model simplifies phage attachment to a single step: irreversible binding. The adsorption efficiency is used to account for unadsorbed phages. Results from phage T4 infections indicated that increasing adsorption efficiency had a similar effect on phage amplification to increasing the initial multiplicity of infection.

Self-Cycling Fermentation was also used as a research tool to study how intracellular levels of host DNA and RNA influence phage productivity during T4 infection. Experiments monitoring

cell burst size and lysis time for cells infected at various points during a SCF cycle revealed that the intracellular RNA level correlates with phage productivity during infection. This work suggests that SCF can be used to complement and enhance the metabolic requirements of organisms in order to maximize productivity.

SOMMAIRE

Les récents développements dans l'application des bactériophages – des virus qui sont parasitiques aux bactéries – n'ont jusqu'ici pas été accompagnés par des innovations dans les stratégies pour leur production. Il y a certainement un besoin de développer des technologies de production efficaces et à grande échelle afin d'en faire bénéficier les industries présentes et futures utilisant les phages. Dans la présente recherche, des paramètres affectant le processus infectieux du phage, tel l'adsorption, les concentrations de matériel génétique et intracellulaire de l'hôte, et le cycle de vie de ces cellules, ont été examinés. Leur influence sur la production de phages virulents et de protéines recombinantes ayant un phage lysogénique comme vecteur d'expression a aussi été étudiée.

La fermentation auto-cyclante (SCF) est un processus cyclique, en semi-continu et automatisé qui maintient une population bactérienne en croissance synchronisée. Ce système a été incorporé à un procédé industriellement pertinent pour la production, en deux étapes, de protéines recombinantes en utilisant des bactériophages comme le vecteur d'expression. Avec la SCF, la productivité du gène exprimé a augmenté comparée à une culture *batch* créée dans des conditions similaires. De plus, la synthèse de protéines a été influencée par le temps auquel la phase de lyse a été incitée dans le cycle de vie de la cellule, suggérant que la production de protéines pourrait être optimisée en combinant le cycle de vie de la cellule avec la SCF.

En outre, un nouveau modèle pour l'adsorption de phages a été proposé et l'impact de l'efficacité d'adsorption du phage sur la production à grande échelle à été démontré. Le modèle proposé simplifie l'adsorption de phage à une étape unique : l'attachement

irréversible. L'efficacité d'adsorption des phages est liée à la proportion de phages qui n'adhérait pas à l'hôte. Les résultats obtenus avec des phages T4 suggèrent que l'efficacité d'adsorption a un effet similaire à augmenter la multiplicité d'infection initiale; le nombre des phages produits pendant l'amplification diminue avec l'augmentation de l'efficacité d'adsorption.

La SCF fut aussi utilisée comme outil de recherche afin d'étudier comment les niveaux intracellulaires d'ADN et d'ARN influencent la productivité des phages pendant une infection par le phage T4. Les mesures du *burst size* et du temps de lyse de cellules infectées à différents temps dans un cycle de SCF ont démontré que le niveau d'ARN intracellulaire était corrélé à la productivité des phages pendant une infection. Cette étude suggère que la SCF pourrait être utilisée pour identifier et contrôler les besoins métaboliques des organismes afin d'augmenter la productivité.

ACKNOWLEDGEMENTS

My deepest gratitude goes to my supervisor, now retired, Dr. David Cooper, who provided the kind of stimulating and challenging work environment where students could cultivate their intellectual prowess in not just research, but life itself. Thank you for the stimulating conversation, especially about the War of 1812.

Also, I am deeply grateful to Dr. Richard Leask, who magnanimously adopted me into his research group and helped take the project in a new direction. In addition, Dr. Dominic Sauvageau, now of the University of Alberta, guided my first research project as summer student and was a major part of the reason I went graduate school. He has provided continuous feedback on the research and offered expertise in the field.

A warm thank you is reserved for the McGill support staff, especially Frank, who was always willing and able to solve technical problems in the laboratory.

To the last of the Falcon Research Group, farewell and God bless, you've had a great run. A special thank you to Eric Arsenaul, Logan Smith and Tobin Brown, who worked on the project as summer students. To the Leask group, especially Paul and Lisa, thank you for the expertise and support.

Josh Kastner, my office-mate, put up with two years of country music and loud banter. Thank you for making the daily grind that much more enjoyable.

One of my fondest memories of McGill will remain my experience as manager of the ChEGSS softball team. Thank you, Team, for making it a fulfilling adventure.

Finally to my darling bride who has translated my dreams into reality and my abstract into French, thank you for embodying everything I love about life.

CLAIM OF CONTRIBUTIONS TO KNOWLEDGE

1) First implementation of Self-Cycling Fermentation (SCF) in a two-stage, semi-continuous production scheme for the production of recombinant proteins using temperature-sensitive phage λ as the expression vector. Using SCF, higher productivities were achieved than in batch experiments under similar conditions.

2) The use of synchronized host cells demonstrated that the point at which induction of protein expression takes place during the cell cycle can impact phage productivity.

3) The SCF system was used as a tool to study cell cycle events such as cell division, genomic DNA and total RNA concentrations.

4) Intracellular events were found to influence bacteriophage infection processes such as burst size and lysis time. The intracellular RNA concentration was found to correlate significantly with burst size and lysis time.

5) A new mathematical model for bacteriophage adsorption to the host cell was proposed. It approximates attachment as a single step and accounts for the adsorption efficiency of the virus particle to the host cell. Experiments validated the assumptions inherent to the model.

6) The adsorption efficiency was found to be a phenotypic trait of the bacteriophage, influenced by physical and chemical properties of the infection medium. It was independent of temperature and Multiplicity of Infection (MOI).

7) The robustness of the adsorption efficiency model was demonstrated by successfully using it to model the adsorption kinetics of viruses from the three largest phage families (Myoviridae, Siphoviridae, and Podoviridae).

8) Limits to the adsorption efficiency model were established. Experiments suggest phages lacking side-tail fibers do not adhere to the adsorption efficiency model.

9) The adsorption efficiency of a phage population was shown to have a marked impact on the number of phages produced during large-scale amplification.

CONTRIBUTIONS OF AUTHORS

Manuscript: "Self-Cycling Operation Increases Productivity of Recombinant Protein in *Escherichia coli.*"
By: Zachary J. Storms, Tobin Brown, Dominic Sauvageau and David G. Cooper

Author	**Contribution**
Zachary Storms	Primary author; wrote entire manuscript. Designed, performed, analyzed experiments.
Tobin Brown	Collected optical density data, assisted in collecting productivity data. Proofread the manuscript.
Dominic Sauvageau	Aided in experimental design, offered technical expertise on SCF and bacteriophages, and edited the manuscript.
David Cooper	Supervised and edited the manuscript.

Manuscript: "Bacteriophage Adsorption Efficiency and Its Effect on Amplification"
By: Zachary J. Storms, Eric Arsenault, Dominic Sauvageau and David G. Cooper

Author	**Contribution**
Zachary Storms	Primary author; wrote entire manuscript. Designed, performed, analyzed experiments.
Eric Arsenault	Aided in experimental design, collected some adsorption data, edited the manuscript.
Dominic Sauvageau	Aided in experimental design, offered technical expertise on bacteriophages, and edited the manuscript.
David Cooper	Supervised and edited the manuscript.

Manuscript: "Modeling Bacteriophage Attachment Using Adsorption Efficiency"
By: Zachary J. Storms, Logan Smith, Dominic Sauvageau and David G. Cooper

Author	Contribution
Zachary Storms	Primary author; wrote entire manuscript. Designed, performed, analyzed experiments
Logan Smith	Collected some adsorption data, edited the manuscript.
Dominic Sauvageau	Aided in experimental design, offered technical expertise on bacteriophages, and edited the manuscript.
David Cooper	Supervised and edited the manuscript.

Manuscript: "The Effects of Host Cell Physiology on Bacteriophage Productivity in Self-Cycling Fermentation"
By: Zachary J. Storms, Tobin Brown, Dominic Sauvageau, David G. Cooper and Richard L. Leask

Author	Contribution
Zachary Storms	Primary author; wrote entire manuscript. Designed, performed, analyzed experiments.
Tobin Brown	Assisted in DNA quantification (agarose gel electrophoresis and densitometry), collected some burst size data, and edited the manuscript.
Dominic Sauvageau	Aided in experimental design, offered technical expertise on bacteriophages, and edited the manuscript.
David Cooper	Supervised and edited the manuscript.
Richard Leask	Supervised and edited the manuscript.

NOMENCLATURE

A	Viably attached phage
b	Burst size; phages produced per cell
C_I	Concentration of irreversible complexes during adsorption
C_{IC}	Concentration of infective centers during adsorption
C_p	Concentration of free (unattached) phages during adsorption
C_{p0}	Initial concentration of phages during adsorption
C_{PR}	Concentration of free phages and reversibly attached phages
C_R	Concentration of reversibly attached phages
C_{h0}	Initial host cell concentration during adsorption
CER	Carbon Dioxide Evolution Rate
CV	Coefficient of Variance
dCER	Derivative of the Carbon Dioxide Evolution Rate
ε	Adsorption efficiency
F	Cell synchrony index; Free phage fraction during adsorption experiment
g	Generation time (doubling time) of the cell culture
H	Bacterial host cell in adsorption model
I	Irreversibly attached phage during adsorption; Equivalent to PH
k	Reaction rate constant
k_La	Volumetric mass transfer coefficient
MOI	Multiplicity of Infection: ratio of virus particles to host cells
MSM	Minimal Salt Medium
N	Number of cells in culture at end of a given time interval
N_0	Number of cells initially present in culture
NB	Nutrient Broth
OD	Optical Density
OUR	Oxygen Uptake Rate

P	Phage particle in adsorption model
PH	Irreversible phage-host complex formed in adsorption; Equivalent to I.
R	Reversibly attached phages
SCF	Self-Cycling Fermentation
t	Time
t_s	Search time of virus to find host cell
t_L	Lysis time: interval between adsorption and cell lysis
T_0	Total initial phage: free phage + infected cells
T_F	Total final phage
TSB	Tryptic Soy Broth
U	Unadsorbed phage (free phage)
υ	Sample volume

TABLE OF CONTENTS

LIST OF FIGURES

LIST OF TABLES

INTRODUCTION

The (bacterio)phage is an obligate parasite. It can only replicate within a bacterial host cell. Generally, the host cell is killed in the process. Because of this, the discovery of bacteriophages in the 1910's [1-2] initiated a flurry of research into their use for the treatment of infectious diseases [3-4]. Soon after their discovery, commercial phage-based therapeutics were sold in North America by companies such as Eli Lilly, Squibb and Sons, and Abbott Laboratories [3]. However, an unsophisticated understanding of bacteriophage specificity coupled with a largely unregulated industry resulted in mostly ineffective products marketed to cure anything from herpes (a virus) to gallstones. Felix d'Herelle, one of the original discoverers of bacteriophages, noted in his memoirs that most commercial phage products available at the time were completely useless against infectious disease [5].

Bacteriophage therapy was almost wholly forgotten in the West after the discovery of antibiotics [6]. It has survived to this day in parts of Eastern Europe and the former Soviet Bloc. Antibiotics were initially so successful at eliminating a wide spectrum of bacteria that premature pronouncements by such reputable authorities as the U.S. Surgeon General allegedly claimed that "it is time to close the book on infectious disease and declare the war against pestilence won!" [7]. Unfortunately, nothing could be further from the truth as new strains of antibiotic resistant bacteria are making headlines the world over [8-10]. In 2007 alone, 25,000 deaths in Europe were caused by multidrug-resistant (MDR) bacteria [11]. The growing presence of MDR bacterial strains today has been accelerated by the overuse and misuse of antibiotics in clinical and agricultural settings [12-14].

While pharmaceutical companies are spurning research and development into novel classes of antibacterials [15], some are calling for a renewed push in antibiotic research to fight MDR strains [16], but others see a fresh opportunity for the forgotten natural remedy—bacteriophages. Research into phage therapy has increased steadily over the past twenty years as evidenced by a quick search on PubMed [15]. In fact, the first regulatory approved human clinical trials of phage-based therapeutics have been completed in North America [17] and Europe [18]. However, researchers recognize that before phage therapy can or should become a mainstream medical practice a great deal of information still needs to be gathered concerning phage-human interactions [19-20], the possible effects of widespread phage therapy use on bacterial populations and mutation capacity [21], and the ecological effects of releasing large quantities of bacteriophages into the environment [15].

Furthermore, the potential phage-based pharmaceutical industry would need fundamental changes to the regulatory and economic framework used today. Encouragingly, engineers, scientists, doctors and regulators are openly discussing the intellectual property rights, economic incentives, and regulatory standards needed for phage therapy to become a reality in the Western world [3, 15, 22]. A team in Belgium has even published the results of a small-scale, quality controlled procedure for producing a phage cocktail intended for human clinical trials at the Queen Astrid Military Hospital in Brussels [23]. The authors intend for this project to serve as a template for producing phage preparations destined for human therapeutic uses on short notice, while meeting proper safety and quality control standards.

The properties of bacteriophages (specificity, fecundity, virulence, rapid evolution) make them suitable for a plethora of

applications beyond human phage therapy. A number of FDA approved products are now available to combat food-borne illnesses such as *Listeria monocytogenes* and *Escherichia coli* O157 on ready to eat meat products [5, 24].

Researchers are investigating other food applications such as using phages to control *Campylobacter jejuni* in chicken guts [25], *Pseudomonas plecoglossicida* in Ayu fish [26], and *Salmonella typhimurium* in ready-to-eat foods [27]. Phage therapy is also being investigated for its efficacy in combating plant disease [28] such as *Erwinia amylovora* infections of apple blossom [29], *Ralstonia solanacearum* infections of tomatoes [30-31], and *Dickeya dianthicola* infections of potatoes [32]. Finally, an EPA-approved pesticide (Agriphage) is now commercially available in the Americas as a biocontrol agent to treat tomato and pepper spot from the US based company Omnilytics [5].

The specificity and high growth rate associated with bacteriophages make them ideal instruments for diagnostic applications. Traditional plate assays for bacterial contamination can take 24 hours or more. By taking advantage of the fast reproductive capabilities of bacteriophages, commercial products have been designed to detect *Mycobacterium tuberculosis* in human sputum samples and the presence of methicillin-resistant *Staphylococcus aureus* on patients entering intensive care hospital wards [5]. Phages are also being studied for their use as biosensors in other applications [33-36], as nano-carriers for drug and enzyme delivery [37-38] and as vectors for recombinant protein production [39-47].

With the advancement of technology, scientists are now able to visualize events at the nanoscale with surprising resolution (e.g. [48]). Consequently, the detailed phage structure, mechanism of

infection, and specific interactions between phage and host cell proteins is now being elucidated [49-51]. While a great deal of effort has been devoted to understanding the minutiae of phage structure and phage-host interactions, surprisingly little work has focused on how these interactions will impact the type of large-scale phage production that would be necessary to support future phage-based industries.

This thesis extends the work of Sauvageau *et al.* who proposed a novel two-stage, self-cycling process for bacteriophage production [52-54]. Sauvageau developed a process for phage production based on Self-Cycling Fermentation (SCF), a semi-continuous, cycling fermentation system that maintains a culture in synchronized logarithmic growth.

This thesis extends the application of Sauvageau's two-stage system to recombinant protein production, evaluates how different infection-related processes are influenced by SCF, and examines the impact of phage adsorption on large-scale phage production. The system was first applied to recombinant protein production using phages as the vector of recombination (Ch. 2). Also, the adsorption of the virus particle to the host cell was rigorously studied (Ch. 3). A new model to understand the adsorption process was proposed, and the significant effect adsorption kinetics can have on phage production was demonstrated. In chapter 4, the robustness of the newly proposed adsorption model was studied by comparing it to a commonly used model and applying it to phage species from the three major families of bacteriophage (Myoviridae, Siphoviridae, and Podoviridae). Finally, initial results from a study on how intracellular properties of the host cell can affect phage productivity are presented (Ch. 5).

Chapter 1 LITERATURE REVIEW

1.1 BACTERIOPHAGES

Bacteriophages are nanometer sized bacterial viruses. They are ubiquitous, averaging concentrations of 10^6 mL^{-1} in aquatic environments [55]. The diversity and sheer volume of phages is striking. There are an estimated 10^{31} specimens [55] undergoing 10^{23} infections every second [56]. The bacteriophage serves an important role in the environment as an ecosystem modifier (releasing fixed organic carbon through bacterial lysis) and a driver of bacterial diversity [55].

Phages reproduce through two general pathways. The first is the lytic cycle. The lytic cycle of a bacteriophage begins with adsorption to the host cell. The phage then ejects its DNA, passing it through the cell membrane into the cytoplasm. Immediately, the host cell reproductive machinery is realigned for phage-directed metabolism. The phage then replicates its genome, produces phage proteins, packages its genome into the capsid, assembles mature virus particles, and lyses the host cell. Mature phage particles are then released to begin the process anew [50].

The second reproductive pathway is called lysogeny. This refers to the case where, instead of destroying its host, the phage develops a hereditary symbiotic relationship with the bacterium. The phage particle is inserted into the bacterium's genome as a prophage. The prophage inhibits all lytic activity and can be passed on from generation to generation of the host cell. However, the prophage can be induced to enter the lytic cycle through a stimulus. For further classifications on the types of phage infections, see Abedon [55].

The majority of classified phages (90%) are tailed phages of the order Caudovirales. Caudovirales have double stranded DNA genomes and fall into three families based on their structures [5].

These three distinct morphologies are illustrated in Fig. 1.1. Myoviridae are characterized by long, rigid, contractile tails; Siphoviridae have long, flexible, noncontractile tails; Podoviridae have short, noncontractile tails. For these three families, the genome is encapsulated in a protein envelope known as the capsid usually exhibiting icosahedral symmetry [5]. The capsid is connected to the tail which is the prime organelle of attachment to the bacterial host and serves as the channel for DNA ejection [49]. Tail fibers protruding from the tip of the tail serve as the principal tools for interactions with host cell receptor proteins [49].

The remaining 10% of phages have various morphologies and genome structures. For example, the inoviridae, or filamentous bacteriophage, consists of a protein filament harboring a single stranded DNA genome that generally replicates by means of persistent or chronic infection. The host cell is not sacrificed, but mature phage virions are continuously excreted [5].

Most of this thesis was conducted with phages T4 and λ. Phage T4 is a typical Myoviridae with an icosahedral capsid encapsulating a 172 kbp linear dsDNA genome. Six double jointed tail fibers protrude from the end of the tail. Phage T4 was likely derived from a wild type strain that exists naturally in the gut of mammals [57]. Phage λ is a temperate Siphoviridae that normally exists in the lysogenic state. An icosahedral head encapsulates the genome of phage λ—a double-stranded DNA molecule 50 kb in length [58]. Both phage T4 and λ use *Escherichia coli* as their host.

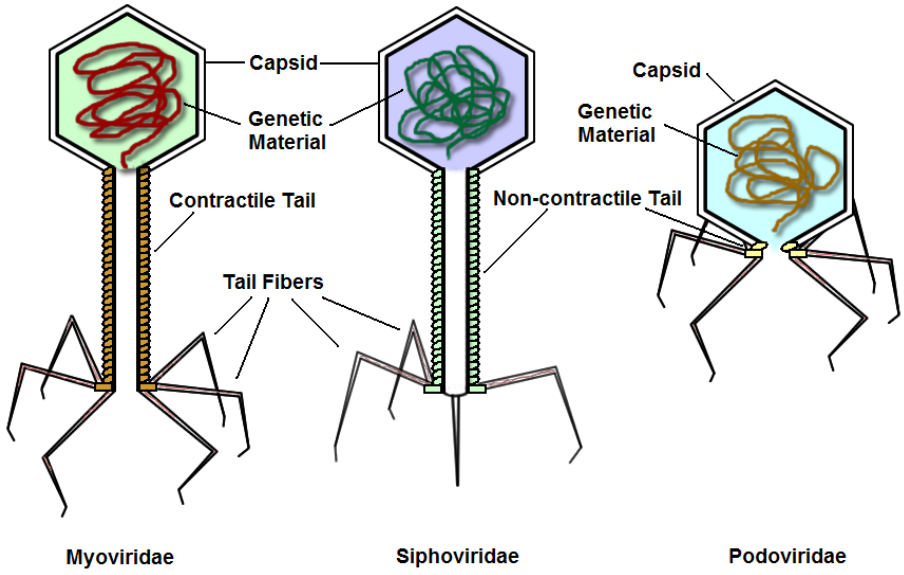

Fig. 1.1 General morphological characteristics of three common phage families.

Bacteriophage adsorption

As the first step in the phage infective process, adsorption to the host cell is an important aspect to consider in phage production. The detailed mechanism of adsorption has been well characterized for phage T4 and it will be described here. Adsorption of other tailed phages is believed to happen in a similar fashion.

The mechanism of phage adsorption has been shown to entail a reversible and irreversible step [59]. The six tail fibers of phage T4 serve as the organelles of reversible attachment. The distal ends of the fibers are mildly attracted to the densely populated lipopolysaccharides on the bacterial surface. The interactions of each fiber are weak enough that one or more may become detached from the surface at any time but the chances of all six becoming detached at the same time are quite slim, allowing the phage to probe the bacterial surface in search of the specific receptor protein [51].

The irreversible attachment is believed to be facilitated by motions of the cell such as swimming and various types of Brownian motion [49]. Once two fibers are reversibly attached to the host cell receptors, the phage remains anchored to the surface while being swayed by the motion of the cell until all fibers are attached with the tail and head pointed upright. This switches the baseplate from a hexagonal to star conformation, triggering tail contraction and DNA ejection. The conformational changes required for the baseplate may be facilitated by the presence of calcium or other cations [49, 60].

A membrane piercing structure present at the tip of the tail tube is used to penetrate the cell membrane [49]. In addition, receptor binding proteins on the tail baseplate recognize and digest external polysaccharides on the cell surface while the peptidoglycan layer is disrupted with glycosidase [61-62]. These actions enable the phage genome to breach the cell envelope as it passes through the tail during ejection. DNA ejection is not triggered by tail contraction but rather specific receptors located in the cytoplasmic membrane, possibly lipids [49].

Although quite complex at the molecular level, rather simple mathematical models have been proven sufficient to model adsorption of a virus population to the host cells. Initially, a simple one step kinetic model was introduced to approximate the early minutes of adsorption [63]. This model is generally inadequate over longer time periods and was soon improved upon with various two step models (sequential, modified sequential, competitive, *etc.*) that included a reversible and irreversible step [59, 64-70]. Numerous environmental variables such as temperature, pH, ion concentration, and the presence of co-factors have been shown to affect phage adsorption kinetics [69, 71-77]. Physiology of the host cell can also be an important parameter to

consider [67, 78]. A more detailed discussion of phage adsorption, including the presentation of a novel one-step irreversible adsorption model, can be found in Chapters 3 and 4.

Phage replication within the host cell

Immediately following injection, the phage works quickly to disrupt the normal workings of the host. Phage promoter genes compete with host promoters for the bacterium's RNA polymerase. In addition, the phage ties up the host RNA polymerase with polymerase binding proteins. Another early step is the degradation of the host's chromosome. The phage breaks down the cell's DNA and RNA and uses some of the parts to construct phage DNA. Additional nucleotides are added through novo synthesis and phage DNA polymerase proteins begin replicating the phage DNA.

The phage maintains tight control over which genes are expressed so that the progeny phages are assembled correctly. In the later vegetative state, tail, head and tail fiber proteins are produced simultaneously. Assembly factors are also generated to aid in putting the pieces together. The phage DNA passes through a portal and is secured within the head. Finally, with a new generation of mature phages complete, a phage-coded lysozyme destroys the cell's membrane.

Monitoring Phage Infection of a Population

The one-step growth experiment is the classic method of monitoring a phage infection of a growing culture [79]. The technique requires the infection of a growing host cell culture with bacteriophages, then diluting the culture to prevent further infection of any free-floating, unadsorbed phages in the medium,

followed by aeration and incubation at the appropriate temperature. Generally, the infection conditions are such that the initial Multiplicity of Infection (MOI), or ratio of phage particles to host cells, is less than 1, ensuring only one virus particle infects a host cell.

Monitoring the phage titer over the course of a one-step growth experiment yields the type of curve shown in Fig. 1.2, which was obtained after treating samples of T4 infecting *Escherichia coli* with 2% chloroform to lyse the cells. The data is reported per infected host cell. After 5 minutes the culture is diluted 10,000 fold; no further adsorption takes place and the concentration remains constant while phage proteins and genomic material are produced within newly infected cells. This period is known as the eclipse. Chloroform treatment terminates phage replication during the eclipse, preventing infected host cells from forming plaques on an agar lawn.

Once the first mature phage particle is assembled within an infective center, the phage enters the rise (or rise rate) defined as the rate of mature phage assembly [80]. This is represented by the 'step' increase in phage titer shown in Fig. 1.2. Soon phage-produced lysozymes accumulate to a lethal level within the cell, marking the termination of the rise and the release of mature phage particles. The entire period between infection of the host cell and lysis is known as the latent period (or lysis time). The rise can also be understood as the range of latent periods exhibited by individual cells within the bacterial population [63].

The burst size, or number of phages produced per cell, can be determined during a one-step growth experiment by comparing the number of infected cells at the beginning of the experiment to the number of newly formed phages at the end of the experiment.

Inspection of Fig. 1.2 yields an eclipse of 20 minutes, a rise rate of 3.21 particles·cell^{-1}·min^{-1}, and a burst size of 72 phages·cell^{-1}.

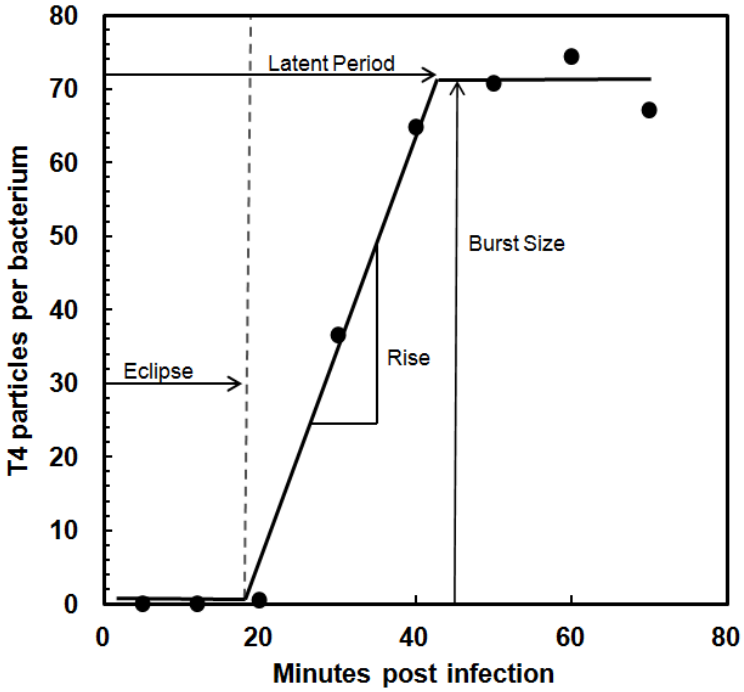

Fig. 1.2 One step growth curve of phage T4 infecting *Escherichia coli*. Samples were treated with 2% chloroform and then assayed for plaque forming units (pfu) on an agar plate.

Effect of phage growth parameters on productivity

Evolutionary and ecological studies have shown the interrelatedness of the major phage growth parameters—adsorption, lysis time, and burst size—with phage fitness (productivity). For simplicity, the time spent searching for a new host cell t_S can be approximated as the adsorption process. The search time (t_S) is primarily a function of host cell density and adsorption rate; therefore, at a given host cell density, t_S is roughly constant [81]. The lysis time t_L is a measurement of the intracellular phase of phage growth [81] while burst size is an indication of phage fecundity. Phage growth rate can be

approximated as $ln(b)/(t_S + t_L)$ [82-83]. Burst size increases linearly with lysis time for the few phage strains studied [83-86]; other functions may be appropriate [83, 87]. Using the eclipse and rise rate estimated from Fig. 1.2, Fig. 1.3 illustrates the influence of lysis time on phage growth for two different search times. Note that if the lysis time is less than the eclipse, no mature phage particles are assembled and the burst size goes to zero.

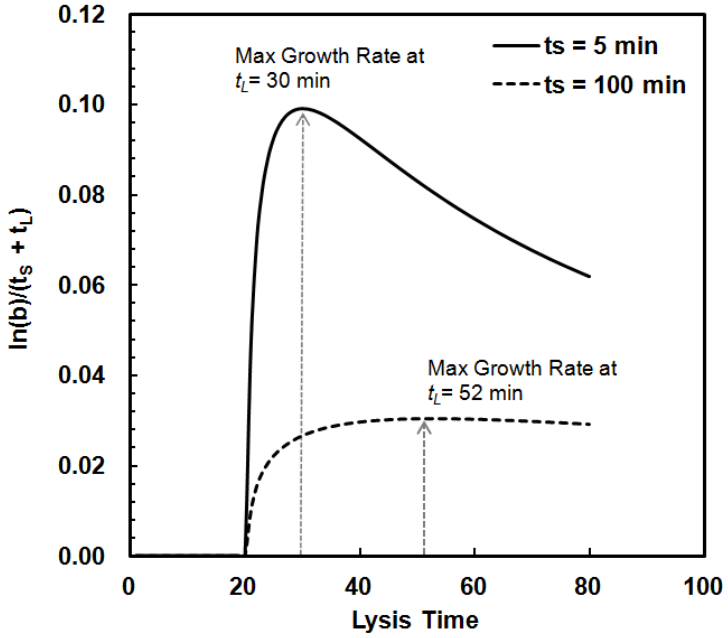

Fig. 1.3 Phage growth rate as a function of lysis time. A short search time (t_s = 5 min), representing an instance of high host cell density and a long search time (t_s = 100 min), representing an instance of low host cell density, are compared.

From the viewpoint of phage foraging, an optimal lysis time exists to balance out the competing effects of generation time (t_S + t_L) and fecundity (b) [81, 86, 88]. At low lysis times, phage fecundity decreases, but progeny virus particles are more quickly released to infect new host cells. As lysis time increases, fecundity increases at the expense of a longer generation time. This reduces the availability of phages to infect new hosts. Therefore, as shown in Fig. 1.3, shorter lysis times are favored at high cell densities

with short search times where newly released virus particles will immediately re-initiate growth. At low host cell densities where the search time becomes much greater, longer lysis times are favored. Evolutionary studies on phage fitness have shown that high host cell densities do in fact select for shorter lysis times [89-90]; however, empirically demonstrating that low host cell densities favor longer lysis times has been more difficult to achieve [87, 90].

Studies on isogenic strains of phage λ, differing only in one specific property, have shown that phage adsorption also places evolutionary pressure on phage fitness. In terms of phage fitness, increasing phage adsorption rate is equivalent to increasing host cell density. Shao and Wang (2008) found that, after holding all other variables constant, a fast adsorbing strain of phage λ achieved a comparable level of phage fitness with a lysis time 30% shorter than a slow adsorbing strain [81]. Further work demonstrated that high adsorption rates can be detrimental to phage fitness in a biofilm [91]. Using phage adsorption to host cells immobilized in a layer of soft agar as a model, the authors propose that if the adsorption rate is too high, sacrificial adsorption to cell debris combined with multiple attachments to cells within the immediate vicinity reduce phage productivity and cause poor plaque formation [91-92].

While evolutionary forces may drive phage growth characteristics over time, the physiological state of the host cell has immediate significant effects on phage infection processes [63, 78, 80, 93-94]. The phage requires numerous nucleic acid precursors, protein precursors, and translation machinery for efficient virus production [80]. Generally, the presence and concentration of these intracellular resources is governed by the physiological state of the host at the time of infection. Each major stage of phage growth, including attachment to the host, DNA

ejection and penetration, and protein synthesis within the host has been shown to be responsive to host cell physiology. Faster growing cells have been shown in multiple instances to decrease the lysis time, increase the phage progeny production rate, and increase the burst size [78, 80].

Higher cell growth rates are associated with a larger cell size and higher levels of genomic DNA, RNA polymerases, ribosomes, nucleoside triphosphates, and amino acids, all of which affect phage growth rate. In a study on the growth of phage T7 within *E. coli*, You *et al.* [80] found that phage infections became increasingly productive as the growth rate of the host increased from 0.7 to 1.7 cell doublings per hour. The eclipse period decreased with increasing host cell growth rate while the rise rate monotonically increased. The authors attribute this observation mainly to the higher concentration and elongation rate of ribosomes at higher host cell growth rates. The concentrations of genomic DNA, amino acids, and host cell RNA polymerases also affected phage growth, although to a lesser degree [80].

Interestingly, the cell volume was found to have a biphasic effect on T7 development. Phage growth initially increased with cell volume, but then decreased as cell volumes became excessively large, possibly due to the dilution of resources in the larger volume [80].

Effect of cell life cycle on phage growth

The few studies that exist on the influence of the cell life cycle on phage productivity support the hypothesis that larger cells with more cell resources increase phage fecundity. At least two studies on Phage T4 have found evidence that burst size of the cell may increase if the cell is infected later in its division cycle [78,

94]. One-step growth experiments on adult cells infected immediately prior to cell division yielded significantly larger burst sizes than the same experiment conducted on young, recently divided cells [94]. The authors suggest that the size of the protein synthesizing system may be the more important variable to consider in phage productivity, not the cell size, in agreement with the analysis of You *et al.* [80]. Similarly, a study on the use of synchronized cultures of *E. coli* in bacteriophage production found evidence that phage productivity was considerably larger for a synchronized culture than an asynchronous one [53]. Metabolic changes due to the synchronization process are suggested as possible reasons for this observation. Importantly, culture growth rate decreased during synchronization but did not lead to a decrease in phage productivity [53].

1.2 PHAGE PRODUCTION STRATEGIES

Large-scale bacteriophage production schemes face many of the challenges typical of bioproduction processes such as temperature [93], medium optimization [78] and aeration [95-96]. Additional factors must be considered in the infection process such as initial MOI [97] host cell density, phage adsorption kinetics [81, 86], and growth rate of the host [78, 98], all of which can have a profound effect on the final phage yield.

Batch fermentation

The simplest and most common method used for phage production is batch fermentation. The basic strategies were pioneered in the 1950s and 1960s; consisting of infecting a batch

culture in the exponential phase of growth at various infection loads [99]. Batch methods have proven reliable and reproducible, and are still commonly employed today [42-43, 100-102]. Unfortunately, batch processes are not without problems—long down times, large equipment footprint, low throughput. These disadvantages have led researchers to seek out alternative production processes.

Fed-batch fermentation

While fed-batch fermentation is a standard technique used to generate high density cell cultures in the bioprocessing industry, it is not widely used for phage production. In fed-batch mode, cells are first grown up to a specified density in batch mode and then switched to nutrient limited fed-batch mode to control the cell growth rate. High cell densities can be achieved by reducing the specific growth rate and consequently, oxygen consumption in the reactor [103]. However, as discussed above, reduced host cell growth rates are generally associated with smaller burst sizes and lower phage productivities. In fact, some studies suggest removal of the carbon source as a control method to terminate phage propagation in infected fermentation systems [104]. Therefore, the tradeoff between high host cell concentrations but slower cell growth rates in fed-batch processes may not lead to significant increases in phage yields. A thorough examination of the subject has not been published in the literature. Although, fed-batch methods have been used for phage-based recombinant protein production as discussed below [39].

Chemostats

While continuous production methods enable higher throughputs and therefore smaller equipment scales than batch processes, they tend to suffer from two important problems with regards to phage production. Firstly, not all particles within a continuously stirred tank have the same residence time. Therefore, some cells may be removed before infection and others before cell lysis, decreasing product yield and potential infective centers in the chemostat [39, 105]. Secondly, some cells may remain in the chemostat for long periods of time, increasing the likelihood of developing resistance [106-107]). In addition, the host cells must be maintained at the threshold population density, where the cell death rate is equal to the host propagation rate, in order to maintain infection over long periods [39].

These drawbacks have led to difficulties in the operation of continuous processes and lower yields than batch systems [39, 105]. Instead, chemostats have shown to be useful tools in the study of co-evolution, phage-host interactions, and phage fitness [107-109].

1.3 PHAGE λ AND RECOMBINANT PROTEIN PRODUCTION

Phage λ is a temperate Siphoviridae that can multiply by both the lytic and lysogenic pathway. Phage λ has a long history in microbiology as a tool to understand molecular genetics, control of intracellular expression systems, and in the formulation of recombinant plasmids [58, 110-111]. The ability to readily switch from the lytic to the lysogenic cycle has enabled researchers to study the feasibility of bacteriophage λ expression systems for recombinant protein production.

Phage λ infection is initiated by adsorption to *lamb* encoded receptors on the surface of the *E. coli* cell. During normal metabolism, these receptors aid in transporting maltose across the cell membrane the cell. Consequently, receptor synthesis is induced by the presence of maltose and repressed by the presence of glucose. Magnesium ions are known to assist in the adsorption process [58].

Conditions determining which pathway phage DNA will take once inside the host—the lytic pathway or the lysogenic pathway—may include the host concentration, mature phage concentration, temperature, or other factors [111-114]. In order to enter the lysogenic state, the Int protein breaks and incorporates the viral DNA into the host chromosome. The *c*I gene product, a protein of 236 amino acids, represses early transcription and blocks late gene expression so that nearly all lytic activity is prevented. Mutations in gene *c*I can make the repressor themolabile, causing it to denature above a certain temperature. The most common mutation of this type is *cI857*. Phages with allele *cI857* become lytic above 38°C and remain lysogenic under 32°C [58].

Over the past 20 years, a number of researchers have investigated the feasibility of using phage λ as a vector for recombinant protein production as an alternative to the traditional plasmid approach. Plasmid production systems tend to suffer from structural or segregational instabilities. Structural instability is the occurrence of a point mutation—a chromosomal rearrangement that leads to loss of product synthesis. Segregational instability is the failure of the expression vector to pass from one cell generation to the next. Segregational instability is particularly troubling because vector free cells will generally grow faster than those containing the plasmid [44].

Phage λ offers a feasible alternative to plasmids for recombinant protein production because it exhibits a high stability in the lysogenic state and a high copy number of the cloned gene in the lytic state. Phage λ has been shown to be stable for over 75 generations in the lysogenic state in a batch culture [44] and for over 12 days in a continuous culture [47]. In order to obtain a high copy number in λ vector systems, the λ-DNA must remain exposed long enough to allow for adequate accessibility to the host transcriptional components. Additionally, lysis of the host cell should be delayed for as long as possible so that cloned gene expression can take place. Keeping these guidelines in mind, Padukone *et al.* [44] suggest that a phage λ system for recombinant protein production should contain the following features: i) ability to switch easily from lysogeny to lytic state ii) deficiency in λ DNA packaging iii) deficiency in ability to lyse the cell in lytic state. The second point refers to genetic modifications to phage λ that impede its capability to package the DNA into the prophage head, therefore maintaining the λ DNA available for transcription of the inserted gene. The last point suggests genetic modifications limiting the phage's lysis capabilities, therefore extending the latent period and consequently increasing the time for recombinant protein production.

Survey of phage λ strains

Table 1.1 summarizes the various phage λ strains reported in the literature for use in recombinant protein production. Note that all of these phage strains contain the mutation *cI857*, making gene *c*I thermolabile. With this mutation, phage λ remains lysogenic below 32°C and becomes lytic above 38°C. The other common factor is that the recombinant protein produced by each

of these phage strains is β-galactosidase, coded for in the *lac* region.

Padukone *et al.* [44] performed some of the earliest studies of phage λ as an expression vector for recombinant protein production. Two recombinant λ strains (λgt11 and λNM1070) were compared using β-galactosidase to monitor expression levels, one of which lacked host cell lysis capabilities (λgt11), the other deficient in lysozyme expressing genes as well as DNA packing functions (λNM1070). Experiments showed that a significantly higher yield of β-galactosidase was achieved using the strain lacking DNA packaging genes.

Other researchers have reported similar results. Park *et al.* [47] saw only a small increase in β-galactosidase activity in the lytic state over the lysogenic state when working with phage λTL, which contains no mutations in cell lysis or λ-DNA packaging functions. However, when this strain was modified to λHL1, containing a deletion of gene Q, a 30-fold increase in β-galactosidase activity was observed in the lytic state compared to the lysogenic state [115]. Gene Q is responsible for the initiation of the whole late region of the lytic state, including DNA packaging and host cell lysis. Oh *et al.* [42] compared three phage λ strains (λSNU1, λSNU2, λSNU3) containing various mutations, which allowed them to investigate which mutations lead to the most efficient recombinant protein production. The strain λSNU1 yielded the highest recombinant protein concentration. This strain is very similar to λHL1, however it contains a mutation in gene S as well as gene Q, which enables the phage to remain in the lytic state for a longer period of time before host cell lysis.

Recombinant protein production strategies using phage λ

Recombinant protein production has been carried out in two general ways: batch and continuous processes. Many researchers have used a batch set-up in which the system is divided into two phases [42, 44, 47, 115]. First, the host cell culture containing the genetically modified λ prophage is grown under lysogenic conditions. Then, at some point during the exponential growth phase, the bacteriophage is induced into the lytic state. All researchers used temperature as the inducing agent. In addition to the usual problems of batch reactors—long start up, shutdown, and clean up periods—the bacterial culture will suffer from nutrient starvation if the induction takes place late in the growth phase.

Park *et al.* [47] investigated a continuous process and a two-stage continuous process as an alternative to the traditional batch approach. In the continuous system, a continuous stirred-tank reactor (CSTR) was used to first grow the lysogenic culture and then induce the lytic state. Stability was a problem for this system. The two-stage system had two CSTR's in series, the first serving as the lysogenic growth stage while the second was operating under lytic conditions and was used for protein production. In this set-up, the dilution rate into the second reactor had a significant impact on product formation and the product was produced at a much lower concentration than in a batch system. However, the two-stage system did have the advantage of separating the lysogenic growth stage from the lytic growth stage, allowing for optimization in each stage. It also avoided the down time associated with a batch reactor.

Table 1.1 Strains of temperature sensitive phage λ modified to express β-galactosidase for studies on recombinant protein production

Phage Strain	*Genotype*	*Comments*	*Source and Reference*
λgt11	*λlac5 cI857 Sam 100*	Deficient in S gene (S^-)	[44, 115]
λHL1	*λlac5 cI857 Qam73*	Deficient in Q gene (Q^-)	[115]
λNM1070	*Wam403 Eam1100 lacZ*$^+$ *cI857 nin5 Sam100*	Incapable of cell lysis (*Sam 100)* Deficient in packaging (*Wam403 Eam1100)*	[44]
λSNU1Q^-S^-	*lacZ cI857 Qam73 Sam7*	Used with P90c in study	[42]
λSNU2$Q^-W^-E^-$	*lacZ Wam403 Eam1100 cI857 Qam73*	Used with P90c in study	[42]
λSNU3$Q^-S^-W^-E^-$	*lacZ Wam403 Eam1100 cI857 Qam73 Sam7*	Used with P90c in study	[42]
λTL	*Lac*$^+$*, trpPOL-E-lacZY, cI*857	Trp promoter is strong promoter for cloned gene	[47]

An exhaustive review of different bioreactor schemes possible for recombinant protein production using bacteriophage λHL1 is given by Chen and Lim [39]. The authors concluded that the

continuous systems result in the washout of a portion of the infected cells, reducing overall performance and lowering product yield. Therefore, a batch system is the better choice of production scheme for recombinant protein expression. The authors also suggested that there exists an optimal cell density for protein production and that yield may be increased by nutrient enrichment after induction (fed-batch operation).

1.4 SYNCHRONIZED CULTURES

Cell cycle analyses are difficult undertakings. The general motivation behind such studies is to map the temporal alignment of events within the cell cycle. Most of the information gathered on cell biology was gleaned from cells undergoing balanced growth. In ideal balanced growth, "every extensive property of the growing system increases by the same factor [116]." In other words, all cell components are increasing at the same time. Balanced growth further assumes genetic homogeneity of the population and that the cell culture remains in equilibrium with an unchanging environment. In practice, for *E. coli*, balanced growth can be reasonably approximated for cell concentrations up to 2×10^8 cells·mL^{-1} [117]. The advantage of balanced growth is that any constituent of the cell (RNA, protein, nucleic acid) can be used as an indication of cell growth.

However, the growth of an individual cell differs significantly from an exponentially growing culture in a number of ways. The mean cell size of a balanced culture remains constant while that of an individual cell increases during a cell cycle. By treating the process as continuous, the balanced growth approximation ignores

the reality of prokaryotic growth because growth and division are discrete cycles for a bacterium. Likewise, rates of synthesis of specific molecules may vary throughout the cell cycle while data collected from a culture will only reveal average rates of synthesis. These limitations have led researchers to devise a multitude of methods to synchronize cell growth. In a synchronous culture, all cells are at the same stage of their interdivision cycle.

As a general rule, when working with synchronous cultures, the cells should emerge from balanced growth essentially normal, meaning the balanced growth has not been disturbed. In addition, more than one interdivision cycle should be produced with the data collected from a specific point in the first interdivision cycle replicating itself in later cycles [117].

Cell synchrony index

In order to quantify to what extent a culture is synchronized, Blumenthal and Zahler [118] devised the cell synchrony index *F*, which measures the fraction of cells undergoing division during time *t* in excess of that expected to divide during balanced growth in the same interval:

$$F = \left(\frac{N}{N_0} - 1\right) - \left(2^{t/g} - 1\right) = \frac{N}{N_0} - 2^{t/g} \qquad (1.1)$$

Where g is the generation time, N_0 is the number of cells at the beginning of the time interval and N is the number of cells at the end of the interval. The left hand side represents the fraction of cells that divided during time t and the right hand side represents the fraction of cells that would have divided had the

culture been growing logarithmically. An index of 0.6 to 0.8 is considered a significant degree of synchrony.

Synchronization methods

One method that has been widely used to study synchronous cultures is the "baby machine" pioneered by Helmstetter [119]. In this technique, adult cells are adsorbed to a filter. Media is circulated on the opposite side of the filter. Newly formed "baby" cells are passed through the filter to the media. It has been shown that the daughter cells passing through the filter grow at the same rate as the parent cells adsorbed to the filter. Since interdivision times within a culture may vary by as much as 10-20% [120], synchrony is generally only maintained for 2-3 divisions [121]. In addition, maximal cell concentrations obtained are on the order of 10^6 cells·mL^{-1}. These limitations preclude Helmstetter's "baby machine" from most industrial applications, but much is published on cell cycle analyses of cultures generated from the device. For example, Cooper [122], measuring rates of DNA synthesis at different growth rates of synchronous cultures generated using the "baby machine," estimated that the C-time and D-time of *E. coli* is 40 minutes and 20 minutes, respectively. The C-time is the period of DNA replication and the D-time is the period between replication and cell division.

Cutler and Evans [123] were able to synchronize *Escherichia coli* and *Proteus vulgaris* by isolating cells in the early stationary phase of growth and then diluting them 7 fold in fresh medium. They determined the optimal harvest point was one half of the generation time after the cells had reached the stationary phase. This method was able to sustained synchrony for 2-3 generations.

Other synchronization techniques focused on modifications to the chemostat such as flow or temperature changes [117], or nutrient addition [124].

Dawson [124] developed a semi-continuous process called the phased culture method. If fresh medium was added to yeast cells at regular intervals, Dawson found that the cells would adjust their doubling time to correspond to the interval of nutrient dosing. In order to avoid an exponential build up of microorganisms, the culture was halved prior to each nutrient dose. This system has also been applied to bacteria [125].

The phased culture method maintains a high level of synchrony over successive generations for an indefinite amount of time. This is not without drawbacks. The time between nutrient additions is arbitrarily set by the operator. If the time is too short, the cells will not double. It if is too long, a period of nutrient starvation ensues. This may have undesired metabolic effects on the organism [125-126].

Self-Cycling Fermentation (SCF)

Self-Cycling Fermentation modifies the continuous phasing approach by using a growth-associated parameter to determine the cycle time [126]. Once the time-based derivative of the variable goes to zero, a feedback control loop is used to halve the culture volume and replenish with fresh media back to the original working volume. The sequence of events involving bacterial growth, harvesting, and replenishing encompasses one cycle. Dissolved oxygen has been the most common control parameter used in SCF [127], although the carbon dioxide evolution rate (CER) has also been used successfully [53-54]. With this mechanism, the cycling time is no longer imposed upon the

bacteria, but rather adapted to the metabolism of the microorganism.

The Self-Cycling Fermentation technique has been extensively studied and used in numerous applications including the degradation of pollutants [128-130], the production of bio-molecules such as surfactin [126, 128-132], sophorolipids [133], and citric acid [134] and the production of bacteriophages [53]. For an exhaustive review of SCF and its applications, see Brown [127].

Modifications to the SCF set-up and operation recently reported in the literature [54] have made it more suitable for industrial applications. The bulky load cells previously used for measuring the volume changes during cycling were replaced with electro-optic level sensors delivering precise, reproducible cycle-to-cycle volumes. In addition, the Carbon Dioxide Evolution Rate (CER), measured in the exhaust gas, was incorporated into the feedback control loop to determine cycle time. This provided a simple, non-intrusive measurement for control. The system proved to be more robust, reliable, and reproducible than previous SCF set-ups [54].

Applying SCF to *Escherichia coli* has led to some unexpected results. Sauvageau *et al.* [54] reported that the metabolism of the organism, as measured by the doubling time, slowed down considerably while cultured under SCF. The organism went from having a doubling time of less than 1 hour in a batch culture to a doubling time of nearly 2.5 hrs during SCF. Carbon source analysis confirmed that the cell did not enter stationary phase during a SCF cycle, but was in fact continuously growing.

1.5 BACTERIOPHAGE PRODUCTION USING SCF

Two-stage, self-cycling process for bacteriophage production

A two-stage system for bacteriophage production based on SCF was recently designed and implemented by Dominic Sauvageau under the supervision of Dr. Cooper [53]. The concept was a semi-continuous, automated process that combined the advantages of batch and continuous processes. The first stage is used to culture the host cells under SCF. When cycling is initiated, the resulting harvest from the first stage can be brought to a second reactor for bacteriophage production. The second stage was operated as a self-cycling infection where a portion of the harvest at the end of each cycle remains in the reactor to initiate a new round of production using fresh host cells from the SCF and fresh medium. Importantly, the control schemes for both reactors were completely de-coupled so that each could be optimized independently.

The motivation for this set-up was three-fold. First, the system incorporates the high phage titers and robustness of batch processes with the high throughput and reduced downtime of continuous processes. Second, separating the host cell growth from the infection reduces the chances of co-evolution. Third, due to the synchronizing effect of SCF, the system allows for the study of host cell physiology and its influence on production. Indeed, synchronous cultures were found to have higher phage productivities during infection than asynchronous cultures [53].

1.6 EXPERIMENTAL APPARATUS

The experimental apparatus, modified from the set-up of Sauvageau and Cooper [53], is shown in Fig. 1.4 (not to scale). A 10·L carboy storing fresh, sterile medium provided the nutrient feed to the reactor. Host cells were cultured under SCF operation in stage 1. The control parameter for cycling was the change in CER (dCER), measured by a CO_2 gas probe in the exhaust gas after passing through a heat exchanger and HEPA filter. The oxygen uptake rate (OUR) was also measured with an O_2 gas probe, though not used for control purposes. The cycling feedback loop and hardware (valves, motor, heater) were controlled using LABVIEW software. For further details on the DAQ, electronics and hardware, see Appendix A.

Instead of a second reactor, shake flask experiments were carried out using host cells from the reactor in stage 1 to monitor bacteriophage production or recombinant protein expression. This facilitated experimental design, especially the study of host cell physiology and its effects on production.

An *Escherichia coli* strain lysogenized with recombinant phage λ modified to over-express β-galactosidase (CY15050) was used to study phage-based recombinant protein expression. *Escherichia coli* ATCC 11303 infected with lytic phage T4 (ATCC 11303-B4) was used as the model system to monitor the effect of SCF on burst size, lysis time, and intracellular DNA/RNA. Studies on phage adsorption kinetics were done on a small scale, details of which can be found in Chapter 3.

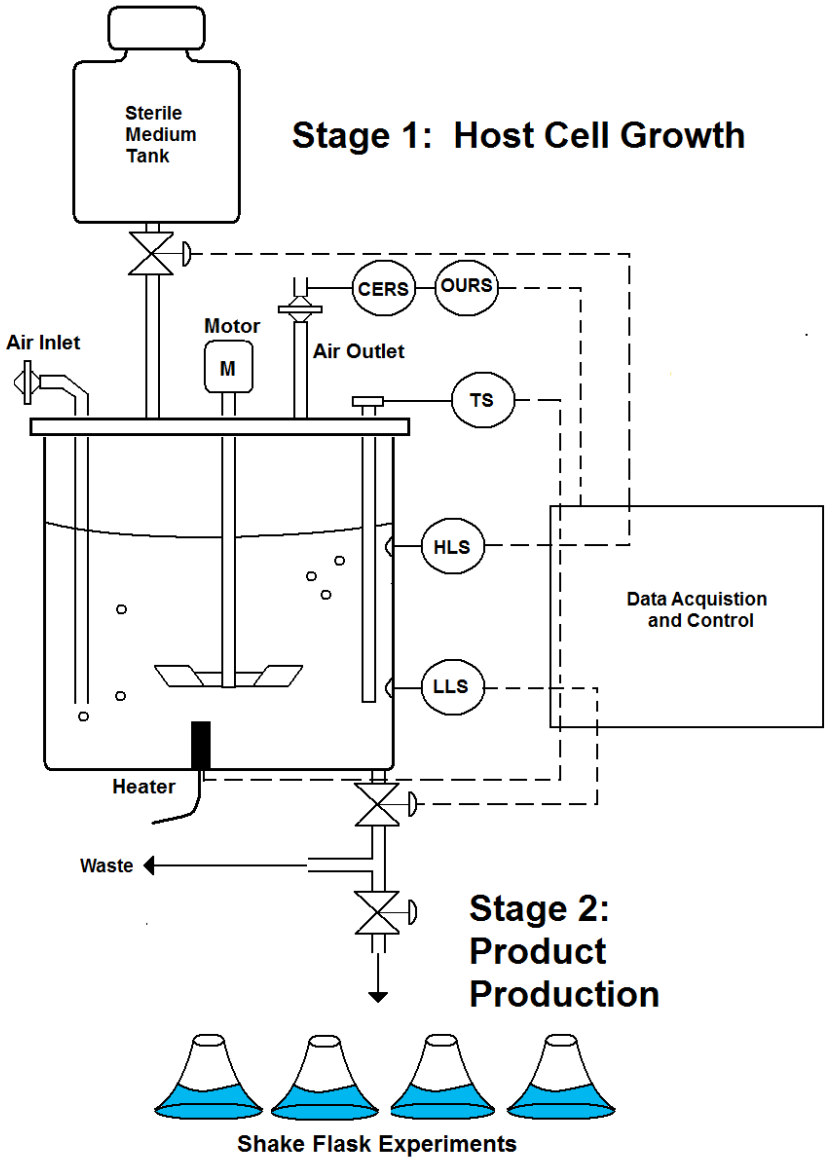

Fig. 1.4 Schematic of experimental apparatus

1.7 OBJECTIVES

The central hypothesis of this thesis is that Self-Cycling Fermentation can be used for recombinant protein production using bacteriophages as the expression vector. The general research question providing the motivation for the manuscripts is how metabolic and physiological changes to the host cell affect individual aspects of the phage life cycle (adsorption, burst size, lysis time). This information was used to maximize productivity in a phage production scheme. The specific objectives of the study are the following:

(1) to study the impact of host cell synchrony on the production of recombinant proteins using bacteriophages as the expression vector (Chapter 2).

(2) to study the effects of adsorption kinetics on large scale phage production and to test the robustness and limits of a new model for bacteriophage adsorption (Chapters 3 and 4).

(3) to study the cell cycle during SCF and the influence of host cell physiology, particularly intracellular RNA levels, on the bacteriophage burst size and lysis time (Chapter 5).

Chapter 2 SELF-CYCLING OPERATION INCREASES PRODUCTIVITY OF RECOMBINANT PROTEIN IN ESCHERICHIA COLI

Published as:

Storms ZJ, Brown T, Sauvageau D, Cooper DG (2012) Self-Cycling Operation Increases Productivity of Recombinant Protein in *Escherichia coli*. *Biotechnol Bioeng.* doi: 10.1002/bit.24492

PREFACE

The first objective of the project was to adapt the two-stage lytic phage production system developed by Sauvageau [53] for phage-based recombinant protein production. The first stage was still operated under SCF, but now culturing a lysogenized *Escherichia coli* strain containing recombinant phage DNA. The first stage was operated under lysogenic conditions optimized for host cell growth. As the system cycled, the harvest could be brought to a second stage, where nutrients could be added and the lytic cycle induced. Over-expression of the cloned gene was achieved by induction of the lytic cycle. The purpose of the study was to demonstrate the suitability of the production scheme, investigate the effects of synchronization on protein expression, and show the proof of concept for industrial application. Importantly, cell cycle effects were observed during protein expression.

The strain selected, CY15050, was obtained from the *E. coli* Genetic Stock Center of Yale University (New Haven, CT). This strain contains the temperature-sensitive prophage λTL which has been modified to over express β-galactosidase [135]. This microorganism was selected because it was well characterized, readily available and easily inducible. The prophage is induced to the lytic cycle above 38°C and remains lysogenic below 32°C. For information on how further genetic modifications to the prophage can increase recombinant gene expression, see [42, 44, 115].

Screening experiments were conducted to determine media composition, β-galactosidase expression, and SCF operation. The media used was a glucose-enriched minimal salt medium. Casein hydrolysate was added in low concentrations to provide a nutrient supplement. The organism was readily induced by raising the

temperature above 38°C and β-galactosidase expression could be monitored using the assay method of Miller [136]. SCF operation was adapted slightly for this organism. While the minimum in rate of change of the CER was still used for control, the start-up medium was adjusted to contain twice as much carbon source as the subsequent cycles. This yielded a stable cycling pattern immediately following the initial, start-up cycle. Additionally, a modification to the LABVIEW VI enabled the operator to view the CER data for all cycles during SCF operation.

This work has been published in *Biotechnology and Bioengineering*. It has been reformatted for presentation here in accordance with the guidelines of the publisher.

2.1 ABSTRACT

Self-Cycling Fermentation (SCF), a cyclical, semi-continuous process that induces cell synchrony, was incorporated into a recombinant protein production scheme. *Escherichia coli* CY15050, a *lac*⁻ mutant lysogenized with temperature-sensitive phage λ modified to over-express β-galactosidase, was used as a model system. The production scheme was divided into two de-coupled stages. The host cells were cultured under SCF operation in the first stage before being brought to a second stage where protein production was induced.

In the first stage, the host strain demonstrated a stable cycling pattern immediately following the first cycle. This reproducible pattern was maintained over the course of the experiments and a significant degree of cell synchrony was obtained. By growing cells using SCF, productivity increased 50% and production time decreased by 40% compared to a batch culture under similar conditions. In addition, synchronized cultures induced from the end of a SCF cycle displayed shorter lysis times and a more complete culture-wide lysis than unsynchronized cultures. Finally, protein synthesis was influenced by the time at which the lytic phase was induced in the cell life cycle. For example, induction of a synchronized culture immediately prior to cell division resulted in the maximum protein productivity, suggesting protein production can be optimized with respect to the cell life cycle using SCF.

Keywords:

Self-Cycling Fermentation, recombinant proteins, *Escherichia coli,* cell synchrony, productivity, bacteriophage vector, β-galactosidase.

2.2 INTRODUCTION

Self-Cycling Fermentation (SCF), a semi-continuous process first developed some twenty years ago [126], has been shown to be advantageous relative to batch cultures in diverse bio-manufacturing applications [131, 133-134, 137]. Operation consists of growing the organism in a batch, harvesting half the volume of the culture broth upon depletion of the limiting nutrient, and then replenishing with fresh medium to recover the original volume, creating a cyclical growth pattern based on the doubling of the organism. The fermentation is referred to as 'self-cycling' since the metabolism of the organism, rather than an operator, dictates the moment at which fresh medium is added.

Recently, SCF was incorporated into a two-stage system for the production of lytic bacteriophages where the host cells were cultured in the first stage using SCF and then brought to a second reactor for phage amplification [53]. This set-up allows for semi-continuous production; harvesting the culture at the end of a SCF cycle to use it as inoculum in the second reactor where production takes place. Compared to batch operation, this production scheme allows for higher throughput at equivalent product concentrations without the long downtimes associated with batch processes. In addition, the operator is given a wide flexibility in operating conditions since the second reactor is completely decoupled from the first stage SCF.

One key feature of SCF is that it induces synchrony in microbial cultures – generally characterized by a narrow distribution of cell ages [127]. As a result, all cells in a population are at the same stage in their life cycle at any given time. Therefore, protein production within a synchronized culture should more closely reflect protein production within an individual cell.

Studies have shown that the rate of protein production can vary during the cell cycle [138-141], suggesting that it may be possible to improve the yield of a recombinant protein production scheme by considering cell life cycle effects on protein synthesis.

Bacteriophage λ has been studied as an alternative to the conventional plasmid-encoded gene product in order to overcome the structural and segregational instabilities associated with plasmid-based recombinant protein production [40-43, 45]. Temperature-sensitive strains of phage λ form a stable, inheritable prophage in the lysogenic state and can be easily induced by raising the temperature to replicate in large numbers in the lytic state [44]. Indeed, there has been renewed interest in incorporating the thermo-inducible phage λ promoters P_L and P_R into plasmid recombinant protein production because temperature activation provides a cheaper, non-toxic alternative to isopropyl-β-D-thiogalactopyranoside, the most widely used induction agent in research [142-144] . The present work used lysogenized *E. coli* containing a temperature-sensitive strain of recombinant phage λ modified to express β-galactosidase in a SCF-based, two-stage production strategy. The lysogenized host cells are cultivated under SCF operation in the first stage and then brought to a second stage where protein production is induced. In this study, the second stage reactor is replaced with shake flasks in order to facilitate experimental design. The influence of culture synchronization on productivity is also demonstrated.

2.3 MATERIALS AND METHODS

Bacterial strain, medium, and cell density measurements

The bacterium used in this study was *Escherichia coli* CY15050 (W3110 Δ*lacU169 tnaA2/λ*TL) obtained from the *E. coli* Genetic Stock Center of Yale University. This is a lysogenized strain containing the *lac*$^+$ recombinant phage λTL. The Δ*lacU169* completely removed the *lac* operon from the host cell chromosome so that β-galactosidase can only be expressed by the phage DNA. Due to a temperature-sensitive mutation in *cI,* a gene repressing lytic activity, λTL is lysogenic below 32°C and lytic above 38°C. Details concerning the construction of λTL can be found elsewhere [135]. Lytic activity and expression of the recombinant gene are induced in λTL by raising the temperature of the culture medium above 38°C.

All experiments were carried out in a minimal salt medium (MSM) containing 6 $g \cdot L^{-1}$ Na_2HPO_4, 4 $g \cdot L^{-1}$ KH_2PO_4, 4 $g \cdot L^{-1}$ NH_4NO_3, 0.2 $g \cdot L^{-1}$ $MgSO_4 \cdot 7H_2O$, 0.014 $g \cdot L^{-1}$ Na_2EDTA, 0.01 $g \cdot L^{-1}$ $CaCl_2 \cdot 2H_2O$, 0.01$g \cdot L^{-1}$ $FeSO_4 \cdot 7H_2O$. For batch growth experiments and induction experiments, the MSM was supplemented with 0.01-$g \cdot L^{-1}$ casein hydrolysate (Oxoid LTD., Basingstoke, England) and 2.0 $g \cdot L^{-1}$ D-glucose. When culturing the cells using SCF, the MSM was supplemented with 0.005 $g \cdot L^{-1}$ casein hydrolysate and 1.0 $g \cdot L^{-1}$ glucose for the second cycle onward. Complete consumption of these compounds was assumed by the end of each cycle.

Two methods were employed to measure cell density. The first was to measure the optical density of a sample of culture medium at a wavelength of 600 nm (Spectrophotometer, Varian, Cary Bio 50) in a 3-mL cuvette. The second method was by

microscopy using a Petroff- Hauser chamber. The microscopic cell count was accomplished using a digital camera (Infinity 1-2C, Lumenera Corporation, Montreal, QC) attached to a Leitz Diaplan microscope (Leica PL Fluotar 40x/0.70 lense). Using the digital camera, three different images of a sample were taken and cells were counted using the Infinity Analyze 5.0 software (Lumenera Corporation). Cell density is reported in cells·mL^{-1}.

β-galactosidase measurements

The assay method used to measure β-galactosidase is described in detail elsewhere [136]. Briefly, the enzyme reacts with the chromogenic substrate *o*-nitrophenol-β-D-galactoside to yield galactose and o-nitrophenyl. *o*-nitrophenyl can be quantified by measuring its absorbance at 420 nm. A unit of β-galactosidase is defined as the amount of enzyme which produces 1 nanomole of *o*-nitrophenol per min at 28°C and pH 7.0. Under the conditions of the assay, 1 nmol·min^{-1} *o*-nitrophenol has an optical density (420 nm) of 0.0045 using a 10-mm light path. Knowing the sample volume of the culture, v in mL, and the reaction time, t in minutes, one can calculate the enzymatic activity units (U) after measuring absorbance at 420 nm and 550 nm (to account for light scattering due to cell debris) with the following equation:

$$\frac{U}{ml} = [OD_{420} - (1.75 \times OD_{550})] \times \frac{1}{0.0045} \times \frac{1\ nmole\ o-nitrophenol}{ml} \times \frac{1}{t}$$

SCF operation

SCF operation is described in detail in a previous publication [54]. The first cycle operated as a normal batch with an inoculum of approximately 2×10^{11} cells. Once glucose, the limiting nutrient,

was depleted from the medium, half the working volume (0.5 L) was harvested and either sent to a collection vessel or used for induction experiments carried out in shake flasks. The contents of the reactor were then replenished with fresh medium to a working volume of 1.0 L. The system was automated such that cycling was initiated every time the required conditions were met.

Furthermore, minor modifications were made to the operation strategy to accommodate the strain of *E. coli* used in this study. In this work, the initial glucose concentration was twice as concentrated in the first cycle as it was for the subsequent cycles. This improved the stability and reproducibility of the cycles.

Fermenter

The reactor set-up is based on that of a previous study [54]. The sensors, valves, heater, impeller, and thermocouple were all connected to a central computer using a LABVIEW programming software that automated the entire process. The reactor had a 1.0-L working volume agitated at 200 rpm and aerated at 0.5 vvm (k_La of 0.93 min^{-1}). The temperature was kept at 31°C in order to keep the cell culture growing under lysogenic conditions. As previously described, the rate of change of the carbon dioxide evolution rate (CER) was used in a feedback loop to determine the cycling time. CER was measured in the fermenter exhaust gas using an IR-spectrometry CO_2 gas sensor (CO2-BTA, Vernier, Beaverton, OR) after passing the air through an in-line HEPA-filter. The units of CER were mmol $CO_2 \cdot L^{-1} \cdot h^{-1}$. The correct volume exchange was achieved during cycling using two electro-optic level sensors at 0.5 L and 1.0 L (ELS-900 Series, Gems Sensors, Plainville, CT) and current-activated solenoid valves.

Some modifications were made to the reactor set-up for this study. A lead-gold electrochemical cell O_2 gas sensor (O2-BTA, Vernier, Beaverton, OR) was added to monitor the oxygen concentration in the reactor exhaust gas and an additional liquid exit stream containing a glass isolator was attached to harvest samples used as inocula for the shake flask induction experiments. The oxygen concentration in the reactor exhaust gas was used to calculate the Oxygen Uptake Rate of the culture. The OUR is reported as $mmol \cdot L^{-1} \cdot h^{-1}$.

Lysogenic growth experiments and induction experiments

All lysogenic growth experiments and induction experiments were carried out in shake flasks. Lysogenic growth experiments mimicked SCF operation in shake flasks and were compared to asynchronous cultures carried out under comparable conditions. They were conducted using a 100-mL inoculum from the end of a batch growth experiment (asynchronous control) or from the end of an SCF cycle. The inoculum was transferred to a 500-ml shake flask and then enriched with fresh MSM such that the working volume was 200 mL with 2.0 $g \cdot L^{-1}$ glucose, 0.01 $g \cdot L^{-1}$ casein hydrolysate and an OD_{600} of 1.4. The shake flask, containing the enriched culture medium, was incubated in an incubator shaker at 220 rpm and 32°C. This protocol was designed to standardize all experiments and mimic the production strategy that would be used in a two-stage process based on self-cycling cultivation. Samples were taken periodically to measure cell density and β-galactosidase activity.

Induction experiments were performed by periodically removing a 20-mL sample from the 500-mL shake flask used for lysogenic growth experiments and immediately transferring it to a

pre-warmed, empty 250-mL shake flask in a separate incubator-shaker at 220 rpm and 42°C for 150 min. In order to monitor the β-galactosidase productivity of the induced cultures, optical density and β-galactosidase activity were measured every 30 min.

2.4 RESULTS

A typical pattern for the growth of bacteria, using SCF operation, is shown in Fig. 2.1 for the first 35 hours after inoculating with the host bacterium. The figure illustrates the expected features of SCF operation; namely a long first cycle (start-up) followed by significantly shorter cycles. What is different from the normal behavior is that in this experiment the bacteria achieved a stable cycling pattern immediately after the first cycle. The second cycle is the beginning of a series of reproducible cycles – the average length of which was 130 min (±6.9 min).

Fig. 2.1A displays the carbon dioxide evolution rate (CER) of the culture growing under SCF. During each cycle, the CER increased for roughly 80 min before reaching a maximum, at which point it decreased precipitously until reaching a minimum; returning to roughly the same value as at the beginning of the cycle. This minimum in CER was used as the monitored parameter to trigger cycling. Fig. 2.1B depicts the oxygen uptake rate (OUR) during SCF operation. The pattern is similar to the CER and the oxygen level in the exhaust gas increases for roughly 80 min during each cycle, reaches a maximum, then decreases to its initial value. The CER is known to be sensitive to pH fluctuations; however, the close agreement between the OUR and CER provides assurance that the broad trends shown in Fig. 2.1

are in fact due to cellular respiration, not changes in pH over the course of a cycle.

Inspection of the OUR curve shown in Fig. 2.1B indicates a decrease in the rate of respiration of *E. coli* CY15050 approximately 30 min into each cycle, well before the maximum OUR is reached. At this point a distinct shoulder in the ascending curve can be observed, reproduced at the same time in each cycle. Meanwhile, the optical density of the culture steadily increased during this time period. Taken together, these two observations imply a decrease in the specific OUR at this point in the cycle, possibly due to the onset of cell division. Note that cycle 1 suffered from some disturbances in the air feed rate, causing the local maxima in Figs. 2.1A and 2.1B located at roughly 3.5 h. However the system was robust and quickly recovered. Normally, CER and OUR increased continuously during cycle 1 until reaching a maximum, indicating no significant decreases in cellular respiration before the onset of a stationary phase.

Fig. 2.1C presents the optical density of the culture at the beginning and end of each cycle. The value of the optical densities at the end of each cycle remained constant throughout the entire SCF operation shown, averaging 2.29 (±0.063).

Cell density measurements of synchronized populations were performed on cultures grown under lysogenic conditions in shake flasks using an inoculum taken at the end of an SCF cycle. These were used to establish the degree of synchrony during growth. Results of one such experiment are shown in Fig. 2.2. The optical density increased linearly throughout the experiment but the number of cells only increased during a short period of the entire growth phase (from 40 to 85 min), yielding a synchrony index of 0.6. Note also that the cell division took place in the middle of the growth cycle, a phenomenon observed in another *E. coli* strain [54]

but not generally seen in other microorganisms undergoing SCF [127]. Neither the biomass nor the cell concentration exactly doubled in experiments carried out in shake flasks. All experiments were standardized so that each shake flask had precisely the same conditions at the start of each experiment, regardless of whether the culture inoculum was obtained from a batch or SCF cycle. Consequently, the harvested cells from the SCF were not diluted exactly in half when used to inoculate the shake flask

Fig. 2.3 compares both growth and β-galactosidase activity of cultures growing under lysogenic conditions (32^{o}C) in shake flasks inoculated (1) with synchronized samples from the SCF or (2) with asynchronous samples from a batch culture, as control. Inspection of the optical density plots reveals that the average growth rate of the synchronized cultures was marginally faster than that of the asynchronous cultures inoculated from a batch. However, it should be noted that the growth rate was slower in shake flasks than in the bioreactor, which is attributed to poorer aeration. The β-galactosidase production by the bacterial cultures growing under lysogenic conditions remained fairly constant throughout the growth cycle. The synchronized cultures displayed a small decrease in specific activity of the product over the first 70 min of growth, possibly owing to the change in culture conditions from a bioreactor to a shake flask.

Induction experiments showed significant differences depending on whether the inoculum used was from a batch (asynchronous population) or SCF (synchronized population). Fig. 2.4 displays results from typical induction experiments. The solid lines of Figs. 2.4A and 2.4B track the optical density of an asynchronous and synchronized culture, respectively, growing under lysogenic conditions in a shake flask at 32°C. The dotted

lines represent samples that have been removed from the shake flask at different times and transferred to another incubator shaker at 42°C, inducing the lytic cycle of the bacteriophage. The time at which a sample is removed from the inoculum and placed at 42°C is referred to as the induction time. Induced asynchronous cultures initiated from batch experiments generally took longer to lyse. For example, within 150 minutes of the induction time, the optical densities of the asynchronous cultures shown in Fig. 2.4A have decreased by less than 10% from their peak values whereas the optical densities of the synchronized cultures have decreased by more than 50%. Note that experiments performed with an induction time of 90 min or greater exhibited little to no evidence of lysis. This was due to the depletion of nutrients within the culture broth prior to lysis of the host population.

Fig. 2.5 displays product formation during induction experiments with inocula from the two types of growth experiments. While the use of both batch and SCF grown cells achieved comparable levels of β-galactosidase activity, the SCF experiments did so 30 minutes faster than their batch counterparts.

Fig. 2.6 highlights some of the differences of producing recombinant proteins using a phage vector in synchronized cultures or batch cultures. Experiments conducted with synchronized cultures obtained from SCF exhibited greater productivity in a shorter period of time. An increase of 50% in the maximum integrated specific productivity of β-galactosidase was observed when compared to cultures obtained from batch experiments. In addition, the maximum in β-galactosidase productivity could be obtained using a significantly earlier induction time for cultures inoculated from SCF samples (45 min compared to 90 min for cultures from batch). Note that the

decrease in productivity was more drastic for synchronized populations. Importantly, cultures from SCF operation also exhibited a bimodal productivity curve where two maxima were observed, at 45 and 90 min. This is in contrast with the batch culture, which had only one maximum, at 90 min. Hypothesis testing (two-sample *t*-tests) revealed that the maxima at 45 and 90 minutes (Fig. 2.6, synchronized cultures) were statistically significant relative to the minimum at 70 minutes with $\alpha = 0.04$ and $\alpha = 0.08$, respectively. Fig. 2.7 highlights the relationship between productivity and cell density at the time of induction in experiments performed with synchronized populations from SCF. The maxima occurred when the lytic phase was induced at the onset or the end of cellular division. The intervening minimum in β-galactosidase activity corresponds to an induction time in the middle of cell division.

2.5 DISCUSSION

The lysogenized *E. coli* strain CY15050 grew as expected under SCF operation. In Fig. 2.1, it can be seen that a reproducible, stable cycling pattern was achieved immediately following cycle 1. Previous operations of the SCF with other bacteria have required up to 8 cycles before a stable cycling period was attained [54, 132, 145]. The improvement demonstrated here is attributed to an alternative start-up procedure. For the first cycle, the concentration of glucose, the limiting nutrient, was set at twice the concentration used for all subsequent cycles. This enrichment of the initial cycle was sufficient to result in an immediate reproducible cycling pattern starting with the second cycle. In control experiments, which were done using the same

glucose concentration for the first cycle as subsequent cycles, the system required 8-10 cycles before a stable cycling pattern was achieved.

Cultures of *E. coli* CY15050 growing with reproducible patterns of operation were found to have a synchrony index of 0.6-0.7, indicating a significant degree of cell synchrony [118]. A previous study on the production of bacteriophage T4 (a lytic phage) using *E. coli* revealed that synchronized cultures achieved higher productivities than asynchronous cultures, possibly due to an increase in burst size [53]. Part of the objective of the current work was to evaluate any advantages synchronized cultures may have over asynchronous cultures when using bacteriophages as vectors in the production of recombinant proteins.

It was thus important to establish whether synchrony was conserved in the protein expression stage (second stage). This was done by using samples from an SCF cycle to inoculate a series of shake flasks for the induction experiments. Fig. 2.2 demonstrates that synchrony is indeed maintained into the second stage. While the biomass increased for roughly 165 min in this figure, almost all cell division took place over a 45-min period in the middle of the generation time. This is important for the procedure as it means that the synchrony established in the SCF reactor, the first stage, can be imposed on the second stage vessel used for production of the recombinant protein.

The next consideration is what effect synchrony has on production. Under lysogenic, exponential growth conditions, β-galactosidase activity is proportional to biomass concentration. Consequently, the specific β-galactosidase activity stayed constant when growing the culture at 32°C (Fig. 2.3). There is little difference between the specific activity of cultures inoculated from a batch and those inoculated from an SCF cycle.

In cultures synchronized by SCF, intracellular processes and metabolic activity are assumed to be in close alignment. Consequently, the viral infective processes taking place within each of the cells, after induction, will also be in close alignment and this should lead to a difference between results from synchronous and asynchronous cultures. This is evident in Figure 4, where, in contrast to the asynchronous cultures from batch, induction experiments of synchronized cultures exhibited a sharp drop in optical density corresponding to a rapid, almost simultaneous culture-wide lysis. Asynchronous batch cultures are characterized by a wide distribution of cell ages and little evidence of alignment of intracellular activity. Therefore, batch cultures, infected in the same manner as the synchronized cultures, display a wider distribution of individual cell lysis times, as evidenced by the slower rate of lysis in Fig. 2.4.

Another important observation was that the production of β-galactosidase in these experiments was significantly faster in synchronized cultures (Fig. 2.5). While activity assays revealed that the total amount of β-galactosidase expressed was of the same order in unsynchronized and synchronized cultures under the same production conditions, given that synchronized cultures lysed significantly sooner, it follows that the maximum in β-galactosidase activity was reached significantly sooner. In order to take the impact of synchronization into account and appropriately compare the productivity of the cultures, the discussion focuses on the integrated specific volumetric productivity defined as the activity of β-galactosidase per unit volume per unit time per unit biomass.

When using bacteriophages to produce recombinant proteins, it can be seen that there is an optimum induction time for the growing culture. It is clear from Fig. 2.6 that, for the

asynchronous batch cultures, the optimum induction time was 90 minutes. Inducing the cultures later in the growth cycle resulted in a poor productivity, likely due to nutrient limitations and onset of stationary phase [39-40, 46, 115].

Also evident from inspection of Fig. 2.6 is that synchronized cultures inoculated from an SCF cycle were characterized by a maximum in productivity that was 50% larger than that of asynchronous cultures. In addition, the optimum induction time of the synchronized cultures was 45 min. Consequently, using synchronized cultures reduced the overall production time by over 40%.

The 50% increase in maximum productivity achieved in synchronized cultures was the result of two factors: 1) synchronized cultures achieved the same level of β-galactosidase activity in a shorter time than unsynchronized cultures and 2) synchronized cultures likely lead to an increase in burst size (phages/cell). Both of these factors can be attributed to the synchronization of the SCF culture. Similar observations can be found in the literature. For example, Rabinovitch, *et al.* [94] found that the age of the cell at the time of infection by a lytic bacteriophage can have a significant impact on the cell burst size. Furthermore, when applying SCF to the production of a lytic bacteriophage, Sauvageau and Cooper [53] observed that a synchronized *E. coli* culture from SCF infected with bacteriophage T4 had a specific volumetric productivity 30% larger than that of unsynchronized cultures under the same conditions.

A surprising feature of Fig. 2.6 is that the synchronized cultures were characterized by the presence of two distinct maxima in productivity, at 45 and 90 min, with a local minimum at 70 min. This trend was not observed in experiments performed with cultures obtained from unsynchronized batch cultures. Fig. 2.7

shows that the maxima in productivity occur when the cells were induced at the beginning and end of cell division and that the intervening minimum occurred for those induced in the middle of cell division. It has been demonstrated that infecting cells right before cell division with a lytic phage leads to greater burst sizes [94]. This can be explained by the higher concentration of the protein-synthesizing system (PSS) per cell present at this moment in the cell cycle and the reassignment of this system to the production of phage-associated particles [94, 146]. This phenomenon explains the presence of the first maximum in productivity for cells induced right before cell division. At this point, the PSS is used for the production of phage particles and the recombinant protein of interest. A similar situation can explain the presence of the second maximum right after cell division, when the PSS is mostly dedicated to the production of phage particles and recombinant proteins upon induction. In contrast, when the lytic stage is induced while cell division is already taking place, a significant portion of the PSS is already assigned to cell division and this hinders the production of the recombinant protein. At this stage, the mechanisms for cell division, phage synthesis and protein synthesis are competing for the same resources within the cell. Also indicative of the re-assignment of cellular functions during cell division, the analysis of the OUR data from Fig. 2.1B suggests a decrease in the rate of cellular respiration during cell division. It can thus be concluded that cell division and the availability of the PSS have a significant effect on protein production – at least one previous study has shown evidence of a decrease in the rate of gene expression during cell division [139]. While further experimentation is needed to fully understand the underlying phenomena, it is clear from Fig. 2.7 that inducing a culture at different times in the cell division process has a

significant impact on productivity and that it is possible to optimize protein production with respect to the cell life cycle.

From the viewpoint of process development, SCF has numerous advantages over a traditional batch culture for the production of recombinant proteins. The production scheme of SCF is similar to a sequential batch procedure, where operators can achieve higher throughputs with a smaller equipment footprint while maintaining the high titers associated with batch processing and avoiding the residence time distribution problems of continuous processes. Additionally, this study has shown that host cell synchronization, a feature of SCF operation, results in higher cell productivities, meaning that the same protein concentration can be achieved in less time and/or with fewer cells than a batch operating under similar conditions. Furthermore, the downstream processing costs can be reduced for an intracellular product such as β-galactosidase by achieving quicker, and complete, lysis of cell cultures while still producing the same levels of proteins with fewer cells. Finally, the operation of SCF is a fully automated process using a non-intrusive measurement for control (CER). These features make SCF an ideal fermentation strategy for use in the recombinant protein production scheme presented here and would likely make it a viable option in an industrial application. Of course, one must consider the requirements for approval by regulating bodies.

Nevertheless, at the very least, SCF currently offers researchers a tool to study how the life cycle of a cell can influence protein expression. For example, the data presented here suggests that inducing protein synthesis prior to cell division results in the highest cellular productivity. The work presented here can serve as a stepping stone for the development of a large scale production process based on SCF that complements and enhances the

metabolic requirements of organisms in order to maximize productivity.

2.6 ACKNOWLDGEMENTS

The authors would like to thank the National Science and Engineering Research Council of Canada as well as the Eugenie Ulmer-Lamothe Fund and Richard H. Tomlinson Doctoral Fellowship of McGill University for providing financial support for this project.

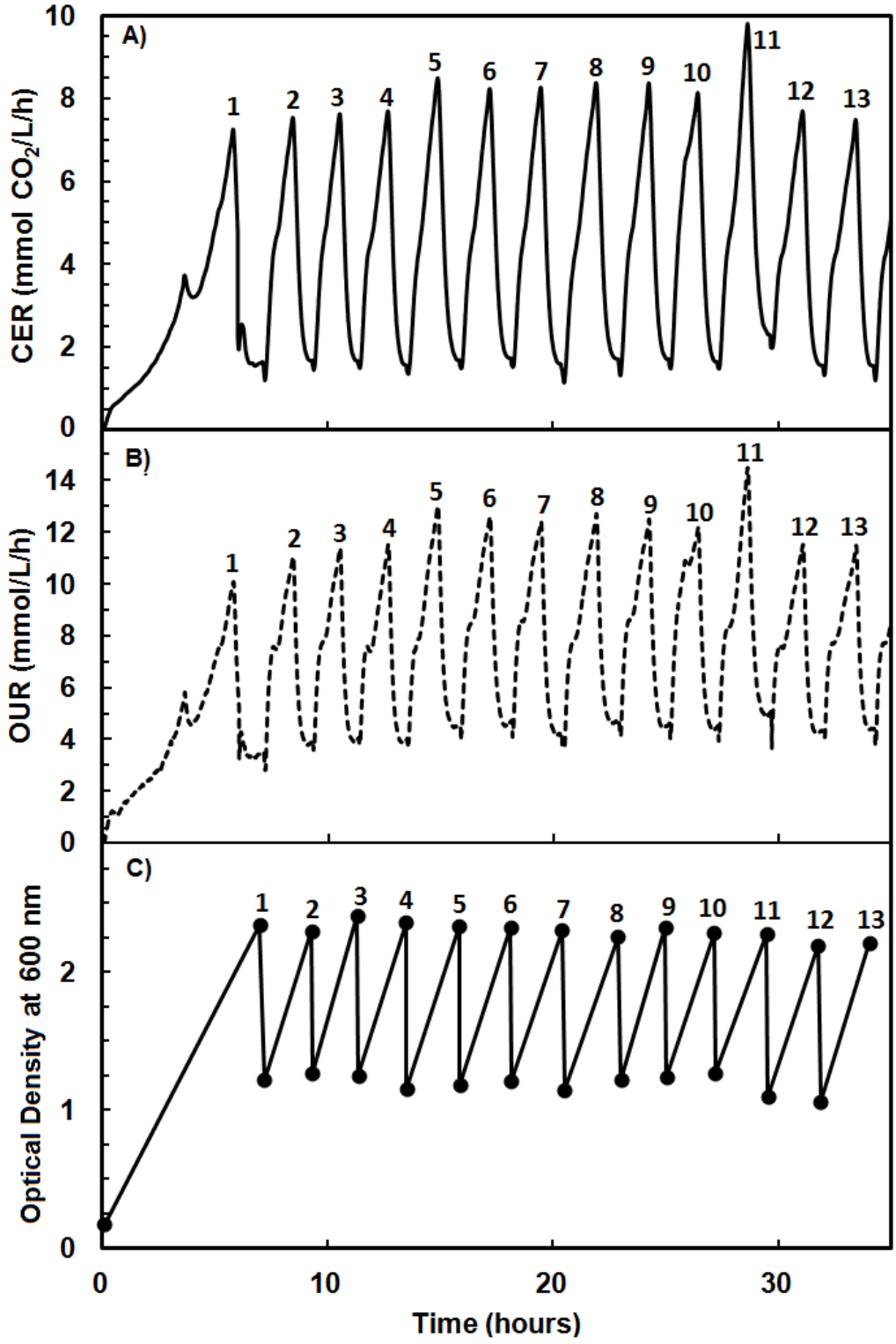

Fig. 2.1 Data for the growth of *E. coli* CY15050 in SCF. The (A) carbon dioxide evolution rate (CER, solid line), (B) oxygen uptake rate (OUR, dashed line), and (C) optical density at 600 nm (•) are shown.

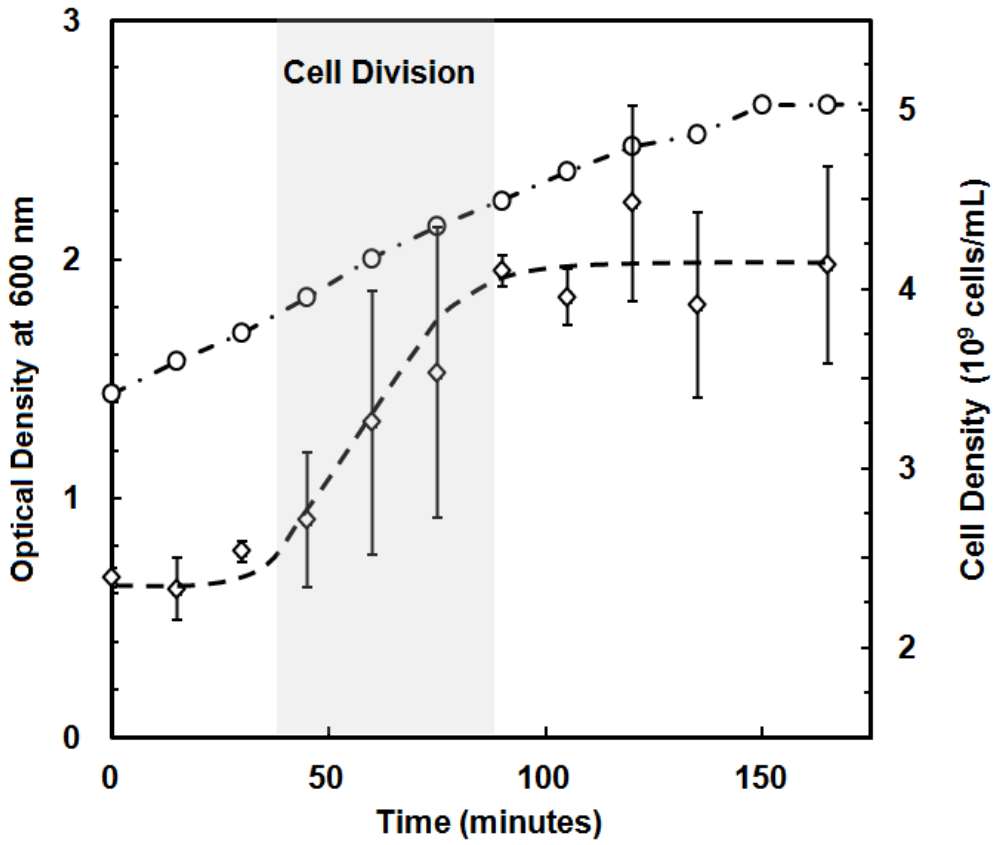

Fig. 2.2 Data for lysogenic growth of a synchronized culture of CY15050 in a shake flask. The inoculum was taken from the end of an SCF cycle and maintained at 32°C for the duration of the experiment. Optical density at 600 nm (○) and cell density (◊) are shown. Note that the dashed line is meant to show the trend in cell division and is not a modeling equation. Error bars represent the standard deviation of the three cell density measurements of each sample.

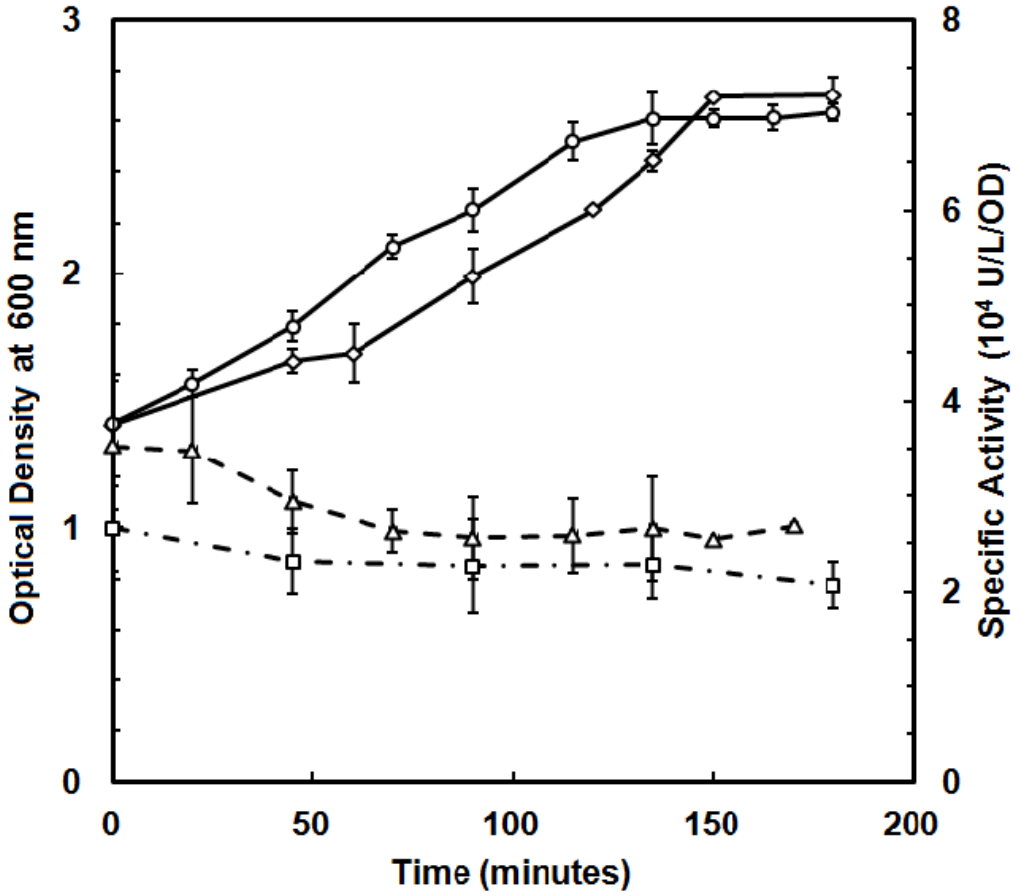

Fig. 2.3 Data for lysogenic growth (32°C) in shake flasks for two types of cultures. These include the optical density of cultures inoculated from batch (◊) or synchronous SCF (○) operation. The specific activity of β-galactosidase is also shown for cultures inoculated from batch (□) or synchronous SCF (Δ) operation. Error bars represent the standard deviation of at least three experiments.

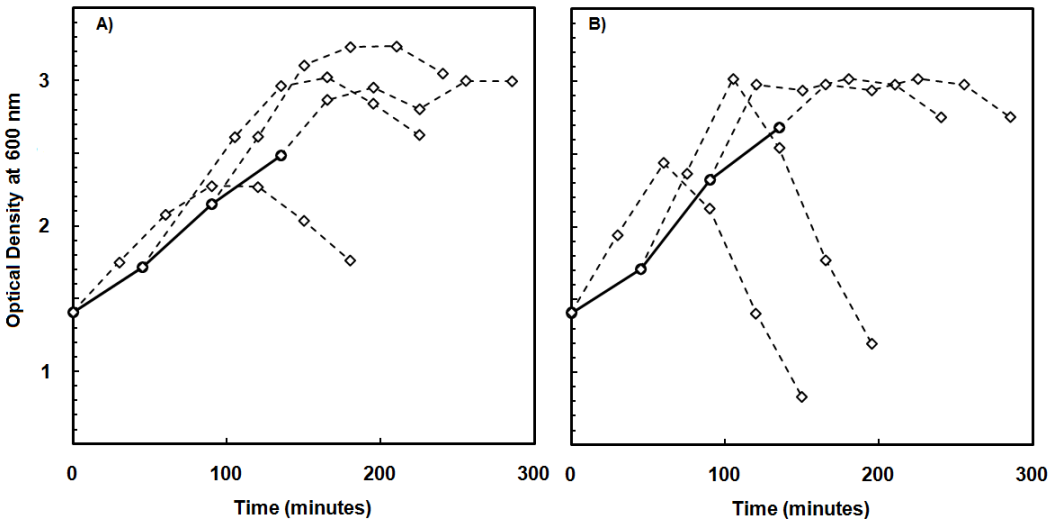

Fig. 2.4 Lytic induction experiments performed using the cultures undergoing lysogenic growth in shake flasks shown in Fig. 3. Samples were taken periodically from these parent flasks and grown at the induction temperature of 42°C. The growth and lysis dynamics of two typical experiments are shown here for comparison. In both (A) and (B) the optical density of the parent lysogenic flasks are circled and connected by a solid line. The induced cultures (◊, dashed lines) from the parent flask inoculated with the harvest of a batch experiment are shown in (A). The induced cultures (◊, dashed lines) from a parent flask inoculated from the harvest of a synchronous SCF cycle are shown in (B).

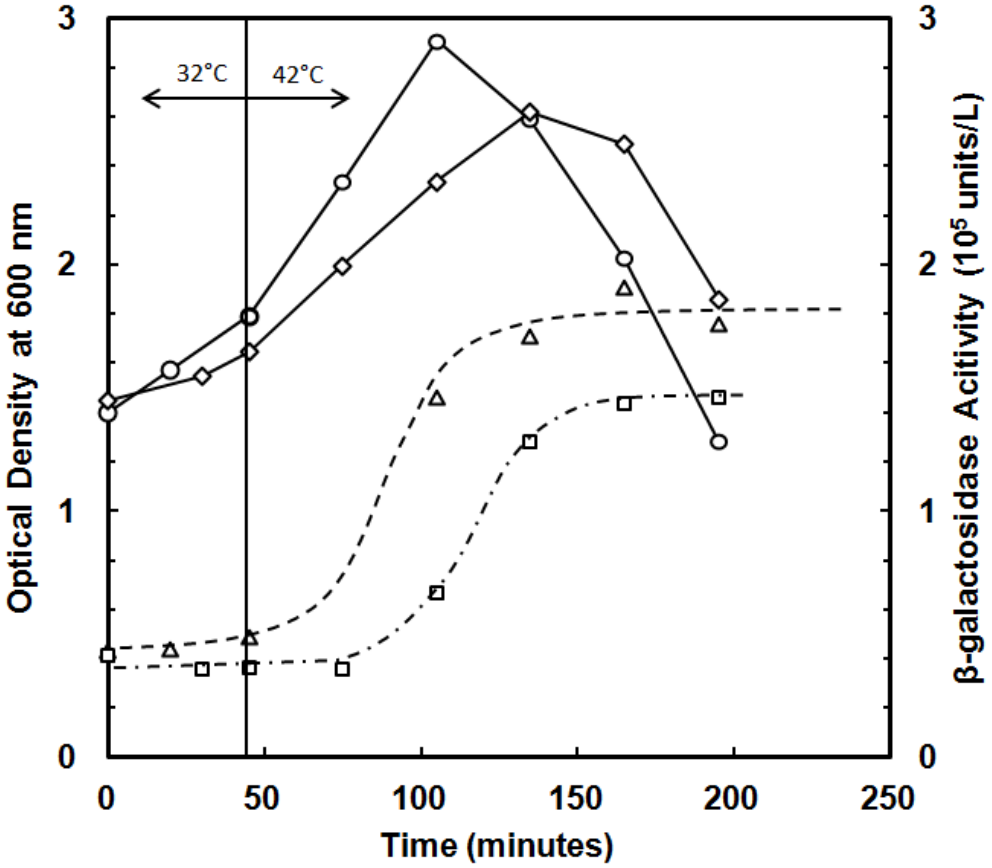

Fig. 2.5 β-galactosidase production for a culture inoculated from synchronized SCF operation (Δ) and induced at 45 minutes by transferring the flask to an incubator at 42°C and for a control flask treated in the same way but using a batch inoculum (□). The dashed lines are meant to show trends and are not the result of a modeling equation. Optical density at 600 nm is also shown for both experiments - SCF inoculum (○) and batch inoculum (◊).

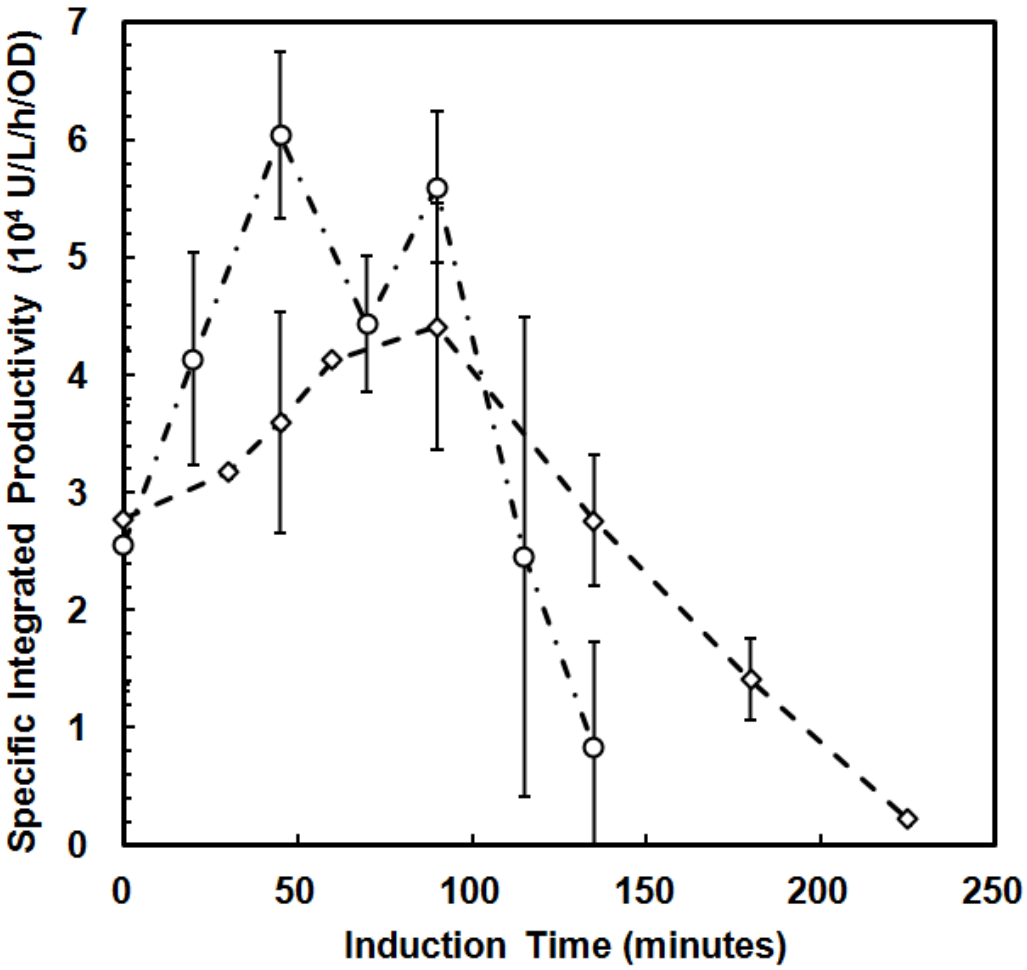

Fig. 2.6 Specific integrated productivity in induced synchronized and batch cultures. Each value of the specific integrated productivity, defined as the units of β-galactosidase activity per unit volume per unit time per optical density unit, was obtained for an individual experiment in which the lytic cycle was induced at the time indicated. Experiments performed with flasks inoculated with cells from the harvest of a synchronous SCF cycle (○) and experiments performed with flasks inoculated with cells from the harvest of a batch (◊) are shown. Error bars represent the standard deviation of at least three replicates.

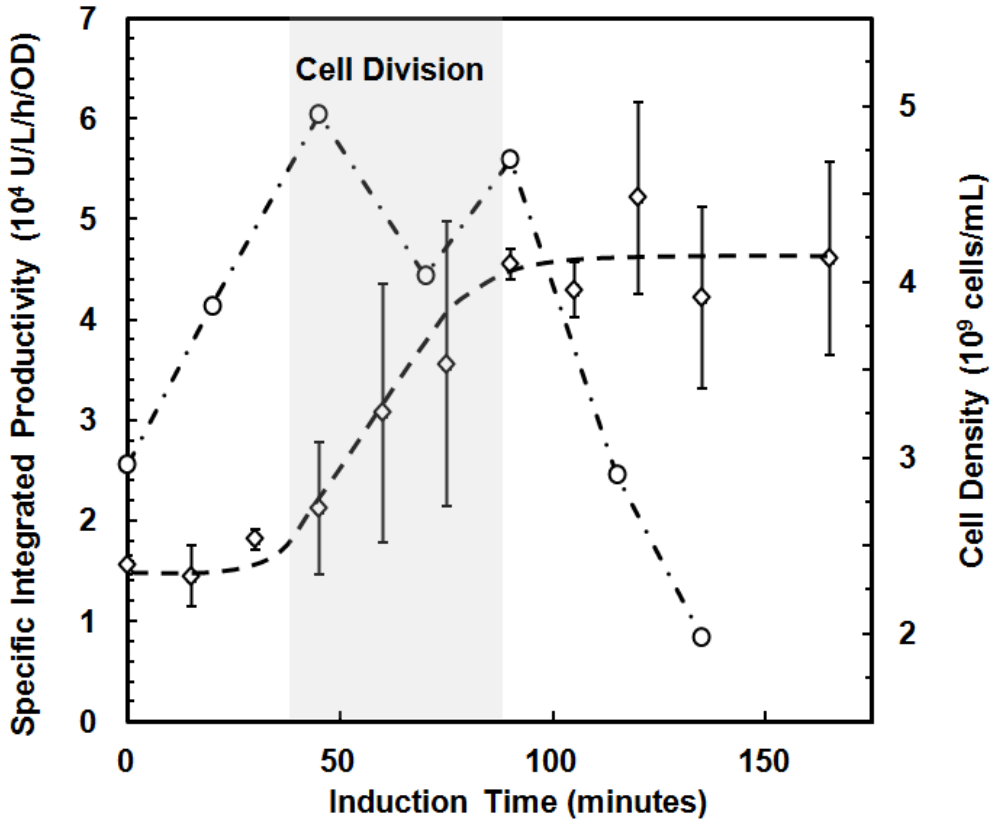

Fig. 2.7 The specific integrated productivity data of the synchronous cultures from Fig. 6 (○) are compared to the cell density of the synchronous culture from Fig. 2 (◊) growing under lysogenic conditions. Note that the dashed line is meant to show the trend in cell density only; it is not the result of a modeling equation. The trend line in cell density serves as an estimate of cell concentration at the time of induction for the specific integrated productivity data shown. Error bars represent the standard deviation of the three cell density measurements of each sample

Chapter 3 BACTERIOPHAGE ADSORPTION EFFICIENCY AND ITS EFFECT ON AMPLIFICATION

Published as:

Storms ZJ, Arsenault E, Sauvageau D, Cooper DG (2010) Bacteriophage Adsorption Efficiency and Its Effect on Amplification. *Bioprocess Biosyst Eng* 33: 823-831.

PREFACE

While researching recombinant protein production using temperate bacteriophage λ, studies on the adsorption kinetics of the bacteriophage to the host cell were carried out in parallel using phage λ and T-series phages. The first experiments were performed on phage T4 and are summarized in this chapter.

Adsorption is the first step in the phage infective process and therefore important to most phage applications. Studies exist on the relationship between phage adsorption and phage fitness [81], plaque formation [92], and ecology [91], but less is reported on the influence of adsorption on large-scale phage production. Part of the motivation for this study was to understand the impact of adsorption kinetics on phage amplification in a fermentation system.

Additionally, initial adsorption experiments yielded data that did not seem to follow traditional adsorption models reported in the literature. After a short period of time, adsorption ceased and a fraction of the phage population, sometimes as large as 50%, failed to irreversibly attach to a host cell. Therefore, the traditional first order adsorption model was modified with the introduction of a new term, adsorption efficiency. In this context, adsorption efficiency is defined as the fraction of the phage population that irreversibly binds to a host cell.

In this study, physico-chemical conditions, host cell physiology, environmental parameters, and infection conditions are shown to influence phage T4 attachment to the host cell. Results indicated that the adsorption rate constant was primarily influenced by the host cell growth conditions while the adsorption efficiency was dependent on the phage and conditions of infection.

In addition, the adsorption efficiency could be modified by adjusting the L-tryptophan concentration in the infection medium, although this tryptophan dependency was found to be a phenotypic trait of the bacteriophage. Finally, batch experiments demonstrated the significant impact adsorption efficiency can have on large-scale phage production.

This study has been published in *Bioprocessing and Biosystems Engineering*. It is presented here in accordance with the reproduction guidelines of the publisher.

3.1 ABSTRACT

Existing models for bacteriophage adsorption are modified with the addition of a new term, adsorption efficiency and applied to a T4-*Escherichia coli* system. The adsorption efficiency is the fraction of phage that adsorb irreversibly to the host. Adsorption kinetics were modeled using the adsorption rate constant (k) and the adsorption efficiency (ε). Experimental data demonstrated that the adsorption rate constant depends strongly on the condition of the host while the adsorption efficiency is a property of the bacteriophage population. The adsorption efficiency exhibited a marked dependence on the concentration of L-tryptophan.

The system was used to study the effect of adsorption kinetics on bacteriophage amplification. Increasing adsorption efficiency had an effect similar to increasing the initial MOI; the number of phages produced during amplification decreased. Optimizing the adsorption efficiency by manipulating the L-tryptophan concentration yielded a 14-fold increase in the number of phages produced.

Keywords:
bacteriophage T4, *Escherichia coli*, amplification, adsorption efficiency, kinetics, L-tryptophan

3.2 INTRODUCTION

Bacteriophage production on an industrial scale has been slow to develop since Felix d'Herelle first discovered what he referred to as an 'infravisible parasite of bacteria' [147]. However, with the ever increasing number of bacteria resistant to antibiotics [148-150] as well as opportunities in diagnostics [151] and recombinant protein production [42, 44-45, 115], there is a growing interest in bacteriophage applications. Realizing these will require efficient, large scale bacteriophage production.

An important factor in production is the first step in the bacteriophage infective process: adsorption to the host cell. Studies on T-even and T-odd bacteriophages have revealed that a number of environmental factors, such as ion concentrations, organic cofactors, pH and temperature, can have a significant impact on the adsorption of the virus to the host cell [69, 71-72, 75]. One of these cofactors is the amino acid L-tryptophan.

T. F. Anderson reported in 1945 that the presence of L-tryptophan greatly increased the plaque count when plating certain strains of bacteriophage T4 on a synthetic medium agar. Further experimentation indicated that L-tryptophan was interacting with the bacteriophage in a process called activation to enable adsorption to the host cell. Other organic cofactors were shown to have similar effects but not as pronounced as those of L-tryptophan [71]. The work of Anderson was corroborated and extended in a series of papers published by G. S. Stent and E. L. Wollman[73-74, 76-77], who determined that the rate of activation of the phage virion by L-tryptophan was proportional to the fifth power of the tryptophan concentration at low concentrations (< 3 $mg \cdot L^{-1}$) suggesting that five molecules of L-tryptophan are necessary for activation. The interaction between the virus and the

L-tryptophan molecule is a reversible reaction and dilution of the phage in tryptophan-free media was shown to lead to deactivation. Finally, decreasing temperature decreased the fraction of phages activated at a given L-tryptophan concentration. At high L-tryptophan concentrations (> 3 $mg \cdot L^{-1}$), the rate of activation is independent of L-tryptophan concentration.

The mechanism of bacteriophage T4 activation by L-tryptophan was elucidated and modeled by Kellenberger et al. in 1965 [152]. The authors proved that in order for phage T4 to adsorb to its host, it must be in an active state; a configuration with all six tail fibers away from the body of the virus. The virus uses the tail fibers to first reversibly bind to the host cell before irreversibly locking its tail to the cell surface. The deactivated state, or retracted state as it is commonly referred to, has the tail fibers retracted against the tail sheath. The authors suggested that there are cofactor-requiring strains of T4 which need six molecules of L-tryptophan per virus in order to enter that activated state; one for each tail fiber. Other studies indicate that the L-tryptophan molecule interacts with endogenous tryptophan residues located on the base plate or tail sheath, leading to the active tail fiber configuration [153-154].

Due to the wealth of knowledge concerning cofactor-requiring strains of T4, the T4-*Escherichia coli* relationship can be easily manipulated to study how the adsorption capability of a bacteriophage affects the amplification of the bacteriophage population. This paper first presents data on the adsorption kinetics of the phage-host system and then investigates how these relate to bacteriophage amplification.

3.3 MATERIALS AND METHODS

Host and bacteriophage

The host bacterium was *Escherichia coli* ATCC 11303. The growth medium was either Tryptic Soy Broth (TSB; Becton, Dickinson and Company, Sparks, MD), Nutrient Broth (NB; Becton, Dickinson and Company, Sparks, MD), or a minimal salt medium (MSM) consisting of 0.014 $g \cdot L^{-1}$ Na_2EDTA, 0.01 $g \cdot L^{-1}$ $FeSO_4 \bullet 7H_2O$, 0.01 $g \cdot L^{-1}$ $CaCl_2 \bullet 2H_2O$, 0.2 $g \cdot L^{-1}$ $MgSO_4 \bullet 7H_2O$, 6.0 $g \cdot L^{-1}$ Na_2HPO_4, 4.0 $g \cdot L^{-1}$ KH_2PO_4, 4.0 $g \cdot L^{-1}$ NH_4NO_3, 2.5 $g \cdot L^{-1}$ glucose, and 0.1 $g \cdot L^{-1}$ Bacto Yeast Extract (Becton, Dickinson and Company, Sparks, MD). MSM was supplemented with different concentrations of L-tryptophan when required (Sigma-Aldrich, St. Louis, MO). These media were also used as infection media.

When samples of host were required, these were grown overnight in shake flasks at 30°C to a concentration of approximately 3×10^9 colony-forming units per mL ($cfu \cdot mL^{-1}$).

Bacteriophage T4 (ATCC 11303-B4) was used in all experiments. A stock solution of bacteriophage T4 suspended in TSB was prepared and stored at 4°C and the titer was verified periodically to ensure no loss in infectious activity. The phage titer of this TSB stock solution was 3×10^{10} plaque-forming units per mL ($pfu \cdot mL^{-1}$) over the course of the study. A second stock solution of phages was prepared by infecting *E. coli* growing in MSM. This stock, referred to as the MSM stock, was also stored at 4°C. It had a titer of 1×10^{11} $pfu \cdot mL^{-1}$.

Phage titer

Phage titers were determined using a modified version of the agar layering technique [63] with an *E. coli* ATCC 11303 lawn to determine the free phage titer. Four milliliters of TSB with 0.75 % agar (w/v) was mixed with 10 μL of *E. coli* fully-grown culture and then poured over a 1.5% (w/v) agar-TSB base. Phage samples were diluted in TSB and aliquots were dropped onto the soft agar lawn and incubated overnight at 37°C for at least 12 hours before the number of plaques was counted. Titers were determined in duplicate and the average is reported.

Adsorption experiments

Adsorption experiments were carried out at either 24°C or 37°C. In all cases, the phages were allowed to equilibrate in the infection medium in an incubator for 45 minutes before experiments were performed. Two types of adsorption experiments were performed: 1) standard infection where the host was grown and infected in the same medium and 2) host-cross infection where the host was grown in one medium and then infected in a different medium. Adsorption experiments were carried out in one of following three media: TSB, NB, or MSM.

Phage and host solutions were prepared separately in sterilized tubes. Phage solutions were prepared by diluting the phage stock in 11 mL of infection medium to the pre-determined titer to be tested. A 1-mL sample of this solution was taken to determine the initial phage titer. The host solution was prepared by centrifuging 10 mL of an overnight host culture, removing the supernatant and re-suspending the pellet in 10 mL of the desired infection medium at the desired temperature. Bacteria

concentrations were diluted to approximately ~10^8 cfu·mL^{-1} and infected at a multiplicity of infection (MOI) of 0.01 unless otherwise stated. Immediately following re-suspension, the host and phage solutions were mixed together in a 30-mL syringe and incubated at the appropriate temperature. Samples of the free phages in the mixture were taken during the experiment by filtering 1 ml of the infection mixture through a 0.2-μm SFCA Corning syringe-filter (Corning Inc, Corning, NY). A fresh syringe-filter was used for each sample. Control experiments showed no statistically significant change of the free phage concentration when the medium was passed through the filter.

Bacteriophage amplification experiment

Bacteriophage amplification experiments were carried out in MSM with different concentrations of L-tryptophan (ranging from 0 to 50 mg·L^{-1}) at 37^{o}C. A 0.4-mL aliquot of phage and a 0.4-mL aliquot of *E. coli* diluted in the desired growth medium were mixed in a microcentrifuge tube at the desired MOI (0.01-1.0) and host concentration (~10^8 cfu·mL^{-1}) to produce the infection mixture. After incubating for five minutes to allow for adsorption to the host cell, the infection mixture was transferred to a shake flask containing 100 mL of the desired growth medium in an incubator shaker at 37^{o}C.

Bacterial growth was monitored throughout the experiment by measuring the optical density of the culture at 600 nm. The infection process was determined to be over after population-wide lysis – determined by the OD_{600} falling to a value below 50% of its peak value. Once the culture had been lysed, a sample was

removed and passed through a 0.2-μm SFCA Corning syringe filter and assayed to determine the phage titer.

3.4 MODEL DEVELOPMENT

Phage adsorption was initially described with a simple first-order reaction mechanism (Eq. 3.1) [63], where *P* is the phage particle, *H* is the host cell, and *PH* is the phage-host complex.

$$P + H \rightarrow PH \qquad (3.1)$$

In such a model, the rate of disappearance of phage can be described by Eq. 3.2, where C_p, C_{h0}, and k are the free phage concentration, the initial host concentration, and the rate constant, respectively

$$\frac{dC_p}{dt} = -kC_{h0}C_p \qquad (3.2)$$

Equation 2 can be solved for the concentration of free phages in solution as a function of time, yielding Eq. 3.3, where C_{p0} is the initial phage concentration.

$$C_p(t) = C_{p0}e^{-kC_{h0}t} \qquad (3.3)$$

A number of modifications to this simple model have been proposed. The most widely accepted is a two-step adsorption process consisting of a reversible and irreversible reaction, proposed by Stent and Wollman [59], which has the advantage of not only being in close agreement with the physical phenomenon,

but also providing an adequate fit for multiple phage/host systems [59, 65, 67]. However, in the case of activated bacteriophage T4, the virus particles have a very low probability of becoming detached once their tail fibers come in contact with the cell surface [51], hence the reaction scheme can be approximated by the model shown in equations (3.1-3).

The situation is complicated for cofactor-requiring strains of T4 because the fraction of T4 particles that are in the active state depends on the concentration of the cofactor. Only phage particles in the activated state are able to irreversibly bind to a host cell. In order to quantify the adsorption capability of a specific virus population, a new term is introduced, adsorption efficiency (ε). Adsorption efficiency is defined as the fraction of a phage population that irreversibly binds to a host cell while those particles that remain free in solution are deemed the free phage fraction (F). Note that $F = 1 - \varepsilon$.

The adsorption model presented in this paper is a modification to the first-order rate equation (Eq. 3.2) that takes into account the adsorption efficiency of the virus. This is accomplished by replacing the phage titer (C_p) in Eq. 3.2 with the effective titer ($C_p - C_{p0}F$). The effective titer represents only those phages that successfully adhere to a host cell by accounting for the portion of the phage population that remains free in solution ($C_{p0}F$). Solving for C_p as a function of time and replacing F with ($1-\varepsilon$) gives equation 3.4.

$$C_p(t) = C_{p0}\varepsilon e^{-kC_{h0}t} + C_{p0}(1-\varepsilon) \qquad (3.4)$$

Equation 3.4 differs from the traditional first-order model (Eq. 3.3) in two ways. Firstly, the coefficient of the exponent is no

longer the initial phage titer but rather the initial effective phage titer, $C_{p0}\varepsilon$. This gives a more realistic representation of the proportion of phages available for adsorption. Secondly, the expression on the right hand side of the equation — $C_{p0}(1-\varepsilon)$— is an indication of the 'inefficient' phages; that is, those phages that fail to adsorb. This term is a constant for a given set of conditions. Note that with an efficiency of one, Eq. 3.4 reduces to the traditional first-order model (Eq. 3.3). Equation 3.4 can be manipulated to express the normalized free phage concentration as a function of time:

$$\frac{C_p(t)}{C_{p0}} = 1 - \varepsilon(1 - e^{-kC_{h0}t}) \qquad (3.5)$$

The efficiency for each medium is approximated by averaging the normalized free phage concentration once adsorption has ceased. The rate constant is determined from the kinetic data. This model is useful because it offers greater insight into the phage adsorption process – by incorporating the competing effects of kinetics and efficiency – than the approaches used in the literature.

3.5 RESULTS

Typical results from some of the adsorption experiments are presented in Fig. 3.1. These are standard infections of *E. coli 11303* using the TSB phage stock in four different media: MSM, NB, TSB or MSM supplemented with 1 $g \cdot L^{-1}$ L-typtophan. The MSM supplemented with 1 $g \cdot L^{-1}$ L-tryptophan was used to observe adsorption kinetics in a medium that was unequivocally saturated

with tryptophan. As each experiment had slightly different initial concentrations of phage, the data for each experiment were normalized relative to the initial phage concentration. Data from each of the four experiments exhibited the same trend; an initial rapid decay followed by a period of no further adsorption. Other experiments (data not shown) all demonstrated that once the final free phage fraction (F) was reached, the value remained unchanged for at least 60 minutes. The proposed adsorption model (Eq. 3.5) was fitted to the data for each medium and is shown as solid lines in Fig. 3.1.

Table 3.1 contains the values of the adsorption rate constant (k) and the adsorption efficiency (ε). Reported values are averages from at least two experiments. The rate constants vary more than an order of magnitude amongst the four media, with MSM displaying the greatest rate constant and TSB exhibiting the smallest. It is important to note that there was no apparent correlation, positive or negative, between the rate of adsorption and the efficiency of adsorption. For example, phage T4 had the fastest rate of adsorption but the lowest efficiency in MSM. In TSB, the virus had the highest efficiency, but the slowest rate of adsorption. In MSM supplemented with L-tryptophan, the virus exhibited both a fast rate of adsorption and a high adsorption efficiency. Table 3.1 also shows that increasing the temperature from 24^{o}C to 37^{o}C during adsorption resulted in 8-fold and 2-fold increases in the rates of adsorption in MSM and TSB, respectively, but, statistically, led to no change in the adsorption efficiency.

Fig. 3.2 shows the adsorption efficiency of phage T4, grown from two different phage stocks, in MSM as the infection medium, as a function of L-tryptophan concentration. The trend for the TSB phage stock displayed a small increase in adsorption efficiency at

low L-tryptophan concentrations (1-7.5 $mg \cdot L^{-1}$). At higher concentrations (7.5-20 $mg \cdot L^{-1}$), the efficiency was a strong function of L-tryptophan concentration and increased to nearly 100%. Above 20 $mg \cdot L^{-1}$, the addition of L-tryptophan had no further effect. The efficiency of the MSM phage stock showed no dependence on the L-tryptophan concentration, remaining above 97% in MSM supplemented with 1 $mg \cdot L^{-1}$ L-tryptophan and 75 $mg \cdot L^{-1}$ L-tryptophan.

In order to verify whether or not the adsorption efficiency represented an equilibrium situation between the virus particles and the host, adsorption experiments were carried out under a variety of host concentrations and MOI's. Fig. 3.3 shows the variation of efficiency with multiplicity of infection (MOI) at 24^0C for two different media, TSB and MSM. Statistical analyses showed no correlation between these parameters.

Several sets of host-cross infections, in which host cells were grown in one medium, collected by centrifugation and infected in a second medium, were carried out. The data for host-cross infections, in which the cells were grown in MSM and infected in either NB or TSB with the TSB phage stock, are presented in Fig. 3.4. Standard experiments where the cells are grown in TSB or NB and infected in the same medium are also shown. As seen in Fig. 3.4, for infections in both NB and TSB, the normalized free phage concentration approached *F* more quickly in the cross infection experiments than in the standard adsorption experiment; the adsorption rate constants increased by an order of magnitude for both cases (2.6×10^{-10} $mL \cdot s^{-1}$ and 3.7×10^{-10} $mL \cdot s^{-1}$, respectively). However, for cross infections carried out in both TSB and NB, the adsorption efficiencies were approximately equal to the efficiencies of the respective infection media, changing by less

than 7%. This small difference is amplified in Fig. 3.4 because of the logarithmic scale.

Fig. 3.5 displays the final phage yield versus initial MOI for phage T4 amplification experiments carried out in MSM at various L-tryptophan concentrations. Each curve demonstrated the same trend. As the initial MOI was increased, the final phage titer decreased. As the L-tryptophan concentration increased from 1 $mg \cdot L^{-1}$ to 15 $mg \cdot L^{-1}$, there was a 14-fold decrease in phage yield.

3.6 DISCUSSION

Validity of proposed model

The traditional first order model for the adsorption of phages to their host (Eq. 3.3) is sufficient to describe many phage-host systems during the first few minutes of adsorption [63]. However, it implies that, provided with enough time, every member of a phage population will adsorb to a host. In fact, while 10 minutes after the onset of adsorption experiments, no further adsorption was observed in all experiments performed in this study, a fraction of the phage population, ranging from less than 1% to around 50% depending on experimental conditions (see Fig. 3.2), always remained free in solution. Therefore, the traditional first order model did not provide an adequate fit for the data obtained in these experiments.

An improvement to the traditional first order model is the two step mechanism proposed by Stent and Wollman. Adsorption described by this model is generally characterized by two exponential decay terms; a fast decay followed by a relatively slow decay. However, this model still has the problem that the phage

population diminishes to zero, a phenomenon that can sometimes be extrapolated from literature data, but is not supported by any of the literature surveyed. Certainly, the systems studied here did not behave in the manner predicted by this two step mechanism.

The new model proposed here (Eq. 3.4) is a hybrid between these two earlier phage adsorption models. It makes use of a first order relationship while recognizing the two step reality of phage adsorption. This model has the advantages of being simple, accurate and robust. It has two modeling parameters: the adsorption rate constant (k) and the adsorption efficiency (ε). The former is an indication of how quickly adsorption takes place, the latter reveals what fraction of the phage population will undergo adsorption. The utility of this new model is that it augments the simpler kinetic model with a quantifiable property of the bacteriophage population, the adsorption efficiency.

Significance of the adsorption rate constant (k) and the adsorption efficiency (ε)

Both the adsorption rate constant (k) and the adsorption efficiency (ε) were shown to be affected, often significantly, by different physico-chemical conditions of the media as well as by physiological conditions of the host. Furthermore, these two parameters were shown to be mutually independent by their different responses to these changes. In fact, k is largely dependent on the state of the host whereas ε is more a property of the state of the virus.

One of the earliest observed methods of increasing the rate of adsorption was by increasing the temperature of the infection medium [69]. This phenomenon was observed in the values of adsorption rate constants in Table 3.1. Note that other

characteristics of the media such as pH, ion concentration, and viscosity[69, 71-72, 75] were not investigated in this study. Aside from the nutrient make-up, many properties of TSB, NB, and MSM are relatively similar (pH, viscosity, etc).

In the past decade, studies have shown that the nutrient make-up of the medium in which the host is grown can have an effect on the rate of adsorption of the virus to the host [67, 78]. Hadas *et al.* found that the adsorption rate of bacteriophage T4 was linearly proportional to total host cell surface area when growing cells in a minimal medium supplemented with various carbon sources and nutrients. Depending on the carbon source, the total cell surface area and the adsorption rate varied over a factor of four [78]. Moldovan *et al* found slightly faster adsorption rates could be obtained in a phage λ-Ymel system when the host cells were grown in a minimal medium in the presence of maltose rather than glucose [67]. It is known that the expression level of LamB, the surface receptor protein required for adsorption of phage λ, varies depending on the carbon source [67]. From these observations, it is evident that the cell size of the host and the density of receptor proteins on the surface of the host are dependent on the nutrient conditions during growth. These variations are, therefore, possible explanations for the order of magnitude differences in adsorption rate constants amongst the data tabulated in Table 3.1. However, these observations alone do not rule out the possibility that the virus itself is accountable for the variation in rate of adsorption from one medium to the next.

Other experiments supported the importance of the growth conditions of the host on the rate of adsorption of the virus. The results in Fig. 3.1 and Table 3.1 indicated that under standard experimental conditions, that is growing and infecting the host in the same medium, the fastest adsorption was observed in MSM.

The slowest adsorption was observed in TSB. However, as shown in Fig. 3.4, when the host was grown in MSM and then infected in TSB, the rate of adsorption of the virus approaches the rates of adsorption attained in infections in MSM under standard conditions. This same trend was observed when growing the host in MSM but infecting with phage T4 in NB (Fig. 3.4). Since the experimental conditions of the virus remain unchanged while those of the host are manipulated in the host-cross infections, the changes in rates of adsorption observed must be caused by different conditions in the host cell. The most plausible explanation is that the morphological and physiological state of the host in MSM leads to the fastest rate of adsorption of the virus. These trends were also seen, although to a lesser extent, in the reverse experiments. When the host was grown in TSB and infected in MSM, the rate of adsorption was closer to that of standard adsorption experiments carried out in TSB.

The second influential factor in Eq. 3.4, the adsorption efficiency (ε), was introduced to account for the fact that the phage population is divided between those that readily adsorb to a host and those that fail to adsorb to a host even after an extended time period. As can be seen in Fig. 3.1 and Table 3.1, this efficiency is unique for each medium. Unlike the rate constant, the efficiency is independent of temperature between 24^{o}C and 37^{o}C – as reported in Table 3.1. In addition, the efficiency was found to be independent of the multiplicity of infection (Fig. 3.3). Regardless of the ratio of virus to host, the fraction of phages that binds irreversibly to the host cells remains the same for a given medium in which the adsorption takes place. This suggests that the adsorption efficiency of the virus population is not merely an equilibrium between the host and bacteriophage and the complex they form, but in fact a property of the virus population. Finally,

from Fig. 3.4, it is clear that the growth conditions of the host have minimal impact on the adsorption efficiency of the virus. In both TSB and NB, there is little change in the adsorption efficiency compared to the infection medium at standard conditions.

In fact, the only experimental condition that brought about significant changes in the adsorption efficiency was the L-tryptophan concentration of the infection medium. From Table 3.1, it can be seen that the increase in efficiency from MSM to NB to TSB parallels a similar increase in L-tryptophan concentration in the media. While it cannot be said with absolute certainty that L-tryptophan is the only factor influencing the adsorption efficiency in these three media, Fig. 3.2 shows how important it is. Here the adsorption efficiency of phage T4 in MSM is increased from roughly 60% to nearly 100% simply by the addition of L-tryptophan to the infection medium.

However, the cofactor requirement of bacteriophage T4 appears to depend on the history of the virus particle. T. F. Anderson reported evidence in 1948 that the L-tryptophan requirement of phage T4 was an inheritable trait [155]. Experimentation in this study with the MSM stock suggests a slightly different conclusion. As shown in Fig. 3.2, phage samples from the MSM stock had an efficiency of over 97% in MSM with and without supplementation of L-tryptophan. Unlike phages produced in TSB, the offspring produced in MSM exhibited no L-tryptophan requirement for adsorption. Note that both the MSM and TSB phage stocks were amplified using the same ATCC strain. In addition, the L-tryptophan dependency was evident when phages produced in TSB were amplified in MSM and then reamplified in TSB. These observations suggest that the L-tryptophan requirement of phage T4 is a phenotypic quality that can be triggered or inhibited depending on the environment of the

bacteriophage particle and not the result of a mutation in the phage DNA.

One way to interpret the tryptophan dependency of bacteriophage T4 is to consider it as a conditional lethal phenomenon. Conditional lethal is a term applied to virus mutants that are only able to replicate under permissive conditions. For example, some temperature-sensitive mutants of bacteriophage T4D can only propagate at low temperatures and are unable to grow at higher temperature [156]. However, as discussed here, the tryptophan dependency of bacteriophage T4 is not a genetic property, but rather a phenotypic characteristic of the virus. In this context, tryptophan dependency can be thought of as a conditional lethal phenotype with a permissivity dictated by the concentration of L- tryptophan.

Other studies in the literature suggest that L-tryptophan increases the rate of adsorption of phage T4 to its host [76]. This phenomenon was observed in the present study, although only a small increase was observed. As shown in Table 3.1, the rate constant of the TSB stock increased approximately 1.8 fold when L-tryptophan was added to the minimal salt medium during adsorption experiments. This change is relatively minor compared to the order of magnitude increase in the rate constant observed between MSM and TSB or NB. L-tryptophan had a much more pronounced effect on the adsorption efficiency of the TSB stock, as is evident in Fig. 3.2.

In summary, the growth medium of the host and the infection temperature have a significant impact on the adsorption rate constant while the phenotype of the phage in response to its environment – including the L-tryptophan concentration of the infection medium – have the most pronounced effect on the adsorption efficiency. The data from this study suggest that the

adsorption rate constant can be strongly influenced by the conditions of the host while the adsorption efficiency is mainly dependent on the conditions of the bacteriophage. Studies with other phage-host systems have suggested a similar conclusion [67, 78].

The new term introduced in this model (ε) could have a more general application. It is reasonable to assume that the concept of adsorption efficiency could be applied to other phage-host systems and possibly other virus-host systems.

Adsorption efficiency (ε) and the efficiency of plating

One historical context in which the adsorption efficiency could be applied is the efficiency of plating. Early phage researchers observed that the plaque count of the same phage preparation varied according to the environmental conditions of the assay. In order to address this phenomenon, Ellis and Delbruck introduced the concept of efficiency of plating [79]. The efficiency of plating (EOP) can be defined as the plaque count determined under stated conditions relative to the plaque count under standard conditions [63]. While the EOP depends on many factors — virus diffusion through the agar, adsorption to the host cell, successful phage replication and lysis of the host cell, etc — the adsorption efficiency of the bacteriophage is quite possibly the most significant mechanism explaining many of the previously reported changes in the EOP. Anderson observed a 10,000 fold increase in the plaque count of bacteriophage T4 when plating on nutrient agar compared to plating the same strain on a defined medium lacking amino acids [71]. This observation is consistent with the presence of tryptophan in the nutrient agar, which can lead to an adsorption efficiency of over 99% as reported in this

paper (see Table 3.1). The efficiency of plating can also change when assaying the same phage preparation with different susceptible bacteria [63] and by varying the salt concentrations of the agar [72]. The adsorption efficiency is almost certain to change with different susceptible hosts and is likely influenced by the ionic environment of the bacteriophage and its host. Therefore, the adsorption efficiency is a plausible mechanism behind the large variation in EOP reported in literature. Additional experiments would have to be done to confirm this hypothesis.

Phage amplification

The data bring out an important property of L-tryptophan. While it can have a significant impact on the adsorption efficiency, it has only a minimal effect on the rate of adsorption. In addition, growth experiments with *E. coli* indicated that L-tryptophan does not have an effect on the metabolism of the host cell (data not shown). Therefore, the addition of L-tryptophan should not affect the physiological parameters linked to adsorption. Consequently, amplifying bacteriophages in MSM supplemented with various L-tryptophan concentrations will only affect the adsorption efficiency of the virus while keeping other amplification parameters constant. It should be noted that the amplification experiments were carried out at 37°C while the majority of the kinetic data was collected at 24°C. As reported in Table 3.1, the warmer temperature increased the adsorption rate constant but caused no observable change in the adsorption efficiency.

The results shown in Fig. 3.5 shed an interesting light on the adsorption efficiency of the bacteriophage. Increasing the adsorption efficiency decreases the overall number of phages produced for given initial conditions of infection. As the L-

tryptophan concentration increases from 1 mg·L^{-1} to 15 mg·L^{-1}, the adsorption efficiency increases from around 60% to over 95% (Fig. 3.2). This, in turn, corresponds to a roughly 14 fold decrease in the final bacteriophage titer obtained from amplification experiments (Fig. 3.5). This negative correlation between adsorption efficiency and final phage titer is due to the fact that a high efficiency of adsorption implies that a large portion of the host cells will be infected and die early in the amplification process. The entire bacterial culture will lyse before it has a chance to propagate to any significant degree. Consequently, more phages are produced at a low adsorption efficiency because it takes significantly longer for the bacteriophage population to lyse the host culture. This allows for the host culture to grow to a higher cell density and therefore produce more virus particles in the process. In this regard, increasing the efficiency is similar to increasing the initial MOI of the production broth.

It seems that the most dramatic changes in phage yield observed in Fig. 3.5 are seen at very low L-tryptophan concentrations (1-5 mg·L^{-1}) where the efficiency ranges from 60% to 70% according to Fig. 3.2. As the L-tryptophan concentration is increased, the phage titer curves tend towards a limit. This happens because, as the L-tryptophan concentration increases, the efficiency becomes very high and the phage production period becomes very short, and consequently, the phage yield is low. As such, the differences in yield are much less pronounced. There seems to be a threshold of approximately 15 mg·L^{-1} L-tryptophan, after which further increases in L-tryptophan concentration do not result in further decreases in phage yield. According to Fig. 3.2, this corresponds to an adsorption efficiency of roughly 95%. Therefore it is reasonable to conclude that above efficiencies of

95%, no further effect on phage yield is observed during production.

3.7 CONCLUSION

The adsorption efficiency appears to be a property of the phage population that is a function of the environmental conditions of infection and the phenotype of the phage stock while the adsorption rate constant is a property that can be significantly influenced by the conditions of the host. An adsorption model that takes into account the adsorption rate constant and adsorption efficiency provided an accurate fit for adsorption data under numerous experimental conditions. The number of phages produced during amplification was found to be negatively correlated with the adsorption efficiency of the virus; decreasing as the efficiency increased. This work demonstrates the importance of considering the adsorption efficiency in any attempt to optimize the production of bacteriophage particles in an industrial process.

3.8 ACKNOWLEDGEMENT

The authors would like to thank the National Science and Engineering Research Council of Canada, the Eugenie Ulmer-Lamothe Fund of McGill University and the Richard H. Tomlinson Doctoral Fellowship of McGill University for providing financial support for this project.

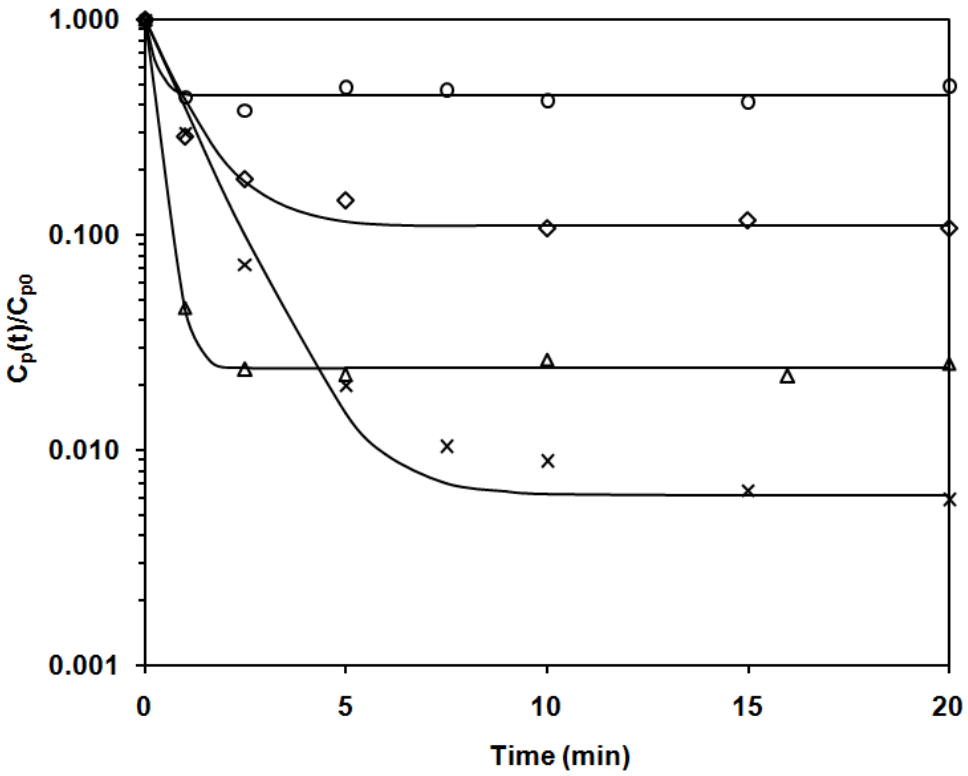

Fig. 3.1 Adsorption experiments of bacteriophage T4 to *E. coli* ATCC 11303 in four different infection media under standard infection conditions: (○) MSM, (◊) NB, (×) TSB and (Δ) MSM + 1.0 g/L L-tryptophan. The phage concentration data are normalized with respect to the initial phage concentration. All experiments were carried out at 24^0C with a host concentration of 10^8 cfu·mL^{-1} and an MOI ~ 0.01 with a phage stock prepared in TSB. The proposed adsorption model is also shown for each medium

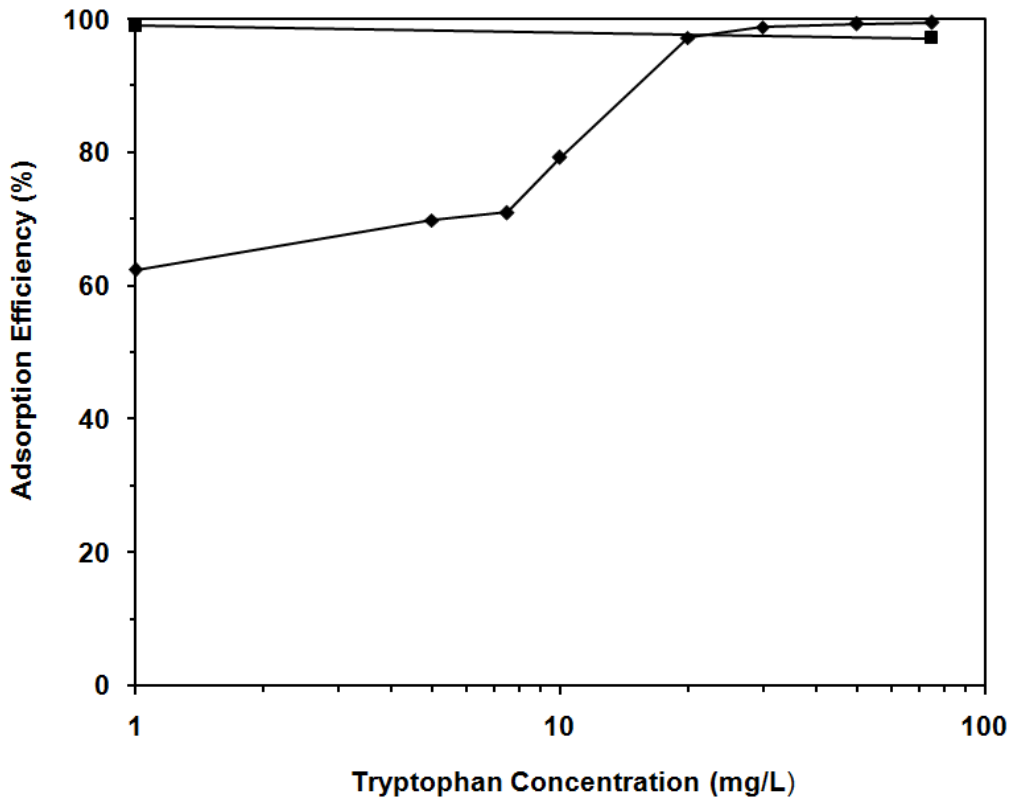

Fig. 3.2 The adsorption efficiency of phage T4 to *E. coli* in MSM versus L-tryptophan concentration under standard infection conditions. The adsorption efficiency was obtained by carrying out adsorption experiments in MSM at various L-tryptophan concentrations at 24^0C with a host concentration of 10^8 cfu·mL^{-1} and an MOI ~ 0.01 Two different phage stocks were used, one stock produced and stored in MSM (■), the other produced and stored in TSB (♦)

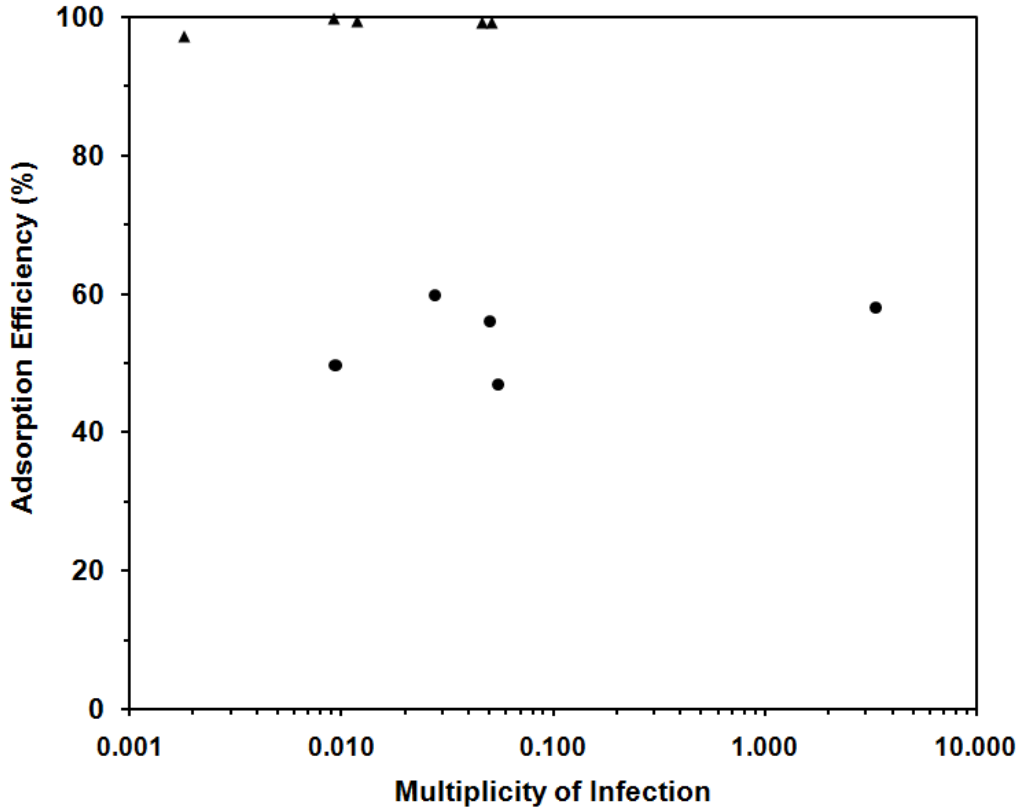

Fig. 3.3 Variation of the adsorption efficiency of phage T4 with initial multiplicity of infection in TSB (▲) and MSM (●) under standard infection conditions. All experiments were carried out at 24^0C with a host concentration of 10^8 cfu·mL^{-1} with a phage stock prepared in TSB

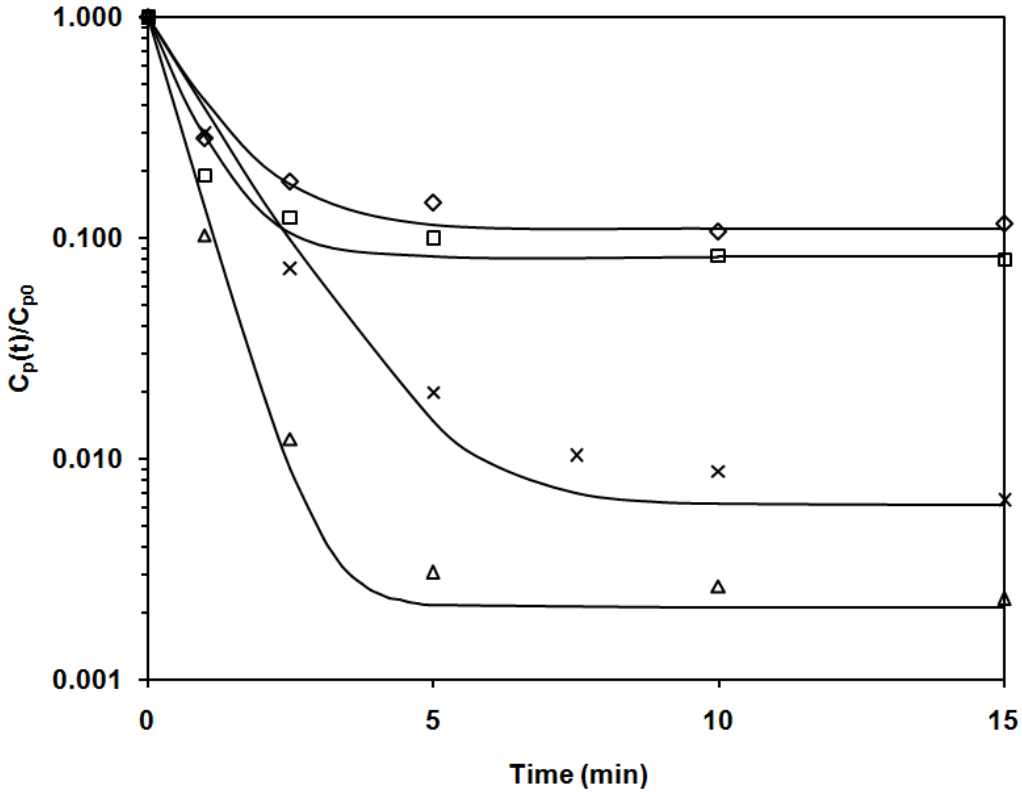

Fig. 3.4 Host-cross infection adsorption experiments. *E. coli* was grown in MSM and then infected in either NB (□) or TSB (Δ). Standard infections, where the host is grown and infected in the same medium – NB (◊) and TSB (×) – are shown for comparison. All experiments were carried out at 24^{0}C with a host concentration of 10^8 cfu·mL^{-1} and an MOI ~ 0.01with a phage stock prepared in TSB. The proposed adsorption model is shown for each experiment

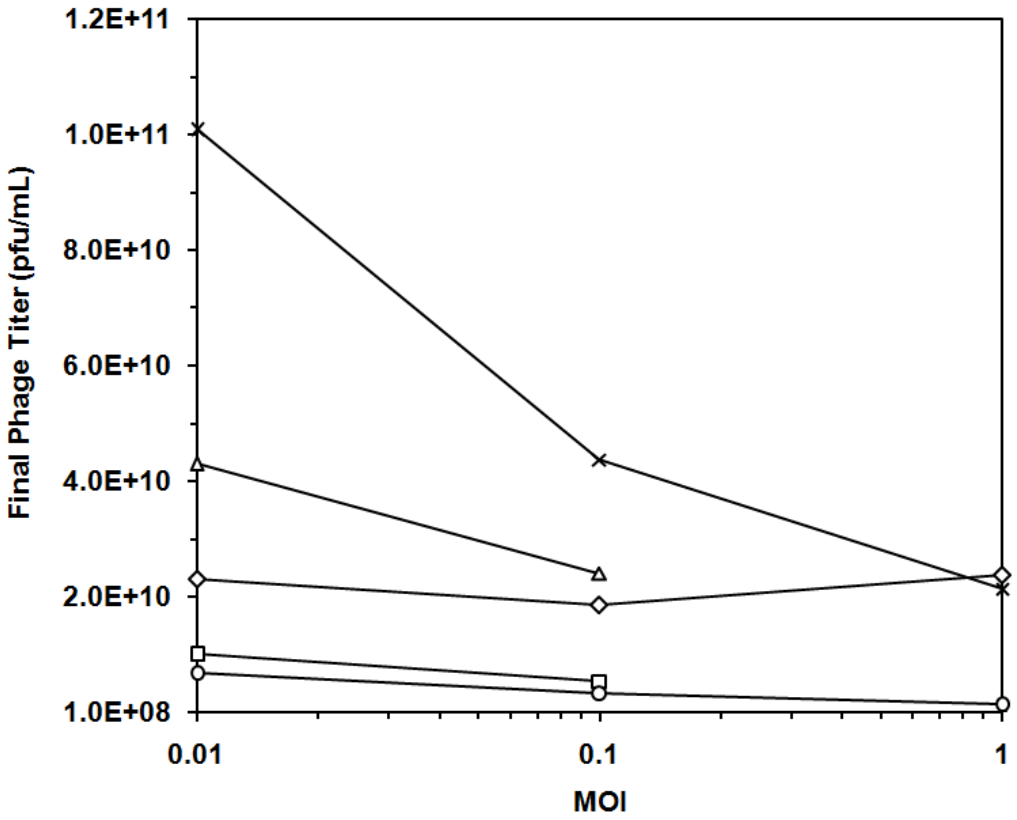

Fig. 3.5 Final phage titer versus initial MOI obtained from amplification experiments. Host cells were infected with a phage stock prepared in TSB and the experiments were carried out in MSM supplemented with L-tryptophan at the following concentrations: 1 mg·L^{-1} (×), 3 mg·L^{-1} (Δ), 5 mg·L^{-1} (◊), 7.5 mg·L^{-1} (□) and 15 mg·L^{-1} (○). All experiments were carried out in 100 mL shake flasks in an incubator shaker at 37°C agitated at 200 rpm

Table 3.1 Efficiency (ε) and rate constants (k) calculated for the TSB phage stock under standard conditions in the minimal salt medium (MSM), MSM with L-tryptophan, tryptic soy broth (TSB), and nutrient broth (NB).

Medium	Temperature (°C)	L-tryptophan Concentration ($mg \cdot L^{-1}$)	ε* (%)	k* ($mL \cdot s^{-1}$)
MSM	24	trace	56 ±11	$3.7 \times 10^{-10} \pm 1.3 \times 10^{-10}$
MSM + 1 g/L Trypt	24	1,000	99 ± 0.9	$6.8 \times 10^{-10} \pm 3.5 \times 10^{-11}$
TSB	24	136	99 ± 1.0	$7.3 \times 10^{-11} \pm 2.5 \times 10^{-11}$
NB	24	36	87 ± 1.7	$3.4 \times 10^{-11} \pm 8.5 \times 10^{-12}$
MSM	37	trace	50	3.0×10^{-09}
TSB	37	136	99	1.5×10^{-10}

*Standard deviations are based on a minimum of two experiments

Chapter 4 MODELING BACTERIOPHAGE ATTACHMENT USING ADSORPTION EFFICIENCY

Published as:

Storms ZJ, Smith L, Sauvageau D, Cooper DG (2012) Modeling Bacteriophage Attachment Using Adsorption Efficiency. *Biochem Eng J* 64: 22-29

PREFACE

In this work, the robustness and limits of the adsorption efficiency model were established by applying it to T-series phages and phage λ.

The robustness of the model was demonstrated by showing its suitability for modeling the adsorption of Myoviridae (T2, T4, and T6), Siphoviridae (T5), and Podoviridae (T7) to *Escherichia coli* under different infection conditions. Also, a rigorous study comparing the performance of the adsorption efficiency model to one of the more commonly used adsorption models, the sequential model, was completed using phage T6. The experimental data validated the assumptions inherent to the adsorption efficiency model.

Analysis of adsorption data collected from two strains of phage λ, one containing side-tail fibers, one without, suggested that the adsorption efficiency is best suited for phage strains containing side-tail fibers. Here, side-tail fibers refer to the tail fibers extending outwards from the base plate. Phage λ has an end tail fiber that protrudes downward from the tail base plate.

This work has been published in the *Biochemical Engineering Journal*. It is reproduced here in accordance with the guidelines set forth by the publisher.

4.1 ABSTRACT

Typically, models of bacteriophage adsorption consider the process in two steps: reversible and irreversible attachment. In this study, a recently introduced one-step adsorption model, the adsorption efficiency model, is used to describe the adsorption of T-series bacteriophages to *Escherichia coli.* The adsorption efficiency model simplifies phage attachment to a single step: irreversible binding. The adsorption efficiency (ε) is used to account for unadsorbed phages. The model accurately describes T-series phage adsorption (T2, T4, T5, T6, and T7) under a variety of conditions. In addition, the model is compared to a commonly used two-step adsorption model, the sequential model. Experimental data support the assumptions of the adsorption efficiency model and suggest that the reversible first step of T-series phage adsorption is equivalent to irreversible attachment under the conditions tested. The adsorption efficiency model was not appropriate for a phage λ strain lacking side tail fibers. However, the model did agree with data previously published for a strain of phage λ possessing side tail fibers similar to those of the T-even phages. This suggests that the adsorption efficiency model applies to phages containing side tail fibers.

Keywords:
Bacteriophage, Adsorption, Adsorption efficiency, Modeling, Kinetic Parameters, Dynamic Simulation

4.2 INTRODUCTION

Bacteriophages are the natural predator of bacteria. Consequently, they have received renewed attention in recent decades for potential applications as biological control agents in the agricultural and food packaging industries; in the control of water-borne pathogens; and in the treatment of bacterial diseases in both humans and animals [5, 17, 24, 157-158]. In addition, their specificity makes them ideal candidates in diagnostic applications [151]. Finally, some researchers are examining their potential as vectors of recombinant protein production [42, 44-45, 115].

Because phage reproduction requires the introduction of its genome into the host cell, the adsorption of the virus particle to the host cell is a necessary step in almost all phage applications. Therefore, developing reliable models of virus-host cell interactions becomes essential for the successful application of bacteriophages. This work looks at the suitability of a recently developed adsorption model to predict the virus-host interactions of tailed phages, specifically, T-series and λ bacteriophages.

The main structural characteristics of the phages used in this study are summarized in Table 4.1. The phages represent three distinct families and exhibit significant differences in tail length and contractility. Also, there is a variety of tail fiber constructs represented. The tail fibers are the organelles used to identify the appropriate receptor protein on the surface of the cell during adsorption to the host. The T-even phages have six very large side-tail fibers (140 nm) while the six fibers of phage T7 are quite small (23 nm) [159-160]. The Siphoviridae studied here (T5, λ and Ur- λ) have one straight tail fiber connected to the distal end of the tail. Phage T5 and Ur- λ complement this end tail fiber with

side-tail fibers protruding outwards from near the base of the tail while λ has only the one end tail fiber [111, 161-162]. The Myoviridae (T2, T4, T6) and Podoviridae (T7) do not have an end tail fiber.

The adsorption of a tailed phage particle to a host cell is a remarkable physiological phenomenon. Generally, upon contact with the host cell, the phage first reversibly attaches to the cell surface with its fibers, and then irreversibly binds to the appropriate receptor protein on the cellular membrane. This prompts conformational changes leading to the opening of the connector, allowing for the release of phage DNA from the capsid into the host cell [163].

A common modeling approach is to simplify phage adsorption into two steps: reversible and irreversible attachment. Numerous models have been published based on this mechanism [59, 64, 66]. Recently, we proposed an alternative interpretation of bacteriophage adsorption, known as the adsorption efficiency model, based on the interactions of bacteriophage T4 with *Escherichia coli* [164]. This model considers that the forward reaction in the reversible step is strongly favored, leading to an irreversible one-step approximation. In the present study, we examine the applicability of this model to other phage-host systems. We also compare and contrast the adsorption efficiency model with one of the most widely used two-step adsorption models, the sequential model.

4.3 MATERIALS AND METHODS

Host and bacteriophage

The host bacterium used for the T-series phages was *Escherichia coli* ATCC 11303. The following media were used for growth of the host and for adsorption experiments: Tryptic Soy Broth (TSB; Becton, Dickinson and Company, Sparks, MD), Nutrient Broth (NB; Becton, Dickinson and Company, Sparks, MD) supplemented with 0.5% NaCl (w/v), and a minimal salt medium (MSM; previously described in [164] supplemented with 2 $g \cdot L^{-1}$ glucose and 0.1 $g \cdot L^{-1}$ Bacto Yeast Extract (Becton, Dickinson and Company, Sparks, MD).

The host bacterium for phage λ was *Escherichia coli* MG1655, obtained from the *E. coli* Genetic Stock Center (CGSC #6300) of Yale University (New Haven, CT). It was cultured in MSM using either glucose or maltose as a carbon source at a concentration of 2 $g \cdot L^{-1}$ (w/v).

The following four bacteriophage strains were used in this study: bacteriophage T2 (ATCC 11303-B2), bacteriophage T5 (ATCC 11303-B5), bacteriophage T6 (ATCC 11303-B6), bacteriophage T7 (ATCC 11303-B38) and bacteriophage λ_{cI857} isolated from a lysogenized strain of MG1655(λ_{cI857}) generously provided by SAIC-Frederick, NCI-Frederick (Frederick, MD). Bacteriophage strains T2, T5, T6 and T7 were amplified using *E. coli* ATCC 11303 in Nutrient Broth with 0.5 % NaCl (w/v), as per ATCC guidelines. Amplified samples were filtered using a 0.2-µm SFCA Corning syringe-filter (Corning Inc, Corning, NY) and the filtrate was stored at 4°C. The titer of each phage stock was

verified periodically to ensure no loss in infectious activity. The data for bacteriophage T4 was from a previous study [164].

Adsorption experiments were performed using samples of host cultures grown overnight, in the medium to be tested, in shake flasks at 200 rpm and 37°C to a concentration of approximately 1 x 10^9 colony-forming units per mL (cfu·mL^{-1}).

Adsorption experiments and phage and infective sites titers

Adsorption experiments were carried out in one of the three media described in section 2.1 (TSB, NB, or MSM) according to the method described in Storms *et al.* [164]. All adsorption experiments were carried out in the growth medium of the host. The host solution (~10^8 cfu·mL^1) was added to the phage solution (~10^7 pfu·mL^{-1}) in a 30-mL syringe at 24°C to a total volume of 11 mL and a resulting multiplicity of infection (MOI) of 0.1. Periodically, 1-mL samples were filtered out of the syringe through a syringe-filter (0.2-µm SFCA Corning syringe-filter – Corning Inc.) and assayed for free phage titer measurements. A fresh syringe-filter was used for each sample.

In some experiments, in addition to measuring the free phage concentration (C_P), the total number of infective centers (C_{IC}) in the phage-host mixture was assayed. This was done by removing a sample from the adsorption broth, diluting 1,000 fold to stop further adsorption, and then plating on an agar plate using the modified layering technique described previously [164]. In this context, infective centers include all irreversibly adsorbed phages (infected cells) and free phages. From these measured values, it is possible to determine the concentration of irreversibly attached phages (C_I) using the equation $C_I = C_{IC} - C_P$. Moreover, in order to

determine the concentration of reversibly attached phages (C_R), samples from the adsorption broth were diluted in tubes containing 2 % chloroform (v/v), which lyses the cells and releases reversibly attached phage particles [70]. These samples were assayed with the agar layering technique, yielding the total concentration of free and reversibly attached phages (C_{PR}). By comparing these samples with free phage samples (C_P), the concentration of reversibly attached phages could be determined using the equation $C_R = C_{P\,R} - C_P$.

4.4 THEORY

Two kinetic models of phage adsorption are summarized below. The first is the sequential model, a variation of the two-step mechanism proposed by Stent and Wollman as an improvement over the earlier, simple first order model [59]. This model remains widely used today [65, 67, 70]. The second is the adsorption efficiency model, describing the adsorption kinetics of bacteriophage T4 taking into account the incapacity of a portion of the phage population to efficiently bind to the host [164]. Note that in each of the models, the adsorption process has been simplified and that the adsorption rate constants k_i depend on many diffusive and physico-chemical properties of the medium, phage and host bacterium. For a more detailed treatment, including the stochastic diffusion of the initial stages of phage adsorption, see the work of Adam and Delbruck [165] or Berg and Purcell [166].

Sequential model

The sequential model describes phage adsorption as a two-step process consisting of a reversible reaction followed by an irreversible one, where *P* is the free phage particle, *H* is the host cell, *R* is the reversible phage-host complex, and *I* is the irreversible phage-host complex.

$$P + H \underset{k_2}{\overset{k_1}{\leftrightarrows}} R \overset{k_3}{\rightarrow} I \tag{4.1}$$

Researchers applying this model have been able to show the reversibility of the first reaction and that the irreversible step is indeed necessary for a successful infection [66, 68-69]. The concentration of each species over time can be calculated by simultaneously solving the following set of ordinary differential equations:

$$\frac{dC_P}{dt} = -k_1 C_P C_H + k_2 C_R \tag{4.2}$$

$$\frac{dC_R}{dt} = +k_1 C_p C_H - (k_2 + k_3) C_R \tag{4.3}$$

$$\frac{dC_I}{dt} = k_3 C_R \tag{4.4}$$

$$\frac{dC_H}{dt} = 0 \tag{4.5}$$

Note that the host cell concentration is assumed to be constant; an approximation valid in this study since adsorption experiments were carried out at room temperature with cell cultures in the stationary phase of growth. Other studies have accounted for bacterial growth [70]. This system of equations can be solved using the ODE45 solver on MATLAB© and the appropriate reaction rate constants can be estimated by fitting the

model to the experimental data and minimizing the error sum of squares.

Adsorption efficiency model

Details concerning the development of the adsorption efficiency model are provided in Storms *et al.* [164]. The model was developed to describe phage T4 adsorbing to *Escherichia coli* and reduces the sequential adsorption mechanism to a one-step reaction mechanism whereby a phage particle (*P*) and host cell (*H*) come together to form an irreversible phage-host complex (*PH*).

$$P + H \xrightarrow{k} PH \tag{4.6}$$

Justification for this simplified reaction mechanism is based on observations in our experiments, and in the literature, that the probability of T4 phage particles becoming detached once their tail fibers have become reversibly bound to the host cell under normal circumstances is very low [51, 167]. The concept of adsorption efficiency (ε) is introduced to explain experimental results showing that in adsorption experiments, unlike the predictions of previous models, the free phage concentration ceased to decrease and reached a plateau after a short time. In some cases, up to 50% of the free phage population failed to adsorb to a host cell [164]. It is important to note that this plateau could not be attributed to equilibrium of the reversible reaction. Adsorption efficiency is defined as the fraction of a phage population that irreversibly binds to a host cell. With this in mind, the concentration of free phages can be solved using the following rate equation:

$$\frac{dC_P}{dt} = -kC_{H0}\{C_P - C_{P0}(1-\varepsilon)\} \quad (4.7)$$

Here, C_{H0} denotes the initial host concentration, which is assumed constant over the course of the experiment, and C_{P0} the initial phage concentration. The term $\{C_P - C_{P0}(1-\varepsilon)\}$ represents the effective titer after taking the adsorption efficiency into account. Equation (4.7) can be solved for the phage concentration as a function of time:

$$C_P(t) = C_{P0}\varepsilon e^{-kC_{H0}t} + C_{P0}(1-\varepsilon) \quad (4.8)$$

In this model, ε is determined experimentally and k can be estimated using the least squares approximation method. This model was shown to fit adsorption data of bacteriophage T4 under a variety of conditions but was not applied to other phage strains.

4.5 RESULTS

Model comparison

Fig. 4.1A displays the data for the adsorption of bacteriophage T6 to *E. coli* in TSB. As shown in the figure, both the sequential model and the adsorption efficiency model effectively predict the free phage concentration of phage T6 during adsorption. However, the two models predict very different behavior of the concentration of reversible and irreversible complexes. The experimental data is in agreement with the values of irreversible complexes given by the adsorption efficiency model (Fig. 4.1B). The sequential model diverges from the experimentally determined values of irreversible complexes by over an order of

magnitude. The concentration of reversible complexes was so small as to be below the detection limit of the assay and is not shown in the figure.

Adsorption experiments

Figs 4.2-5 contain results from adsorption experiments with phages T2 (Fig. 4.2), T5 (Fig. 4.3), T6 (Fig. 4.4) and T7 (Fig. 4.5). Each phage was tested in the following three media: minimal salt medium (MSM), tryptic soy broth (TSB), and nutrient broth (NB) with 0.5% NaCl. In each case, the adsorption efficiency model was fitted to the data. The values for ε were determined from the experimental data and k-values were estimated using the least sum of squares approximation method. The model parameters are tabulated in Table 4.2 and Table 4.3. As can be seen in the figures and the table, the kinetics of adsorption vary widely depending on phage and medium.

The adsorption data of Phage T2 are summarized in Fig. 4.2 and show very large differences in behavior. While the data are very similar for both TSB and MSM – adsorbing quickly with efficiencies exceeding 0.99 – the phage in NB adsorbs with poor efficiency ($\varepsilon = 0.09$).

Phage T5 adsorption data are presented in Fig. 4.3. The system exhibits quick kinetics but poor adsorption efficiencies in both TSB and MSM. The other extreme is a relatively high adsorption efficiency in NB (0.95), but with slower kinetics. In fact, with a k-value of 6.9×10^{-10} mL·min^{-1}, phage T5 exhibits the slowest adsorption kinetics of all the systems studied in NB medium.

The adsorption patterns of phage T6 are different for all three media (Fig. 4.4) but, as shown in Table 4.3, in general, it has a low adsorption rate constant, yielding slower adsorption kinetics. The adsorption efficiency varies from 0.77 in MSM to 0.97 in TSB and NB.

The adsorption of phage T7, shown in Fig. 4.5, is notable for its low to moderate adsorption efficiency in all three media, ranging from 0.23 in TSB to 0.49 in NB. The kinetic data for phage T7 (Table 4.3) indicates that it displays the fastest adsorption rate in TSB and the slowest in NB.

Fig. 4.6 is different from the previous experiments in that it shows kinetic data of phage λ adsorbing in one medium (MSM) but for host cells grown in one of two different carbon sources. When using *E. coli* cells grown on glucose, phage λ exhibits very slow adsorption kinetics. However, when infecting cells grown on maltose, phage λ adsorbs rapidly and with great efficiency.

4.6 DISCUSSION

The focus of this study is two-fold: 1) to compare the performance of the adsorption efficiency model to the sequential model, one of the most widely used phage adsorption models, and 2) to test the applicability of the adsorption efficiency model to compare the behavior of different members of the T-series phages.

Comparison of sequential and adsorption efficiency models

The sequential model and the adsorption efficiency model have a number of key differences in how they treat bacteriophage adsorption to the host cell. The sequential model simplifies the process to two steps as shown in equation (4.1). The first step is

the formation of a reversible complex *R* and the second is the formation of an irreversible complex *I*, representing an infected cell. The free phages *P* exist in equilibrium with *R*. However, *R* can also further adsorb to form *I*, shifting the equilibrium to the right and eventually leading to the irreversible adsorption of all phages in solution. The benefit of this reaction mechanism is that it makes use of three reaction rate constants, making the sequential model very robust. Also it is representative of the physiological process. It has been used to describe the adsorption of bacteriophage in a variety of different systems [65-67, 70].

The adsorption efficiency model simplifies bacteriophage adsorption even further than the sequential model. It assumes that the forward reaction is highly favored in the equilibrium between *P* and *R*, making the prospect of a reversible complex reverting back to a free phage and independent bacterial host cell unlikely. In addition, the reaction step from $R \rightarrow I$ is also highly favored over $P + H \leftarrow R$. For these reasons, the concentration of reversible complexes is assumed to be insignificantly small and the reaction scheme is simplified to the first order mechanism shown in equation (4.6). The adsorption efficiency model was developed for bacteriophage T4, whose adsorption is well understood and known to exhibit characteristics warranting the assumptions inherent to this model

A previous study has shown that the adsorption efficiency model fits phage T4 adsorption data at various multiplicities of infection (MOI) in a variety of media [164]. Furthermore, adjusting the adsorption efficiency significantly impacted bacteriophage amplification [164]. However, at the time it was not at all clear whether the adsorption efficiency model would be valid for other phage systems.

In order to fully compare and quantify the performance of the sequential model and the adsorption efficiency model, further experiments have been performed with other phages. Phage T6 adsorbing in TSB was selected as a case study for these experiments due to its relatively slow kinetics and high adsorption efficiency. Both the sequential model and the adsorption efficiency model perform well in predicting the free phage concentration of phage T6 during adsorption (Fig. 4.1A). The errors (sum of squares) on the models are 0.01 and 0.007 for the sequential and adsorption efficiency models, respectively. The divergence between the two models only becomes apparent when examining their predictions of the concentration of reversible and irreversible complexes (Fig. 4.1B). The free phage data in Fig. 4.1A appears to reach equilibrium after approximately 30 minutes, after which further adsorption is minimal. If phage T6 adsorption evolved according to the sequential model, the adsorption dynamics would be such that, as the free phage concentration decreased in solution, the concentration of R would first accumulate in equilibrium with P and then slowly react to form I. This was not observed in the experimental data reported in Fig. 4.1B, where the concentration of reversible complexes was negligible.

On the other hand, the adsorption efficiency model assumes that the reversible first step of the sequential model is preferentially directed towards R. In addition, the conversion from reversible to irreversible complex ($R \rightarrow I$) is assumed to happen very quickly. Therefore, the concentration of reversible complexes should be inconsequentially small. The leveling off of the normalized free phage concentrations in Fig. 4.1A is accounted for not with an equilibrium reaction, but with ε, the adsorption efficiency. Using this approach implies that, as the number of free

phages decreases, the quantity of irreversible complexes must increase correspondingly. The plateau in the free phage data shown in Fig. 4.1A is not an equilibrium between reversibly and irreversibly attached phage particles, it is the result of mature phage particles unable to adsorb to a host cell [164].

As can be seen in Fig. 4.1B, the adsorption efficiency model fits the experimentally determined concentrations of *I* significantly better than the sequential model. In addition, the concentration of *R* was below the detection limit of the assay. This further substantiates the adsorption efficiency model, which predicts R to be close to zero. The sequential model deviates from the experimental values by over an order of magnitude throughout much of the experiment. In fact, there is no evidence for the accumulation of reversible complexes. The data shown in Fig. 4.1B validate the assumptions inherent to the adsorption efficiency model.

Other studies have also reported cases where the concentration of reversible complexes was negligible. Crawford and Goldberg [167] reported that "attachment of T4 to *E. coli* B was essentially equivalent to infection at temperatures between 20°C and 42°C." The authors did find significant levels of reversible attachment when adsorbing phage T4 to a mutant of *E. coli* B strain with a reduced concentration of receptor proteins on its membrane. The authors suggest that at least three tail fibers must come in contact with the lipopolysaccharides on the cell surface to initiate the conformational changes to the phage tail associated with irreversible binding [167]. Another study using phage T5 reported similar findings: Heller and Braun [168] found evidence that the reaction from $R \rightarrow I$ happens rapidly in experiments where phage T5 adsorbs to *E. coli* F, which contains a great deal of the

outer membrane protein FhuA (formally known as *tonA*-coded outer membrane protein) on its cell surface. However, when adsorbing to a mutant F strain containing a diminished amount of FhuA, phage T5 easily desorbs from the host cell. The protein FhuA mediates the transfer of ferrichrome bound iron across the cell membrane and serves as the receptor protein for phage T5 [168].

Application of adsorption efficiency model

The suitability of the adsorption efficiency model in describing the adsorption kinetics of three other T-series phages is evident in Figs. 4.2-5. All studies were carried out at 24°C with an MOI of approximately 0.1. Adsorption efficiency has been shown to be independent of temperature between 24°C and 37°C and of MOI over a wide range of values [164].

One of the most dramatic observations from these experiments is the marked dependence in adsorption kinetics and efficiency on the media used for the experiments, which can be seen for all five of the T-series phage strains. The rate constants, for a single phage species, can vary by more than an order of magnitude and the adsorption efficiency range from less than 10% to over 99% (Tables 4.2 and 4.3). Interestingly, there is no obvious correlation between adsorption efficiency and rate constant. As well, there is no one medium clearly advantageous for adsorption for all four phages.

The T-even phages, all Myoviridae, are serologically related and morphologically similar. Therefore, it is somewhat surprising to see such large differences in adsorption behavior in each of the media. For example in MSM, the adsorption efficiency of phages T2, T4, and T6 are 0.99, 0.56, and 0.77, respectively. The

interactions of components in the different media with the phage tails are the likely explanations for these large variations seen in efficiency. For example, many studies have shown that certain strains of phage T4 have a tryptophan dependency for adsorption [71, 73-74, 76-77, 152]. A previous study has shown that the adsorption efficiency of phage T4 in MSM is a strong function of the L-tryptophan concentration [164]. Therefore, the low adsorption efficiency of phage T4 in MSM can be explained by the trace amount of L-tryptophan found in this medium. In contrast, phage T2 exhibits the highest adsorption efficiency of the three strains in MSM. Multiple studies have shown that the adsorption of phage T2 is ion-dependent [66, 69]. Specifically, an optimum concentration of ions leads to quick and irreversible adsorption. This may explain why phage T2 adsorbs with an efficiency of 99% and a reaction rate constant of 9.8×10^{-9} $mL \cdot min^{-1}$ in MSM, a medium with high ionic concentrations. It should be noted that phage T2 has been shown to exhibit reversible adsorption under certain conditions such as low temperatures [66].

An essential part of phage adsorption is the presence of the appropriate receptor on the cell surface. Mutant strains lacking a specific receptor protein will exhibit resistance to phage infection. For example, strains of E. coli completely lacking FhuA are completely resistant to phages T1 and ϕ80, which use FhuA as the receptor protein [169]. The T-series phages studied here use a variety of receptor proteins. Phage T2 can use either OmpF or Ttr as a receptor protein [170], phage T4 attaches to lipopolysaccharides (LPS) or OmpC [171], phages T5 and T7 bind to the protein FhuA [172-173], and phage T6 uses the tsx protein as a receptor [174]. It is improbable that the E. coli strain tested produces each of these receptor proteins in the same quantities in

each of the three media tested. It is more likely that the density of a specific receptor protein varies from one medium to the next, therefore impacting the adsorption rate.

The robustness in the application of the adsorption efficiency model to a range of bacteriophage species is apparent in the adsorption data for phages T5 and T7 (Fig. 4.3 and Fig. 4.5). As members of the Siphoviridae and Podoviridae families, respectively, phages T5 and T7 differ significantly in morphology from the T-even bacteriophages. While Myoviridae have a contractile tail and six long, jointed tail fibers, phage T5 has a non-contractile tail with three short, L-shaped tail fibers which enable attachment; as well as a single long, straight fiber that crosses the host cell envelope upon infection [161]. In contrast to both Myoviridae and Siphoviridae, the tail of phage T7 is so short (23 nm [175]) that evidence suggests it must be extended in order to deliver the viral DNA across the cell wall and into the cytoplasm [176]. However, Figs. 4.3 and 4.5 illustrate that the adsorption of these distinct phage species can still be described with the adsorption efficiency model.

Limits of Adsorption Efficiency Model

While the adsorption efficiency model provides a suitable fit to the adsorption kinetic data of the T-series phages shown here, it is important to note that no model is without limitations. This is especially true in the case of virus-host cell interactions. In their exhaustive review article of bacteriophage adsorption, Rakhuba *et al.* [171] doubt the "feasibility of creating a general model embracing the whole spectrum of existing bacterial viruses and their hosts." Instead, they remark that interactions between the virus and host cell are population and species specific.

The adsorption efficiency model also has limitations as we found that it did not represent phage-host interactions of bacteriophage λ well. The adsorption kinetics of bacteriophage λ was tested under a variety of conditions and not once did the adsorption efficiency model provide a suitable fit. Kinetic data of Phage λ adsorbing to *E.coli* MG1655 grown in MSM using two different carbon sources is shown in Fig. 4.6. Note that phage λ adsorbs much more easily when the host cells are grown on maltose rather than glucose. The difference in the adsorption behavior of phage λ is a function of the concentration of receptor proteins on the cell surface. Phage λ uses maltoporins encoded by the *lamB* gene as a receptor protein [58]. Maltoporins regulate transportation of maltose across the cell membrane and therefore they exist in high quantities when the cell is growing on maltose. This, in turn, makes maltose grown cells easy targets of phage λ as can be seen in Fig. 4.6. When growing on glucose, the cells produce a much smaller quantity of maltoporins, thereby making it difficult for the virus to bind to the cell.

However, an ε value would be meaningless for this phage since the free phage concentration continuously decreases. As is evident in Fig. 4.6, trying to force the adsorption efficiency model on the data results in a rather inadequate description of the adsorption. In fact, the dual-time scale nature of the phage λ adsorption to maltose grown cells, where adsorption is relatively fast for the first 20 minutes and then slower after that, makes the sequential model a very suitable fit for this system. More rigorous studies on modeling the adsorption kinetics of phage λ using the sequential model are reported elsewhere [67].

The data suggests that the presence of side fibers attached to the phage tail may be an influential factor in determining which adsorption model is most appropriate for a specific species. The

only phage studied that did not fit the adsorption efficiency model was phage λ, which also lacks side-tail fibers. The λ strain used here contains only the single J-coded straight fiber protruding from the end of the phage tail. Among the T-series phages studied, phage T5 is most similar in structure to phage λ as they are both Siphoviridae. However, in contrast to phage λ, phage T5 contains three additional short tail fibers to aid attachment and fit the adsorption efficiency model well. The combined results of this study suggest that the presence of side-tail fibers is necessary to ensure that the phage has a low probability of detaching after the initial reversible attachment. To test this hypothesis more rigorously, one needs to compare isogenic phage strains that differ only in the number of side tail fibers.

Data from literature supports this theory. While the single tail fiber variant is typical of commonly studied λ strains, it is in fact a recombinant of the original wild-type phage λ [162]. The variant designated as Ur-λ by Hendrix and Duda is thought to be nearly identical to the λ strain originally isolated for laboratory studies in 1951. However, it contains on average 6 conical long side tail fibers similar to those of T4-like phages, roughly 80 nm long with 3 straight segments connected by flexible joints [162]. Fitting the adsorption efficiency model used here to the adsorption data published by Hendrix and Duda provides an adequate fit (ε = 0.97, k = 1.1 x 10^{-8} mL·min^{-1} for *E. coli* growing on maltose; ε = 0 .73, k = 6 x 10^{-9} mL·min^{-1} for *E. coli* growing on glucose) providing further evidence that the presence of side-tail fibers may be the critical criterion in determining whether or not a phage strain will fit the adsorption efficiency model.

4.7 CONCLUSION

The adsorption efficiency model presented here is compared to one of the more widely used bacteriophage adsorption models, the sequential model. Experimental data support the assumptions inherent to the adsorption efficiency model and demonstrate its aptness in describing the adsorption kinetics of T-series phages. Adsorption experiments with T-series phages revealed a wide range of adsorption behavior depending on the phage and the medium. In each system tested, the adsorption efficiency model provided an excellent fit to the experimental data. However, the model is not without limitations. It was unsuitable for phage λ; possibly due to a lack of side-tail fibers. However, in applications, such as diagnostics and drug delivery, with the appropriate type of phage, the adsorption efficiency model would be the more useful choice for modeling phage attachment.

4.8 Acknowledgements

The authors would like to thank the National Science and Engineering Research Council of Canada, the Eugenie Ulmer-Lamothe Fund of McGill University and the Richard H. Tomlinson Doctoral Fellowship of McGill University for providing financial support for this project.

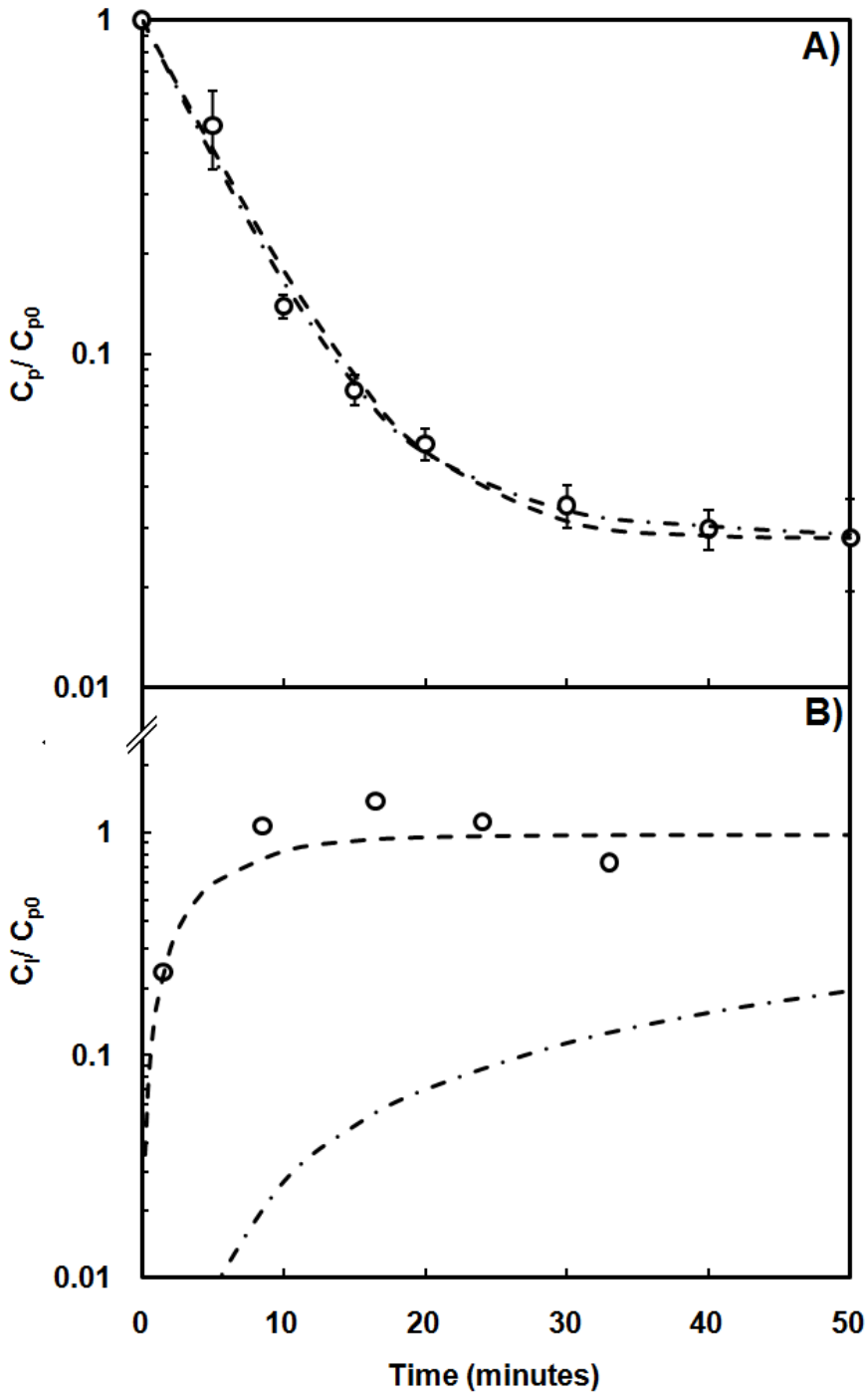

Fig. 4.1 Comparison between the adsorption efficiency model and the sequential model. A) The free phage concentration C_P (○) of bacteriophage T6 adsorbing to *E. coli* in TSB. The free phage concentrations are normalized with respect to the initial phage titer. B) The concentration of irreversible complexes C_I (○) of bacteriophage T6 adsorbing to *E. coli* in TSB. The concentration of irreversible complexes is normalized with respect to the initial phage titer. All experiments were carried out at 24°C at an MOI of ~0.1 with a host cell concentration of ~$1x10^8$ cfu·mL^{-1}. The adsorption efficiency model (- -) and the sequential model (- · -) are shown for comparison in both A) and B).

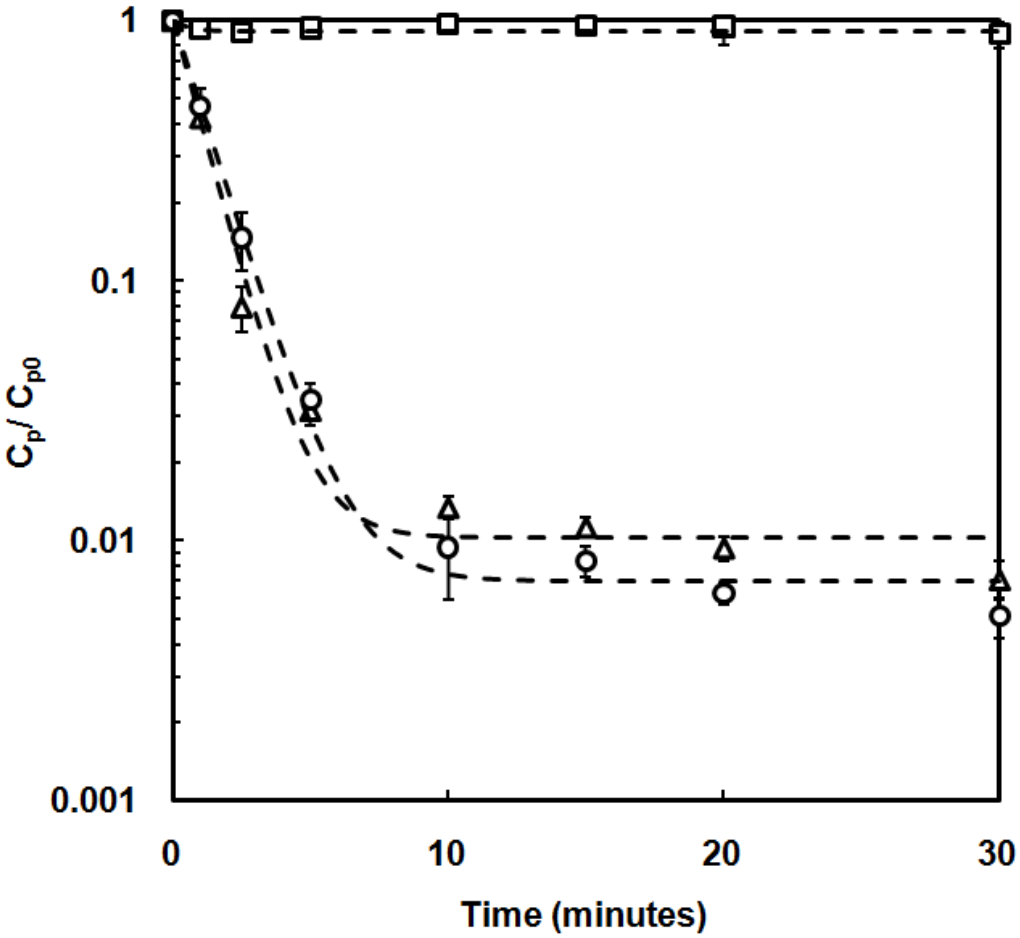

Fig. 4.2 Adsorption of phage T2. Experiments performed in three media: MSM (Δ), NB (□), and TSB (○). Free phage concentrations are normalized with respect to initial phage titer. All experiments were carried out at 24°C at an MOI of ~0.1 with a host cell concentration of ~$1x10^8$ cfu·mL^{-1}. The adsorption efficiency model is shown for each medium as a dashed line. Error bars represent the standard deviation of three experiments.

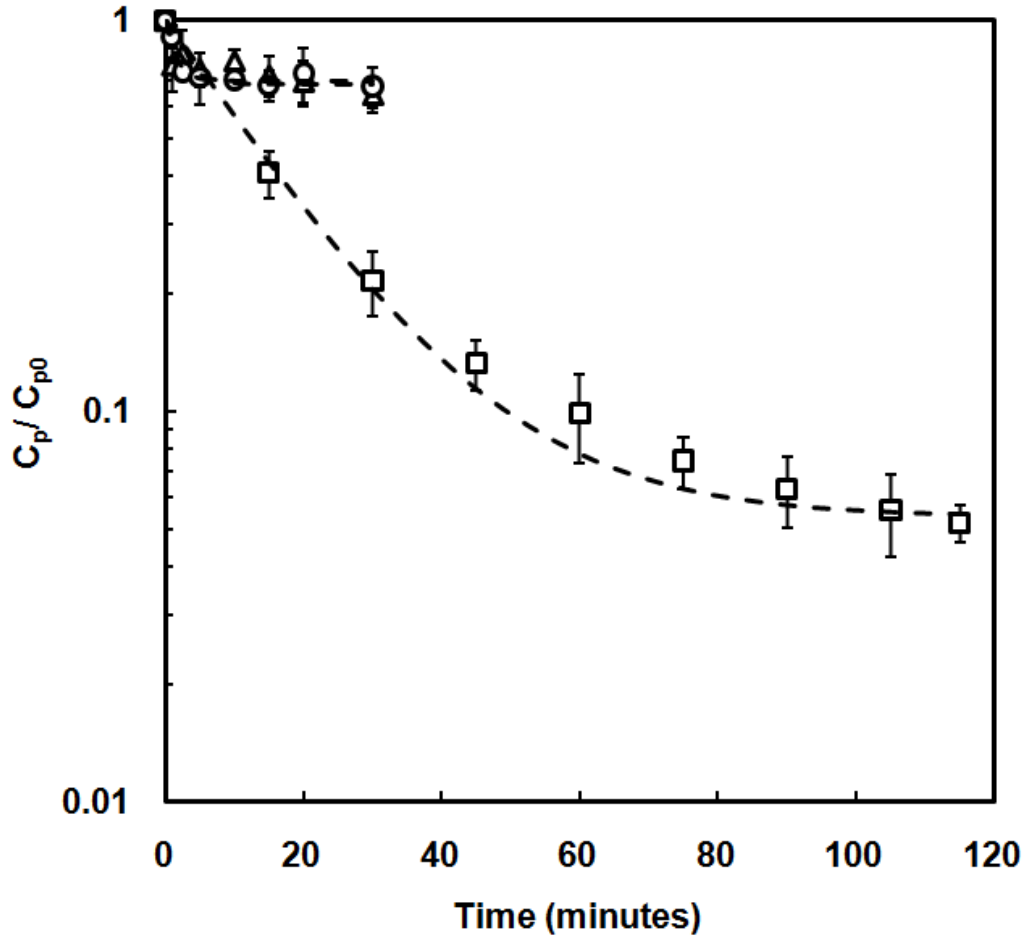

Fig. 4.3 Adsorption of phage T5. Experiments were performed in three media: MSM (Δ), NB (□), and TSB (○). Free phage concentrations are normalized with respect to initial phage titer. All experiments were carried out at 24°C at an MOI of ~0.1 with a host cell concentration of ~$1x10^8$ cfu·mL^{-1}. The adsorption efficiency model is shown for each medium as a dashed line. Error bars represent the standard deviation of three experiments

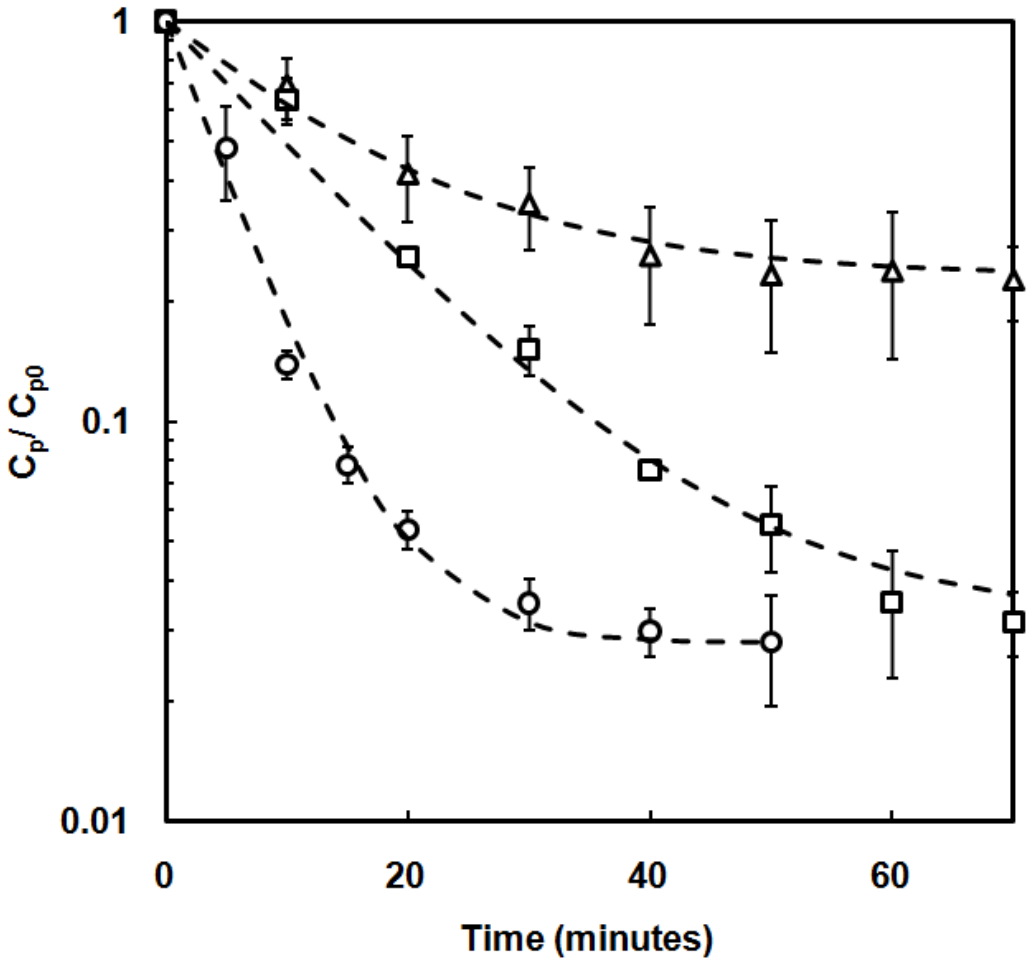

Fig. 4.4 Adsorption of phage T6. Experiments were performed in three media: MSM (Δ), NB (□), and TSB (○). Free phage concentrations are normalized with respect to initial phage titer. All experiments were carried out at 24°C at an MOI of ~0.1 with a host cell concentration of ~$1x10^8$ cfu·mL^{-1}. The adsorption efficiency model is shown for each medium as a dashed line. Error bars represent the standard deviation of three experiments.

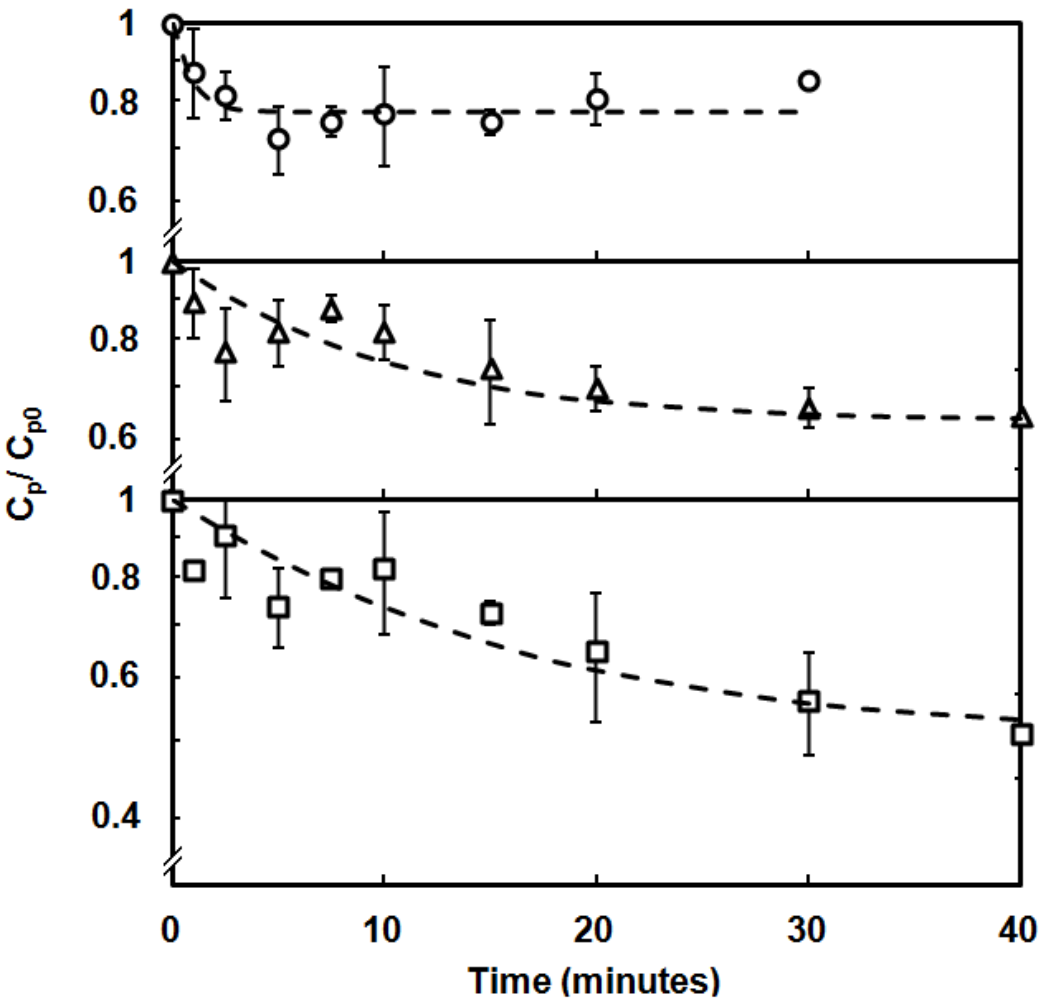

Fig. 4.5 Adsorption of phage T7. Experiments were performed in three media: TSB (○), MSM (Δ), and NB (□). Free phage concentrations are normalized with respect to initial phage titer. All experiments were carried out at 24°C at an MOI of ~0.1 with a host cell concentration of ~$1x10^8$ cfu·mL^{-1}. The adsorption efficiency model is shown for each medium as a dashed line. Error bars represent the standard deviation of three experiments.

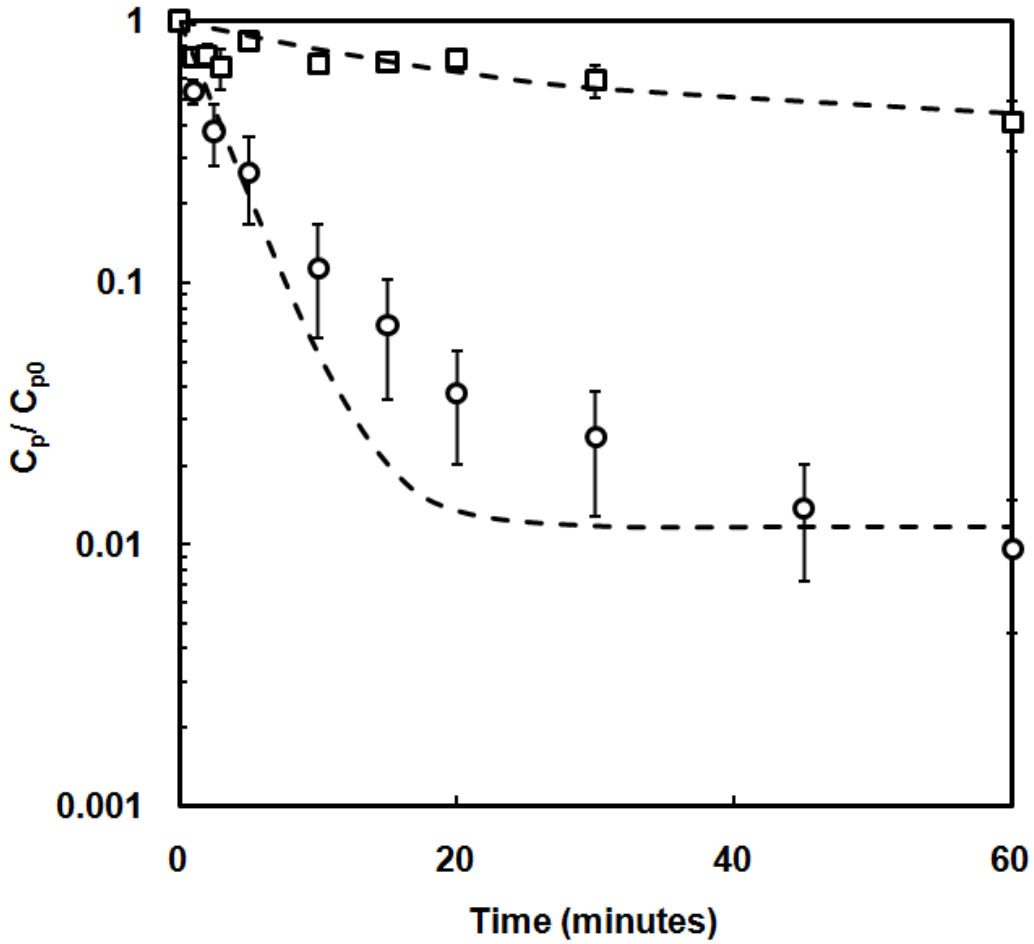

Fig. 4.6 Adsorption of phage λ in MSM. Free phage concentrations are normalized with respect to initial phage titer. Host cells were grown on either glucose (□) or maltose (○) prior to adsorption. All experiments were carried out at 24°C at an MOI of ~0.1 with a host cell concentration of ~$1x10^8$ cfu·mL^{-1}. Error bars represent the standard deviation of three experiments

Table 4.1 Characteristics of phage strains tested.

Phage	Structure and Dimensions						
	Capsid	Tail		Side-Tail Fibers		End Tail Fiber	References
	Size (nm)	Contractile	Length (nm)	Number	Length (nm)	Length (nm)	
T2	65 x 80	Yes	120	6	140		[159, 177]
T4	65 x 80	Yes	120	6	140		[159, 177]
T5	90 x 90	No	250	3	80	50	[161]
T6	65 x 80	Yes	120	6	140		[159, 177]
T7	60 x 60	No	23	6	32		[160, 175, 178]
λ	60 x 60	No	150	0		23	[111, 179]
Ur- λ	Similar to λ	No	Similar to λ	6	80-85	Similar to λ	[162]

Table 4.2 Adsorption efficiencies for T-series phages in three media.

Phage	Adsorption Efficiency[a] (ε)		
	MSM	TSB	NB
T2	0.99 ±	0.99 ±	0.09 ±
T4[b]	0.56 ±	0.99 ±	0.87 ±
T5	0.31 ±	0.30 ±	0.95 ±
T6	0.77 ±	0.97 ±	0.97
T7	0.37 ±	0.23 ±	0.49 ±

[a]Mean values with the standard deviation of three replicates. [b] Phage T4 data from reference [164].

Table 4.3 Adsorption rate constants for T-series phages in three media.

Phage	Adsorption Rate Constant[a] (k, mL min^{-1})		
	MSM	TSB	NB
T2	$9.8 \times 10^{-9} \pm 3.6 \times 10^{-10}$	$5.2 \times 10^{-9} \pm 9.1 \times 10^{-10}$	$9.3 \times 10^{-10} \pm 6.9 \times 10^{-10}$
T4[b]	$2.2 \times 10^{-8} \pm 7.8 \times 10^{-9}$	$4.4 \times 10^{-9} \pm 1.5 \times 10^{-9}$	$2.0 \times 10^{-9} \pm 5.1 \times 10^{-10}$
T5	$2.5 \times 10^{-8} \pm 1.3 \times 10^{-8}$	$5.3 \times 10^{-9} \pm 2.5 \times 10^{-9}$	$6.9 \times 10^{-10} \pm 5.2 \times 10^{-11}$
T6	$3.4 \times 10^{-9} \pm 5.2 \times 10^{-10}$	$9.7 \times 10^{-10} \pm 5.8 \times 10^{-11}$	$9.3 \times 10^{-10} \pm 2.5 \times 10^{-11}$
T7	$5.7 \times 10^{-9} \pm 3.1 \times 10^{-9}$	$6.2 \times 10^{-9} \pm 3.8 \times 10^{-9}$	$9.7 \times 10^{-10} \pm 5.8 \times 10^{-11}$

[a]Mean values with the standard deviation of three replicates. [b] Phage T4 data from reference [164].

Chapter 5 THE EFFECTS OF HOST CELL PHYSIOLOGY ON BACTERIOPHAGE PRODUCTIVITY DURING SELF-CYCLING FERMENTATION

In preparation for submission to *Microbial Cell Factories*:

Storms ZJ, Brown T, Sauvageau D, Cooper DG, and Leask RL (2012) The Effects of Host Cell Physiology on Bacteriophage Productivity in Self-Cycling Fermentation

PREFACE

This is a preliminary study further exploring how the state of an individual cell at the time of a phage infection can influence the productivity of the process. The results presented in Chapter 2 revealed that the cell life cycle can be an important consideration in production systems. While that work used a temperate phage λ system, studies on lytic phages have also shown the influence of the cell cycle on phage productivity [78, 80, 94]. In each of those studies, intracellular properties related to the metabolic state of the host, particularly RNA levels, were hypothesized to influence phage productivity

Of particularly relevance to this study is the work of Sauvageau and Cooper in which synchronized *Escherichia coli* cells cultured under SCF were implemented in a phage T4 production system [53]. The authors reported an increase in phage T4 productivity using synchronized host cells cultured under SCF compared to an asynchronous batch system. Their work implies that synchronized cultures are able to achieve larger burst sizes and (or) shorter lysis times.

This final chapter presents results that attempt to explain the increase in phage productivity observed by Sauvageau and Cooper in synchronized cultures, and the protein expression data presented in Chapter 2 of this thesis. The lytic *Escherichia coli*-T4 system was chosen as the model microorganisms, although other phage-host systems would be expected to yield similar trends. The intracellular levels of genomic DNA and RNA were monitored during individual SCF cycles. In addition, the burst size and lysis time of cells infected with phage T4 at various points in the SCF cycle were determined. A correlation between intracellular RNA and phage productivity was observed.

This preliminary data suggests further work, particularly monitoring specific RNA expression levels during the cell cycle and phage infection, would shed light on the influence of intracellular properties on phage productivity and the advantage of using synchronized cells in fermentation processes.

5.1 ABSTRACT

Self-Cycling Fermentation (SCF), a semi-continuous bioprocess that synchronizes cell growth by applying an automated, self-cycling operation, was used to study how intracellular levels of genomic DNA and RNA influence phage productivity during a T4 infection. A comparison of DNA and RNA concentrations in cultures of *Escherichia coli,* the host cell used in this study, during early (synchronizing) and late (synchronized) SCF cycles demonstrated the marked reduction in cycle-cycle variability observed in synchronized cultures. Experiments monitoring cell burst size and lysis time for cells infected at various points during a SCF cycle revealed that intracellular RNA levels are correlated to phage productivity during infection. Also, the increased presence of abortive infections late in the SCF cycle led to a dramatic decrease in phage production. This work helps explain advantages associated with SCF in phage or phage-based production systems reported in the literature.

Keywords:

Self-Cycling Fermentation, *Escherichia coli*, cell physiology, bacteriophage production, synchronization, burst size

5.2 INTRODUCTION

The growth of an individual cell differs significantly from the growth of a cell culture. The mean cell size of a balanced culture remains constant while that of an individual cell increases exponentially during a single cell cycle [180]. Likewise, rates of synthesis of specific molecules may vary throughout the cell life cycle while data collected from a culture will only reveal average rates of synthesis. Recent work has shown that these averaged events within the cell cycle may help explain productivity trends seen in bacteriophage-producing bioprocesses [53, 181]. In addition, it was recently shown that cell size can be a determinant feature in influencing the outcome of a bacteriophage infection. For example, a ~2 fold increase in cell volume at the time of a λ infection was reported to raise the probability of lytic growth, possibly due to the greater presence of cellular resources within the larger volume [114].

In order to study intracellular events at the culture-wide scale, a variety of approaches have been used to induce cell synchrony—cell growth characterized by a narrow distribution of cell ages. For example, submitting bacterial cultures to periodic intervals of low temperatures, chemical stimulants, or nutrient starvation has been shown to induce synchrony. However, these methods are likely to also cause changes to the regular metabolic function of the cell [117]. Another approach called continuous phasing cultures cells in a semi-continuous manner where half the reactor volume is harvested and replenished with fresh media at regular time intervals [124-125, 182-183]. When working with yeast, Dawson found that the organisms adjusted their doubling time to the period of the cycling, resulting in synchronized growth [124]. However, when applied to bacteria cultures, the

microorganisms struggle to adjust their doubling time to the operator-selected cycling period [126]. Nonetheless Fritsch *et al.* (2005) reported high levels of synchrony when applying continuous phasing to the bacteria *Cupriavidus necator* [125]. However, they did find that the highest levels of synchrony were obtained when a significant period of nutrient starvation existed at the end of each cycle.

Self-Cycling Fermentation (SCF) [126] is a modification to continuous phasing where a feedback loop is established to cycle the system once a limiting nutrient is depleted. This system leads to synchronized cultures with many marked advantages. The cell densities obtained are comparable to those of a batch, it can easily be set-up to run as a semi-continuous, fully automated process using non-intrusive instrumentation, and synchrony indexes upwards of 0.6 can be readily achieved. This method has been investigated for diverse potential industrial applications and performs as well as, or better than, a batch under numerous bioprocessing conditions including the degradation of pollutants [128-130], the production of bio-molecules such as surfactin [126, 131-132], sophorolipids [133], and citric acid [134], recombinant protein production [181] and the production of bacteriophages [53]. In spite of all this, a detailed characterization of the cell life cycle events taking place throughout the SCF cycle has yet to be undertaken.

This study is a first step towards understanding how the cell life cycle influences the physiology and productivity of cells growing under Self-Cycling Fermentation. The genomic material and total RNA of cultures were monitored during SCF cycles as these have been shown to change throughout the cell cycle and suggested as possible physiological characteristics that will influence the outcome of bacteriophage infections [78, 80, 125]. This research

had two complementary goals. In the first section, *Escherichia coli* was used as a model microorganism to study the cell cycle events of cultures growing under SCF. The second goal was to understand how metabolic events within the cell influence the productivity of a bacteriophage infection.

5.3 MATERIALS AND METHODS

Microorganisms and medium

The microorganisms used in this study were *Escherichia coli* ATCC 11303 and bacteriophage T4 (ATTC 11303-B4). The bacteria was cultured in a minimal salt medium (MSM) at 37°C containing 3 $g \cdot L^{-1}$ D-glucose (limiting nutrient) and 0.25 $g \cdot L^{-1}$ yeast extract described previously [54].

Reactor and SCF operation

The reactor set-up in this study is the same as was previously described in Sauvageau *et al.* [54]. Briefly, a custom-made 4-L stainless steel reactor with a 1-L working volume aerated at 0.5 vvm ($k_L a$ of 0.93 min^{-1}) and agitated at 200 rpm was used for SCF experiments. The carbon dioxide evolution rate (CER), measured with a CO_2 gas sensor (CO2-IN, Vernier) in the air exhaust stream, was the measured variable used to control cycling in the system.

Roughly 3×10^{10} cells from an overnight culture were used to inoculate the reactor. Once the limiting nutrient was depleted, indicated by a minimum in the change in CER (dCER), half the culture volume was harvested and the working volume of the reactor was refilled to its initial volume (1.0 L) with fresh media.

OD_{600} and biomass measurements

Cell density was monitored by measuring the optical density of the culture at 600 nm using a spectrophotometer (Varian, Cary Bio-50). Conversion of the optical density to cell dry weight was achieved by generating a calibration curve during batch growth. Ten-milliliter samples were periodically removed, centrifuged at 10,000 × g for 10 minutes, re-suspended in distilled water after removal of the supernatant and incubated overnight at 80°C. Gravimetric analysis was used to determine the dry weight of cell biomass. It was found that a cell culture at an OD_{600} of 1.0 had a dry weight of approximately 0.5 $g \cdot L^{-1}$.

Isolation and analysis of RNA/DNA

Samples of *Escherichia coli* (ATCC 11303) were collected during logarithmic growth in 0.5 mL aliquots, centrifuged at 14,000 × g for one minute, and stored at -80°C. After thawing and decanting the supernatant, the pellet was re-suspended in 100 µL of TE buffer (10 mM Tris·Cl, 1 mM EDTA; pH 8.0) containing 1 $mg \cdot mL^{-1}$ lysozyme (Sigma-Aldrich, St. Louis, MO) and incubated for 5 minutes at room temperature. Subsequently, an RNA/DNA purification kit from Norgen Biotek Corp (Ottawa, ON) was used to isolate genomic DNA and total RNA from each sample.

Genomic DNA samples isolated from three early and three late cycles were analyzed by agarose gel electrophoresis; densitometry was used for quantification. A detailed protocol can be found in Maniatis (1989). Briefly, Tris Acetate running buffer (0.04 M Tris-acetate, 0.001 M EDTA) was used to form 0.8% (w/v) agarose gels. Gels were stained with ethidium bromide (0.004 % (v/v)), added before casting. Each well was loaded with 2 µL of loading buffer, 2 µL of a capsid DNA standard (40 $\mu g \cdot mL^{-1}$), and 5

μL of the sample genomic DNA. After running the gels for approximately 1 hour at 80 mA, an image was captured using a Gel-Doc apparatus (Bio-Rad Laboratoires, Inc., Hercules, CA) and the software Quantity One 4.2.2 (Bio-Rad Laboratoires, Inc., Hercules, CA). The band intensities of the genomic DNA in each sample were compared to the intensity of the capsid DNA standard using ImageJ, an open source software, in order to determine the DNA concentration.

The total RNA concentration was determined by measuring the absorbance of light in each sample at 260 nm and 280 nm using a Genova UV-visible spectrophotometer from Jenway (Bibby Scientific Limited, Staffordshire, UK). The total RNA concentration is then given as $40 \times ABS_{260} \times$ Dilution factor.

Burst size measurements

Phage burst size (*b)* was determined using a standard protocol modified from methods reported in the literature [79, 86]. A 1-mL sample of *Escherichia coli* 11303 at a concentration on the order of 10^8 cells·mL^{-1} in MSM (with 0.3% (w/v) glucose, 0.025% (w/v) yeast extract) was mixed with phage T4 at an MOI of 0.1 to limit the chance of superinfection. L-tryptophan (40 μg·mL^{-1}) was added to the infection broth to assure a high adsorption efficiency of the phage to the host cell. After incubation for 5 minutes at 37°C, a 10 μL aliquot was removed and diluted 10,000 fold in fresh media to a final volume of 10 mL. A 1-mL sample was removed and assayed for the total phage (T_0, free floating phages plus bacteria infected with phage). The original infection broth was vortexed with 2% cholorform and then assayed to determine the unadsorbed phage concentration (*U*). The remaining culture was incubated in a 250 mL shake flask at 37°C and 220 rpm for 35

minutes. A 1-mL sample was removed and diluted a further 10 times to avoid infection of host cells by the newly formed phages. This culture was incubated an additional 15 minutes at 37°C and 220 rpm. At 50 minutes, three 1-mL samples were removed and assayed for final total phage (T_F). Burst size was then calculated as $b = T_F/(T_0 - U)$.

Lysis time measurements

Lysis time was determined by closely following the evolution of a Phage T4 infection using spectrophotometry. A 1-mL sample of *Escherichia coli* ATCC 11303 at a concentration on the order of 10^8 cells·mL^{-1} in MSM (with 0.3% (w/v) glucose, 0.025% (w/v) yeast extract) was mixed in a sterile 3-mL disposable cuvette with a pre-warmed 1-mL aliquot of phage T4 at an MOI of ~1.5. At this MOI the majority of the cell culture was infected with only one virus particle. The mixture was incubated at 37°C for two minutes before an additional 1-mL of media was added. The cuvette was then transferred to an incubator shaker at 220 rpm and 37°C for the remainder of the experiment. The optical density of the mixture was monitored every 5 minutes for 20 minutes, and every 2 minutes thereafter. Cell lysis was generally well defined on the curve, represented by a significant drop in the culture optical density. Here the lysis time is defined as the peak in the optical density, this point representing the onset of lysis.

Statistical testing

Two-way ANOVA was used to evaluate the differences between early and late cycle optical densities, DNA concentrations, and total RNA concentrations. In addition, the variability between early and late cycles was compared using two-tailed t-tests on the

coefficient of variance (CV) of each pair of data sets. Finally, a linear regression was run on the burst size and lysis time measurements with respect to specific RNA concentration. The significance of the slope was tested using the f-statistic (H_o: $\beta_1 = 0$). All tests were performed at the 95% confidence interval.

5.4 RESULTS

The relative amounts of biomass, specific genetic material, and RNA were monitored in both synchronizing (early) and synchronized (late) SCF cycles. Early cycles (2nd or 3rd cycle of the fermentation process) generally displayed more variability and less synchrony. Synchrony has been shown to develop to a significant degree within 8-10 cycles [54, 181]. Here, the term late cycles refers to cycles greater than cycle 10.

Cell growth, DNA synthesis and intracellular RNA

Figure 5.1 compares typical cell growth data obtained from early and late cycles. Regardless of cycle number, the absorbance reading at 600 nm increased continuously (Fig. 5.1A). The data suggests that the growth rate is consistent from cycle to cycle. Here growth rate is defined as the rate of biomass production, not the increase in cell number, which will display significantly different profiles in early and late cycles [54, 181]. The decrease in growth observed towards the end of each cycle is probably due to metabolic changes triggered by the depletion of the limiting nutrient and not cell division. Previous work has shown that cell division in this system occurs during the middle of the cycle, from roughly 50 to 120 minutes for a cycle time of 200 minutes [54].

The normalized concentration of DNA during early and late cycles is shown in Fig. 5.1B for comparison purposes. The DNA concentration began to noticeably increase after 40 minutes during the early cycles and after 80 minutes during the later cycles. By 140 minutes, the DNA concentration had doubled in value for both the early and later cycles. In an average *E. coli* B/r cell undergoing balanced growth at 37^0C with a doubling time of 40 minutes, there are 2.1 molecules of DNA with a molecular weight of 2.5×10^9 g·mol^{-1} [180]. Therefore, a cell culture of 10^9 cells·mL^{-1} would have a total DNA concentration of 9 μg·mL^{-1}. Or, knowing that the total DNA comprises 3.1 % of the cell dry weight [180], a DNA concentration of 15-30 μg·mL^{-1} should be obtained based on the cell dry weight (0.5-1.0 g·L^{-1}). Using agarose gel electrophoresis combined with densitometry, DNA concentrations between 4 and 20 μg·mL^{-1} were obtained, in agreement with these theoretical calculations.

In contrast to the cellular DNA contents, the total RNA within the culture increased rapidly early and then reached a plateau in SCF cultures (Fig. 5.2A). This trend gives rise to the maximum in the specific RNA, defined as amount of RNA per cell dry weight, observed at 40 minutes for the late cycle (Fig. 5.2B).

Two-tailed t-tests on the Coefficient of Variance (CV) revealed the difference in reliability and reproducibility between early and late cycles. The average CV of the optical density, DNA concentration, and total RNA concentration of the later cycles was 23% (P=0.068), 60% (P=0.05), and 67% (P=0.009) smaller than the CV of the earlier cycles, respectively. The larger variability in the early cycle data manifests itself visibly in the error bars of Figs. 5.1 and 5.2. The early cycle data, notably the total DNA and RNA, was markedly less reproducible, making trends difficult to distinguish.

This may explain why two-way ANOVA comparing the RNA and DNA data between early and late cycles yielded no significant difference in the trends ($P>0.05$).

Phage productivity

Infection of the cell culture by phage T4 was used to monitor how metabolic and cell cycle effects could influence phage productivity during a SCF cycle. Figure 5.3 displays the cell burst size (Fig. 5.3A) and lysis time (Fig. 5.3B) for samples periodically removed from early cycles and infected with phage T4. A maximum burst size of 47 phages/cell was observed at 40 minutes followed by a steady decrease for the remainder of the cycle. Burst sizes as low as 20 or less were observed at the end of each cycle. Meanwhile, the lysis time varied by close to 20% when infection was triggered at different times in a cycle. The fastest lysis times were observed 30 to 50 minutes into each cycle, corresponding to the maximum burst size. The slowest lysis times were recorded near the end of each cycle, also when the burst size was smallest. In addition, both burst size and lysis time were correlated to specific RNA concentration of the culture (see insets of Fig. 5.3). Higher levels of intracellular RNA corresponded to larger burst sizes (f-test on significance of slope, $P=0.001$) and shorter lysis times (f-test on significance of slope, $P=0.051$). Taken together, the burst size and lysis time data imply phage productivity reached a maximum of 100 pfu·cell^{-1}·h^{-1} and minimum of 34 pfu·cell^{-1}·h^{-1} depending on the time of infection during a single cycle.

The burst size data summarized in Fig. 4.3 was generated using 10-μL aliquots from the same phage stock for each experiment. Therefore, the measured value of T_0, the initial total phage (free phage + infective centers), would be expected to remain

constant from one experiment to the next. This was not the case. The value of T_0 detected in the plate assays varied by over 50% throughout a SCF cycle (Fig. 5.4A). The true value of T_0, based on the stock solution titer, includes unadsorbed phages (U), infected host cells (viably attached phage, A) and any abortive infections. Superinfection was minimized by using a MOI of 0.1 while adsorption to cell debris or non-host cells (i.e. the container wall) was insignificant (data not shown). The value of U is shown to be constant for all infections (Fig. 5.4A), indicating that the number of infected host cells A is decreasing with cycle time (Fig. 5.4B), implying an important increase in abortive infections late in the cycle. This in turn, leads to an order of magnitude decrease in the phage titer generated during the burst size experiment (T_F, final infective centers, Fig. 5.4B).

5.5 DISCUSSION

Under SCF operation, the culture displayed a highly reproducible optical density pattern from cycle to cycle as shown in Fig. 5.1A. This would lead one to believe that early and late cycles shared identical growth profiles. However, while the optical density in this case is an indication of the increase in biomass this does not have to be due to an increase cell number. In fact, for the late cycles, the optical density measurements give an indication of increasing cell size until cell division occurs. Previous work has shown that in early, unsynchronized cycles, there is a random distribution of cell ages and cell division takes place throughout the cycle [54]. The cell size is randomly distributed since cell mass increases exponentially during the cell cycle [180] and the

interdivision times of individual cells within a culture can vary by 10-20% around a mean [120].

Later cycles are characterized by synchrony indices upwards of 0.6 [54, 127, 181]. Cell division occurs over a narrow time period within the cycle during synchronized growth. For this system, cell division is between 50 and 120 minutes [54]. Therefore, while the optical density data implies a similar level of biomass present in early and late cycles, the profile of the individual cells forming that biomass is quite different between early and late cycles. A random distribution of cell ages is not found in late cycles. During late cycles, the cells are the most mature in the period immediately prior to cell division (20-50 minutes). These cells should have the largest quantity of genomic material and RNA while the young, newly formed cells found immediately after cell division (after 120 minutes) should have the smallest. One would expect a less clearly defined trend from the early cycle data, due to greater variability from cycle to cycle and the more random distribution of cell ages as cultures in these cycles are only beginning to synchronize. The data from Figs. 5.1 and 5.2 supports this hypothesis.

The specific RNA concentration in late cycles increased for the first 40 minutes, reached a maximum of 6.5% of cell dry weight, and then decreased slowly for the remainder of the cycle (Fig 5.2B). The maximum occurred when the cells were oldest, immediately prior to cell division. During the early cycles, when the system is only beginning to be synchronized, a similar trend existed. However, the large error bars warrant caution when interpreting the results and the RNA data collected displayed considerably more scatter.

Interestingly, the increase in total RNA preceded DNA replication during the cycle. The cells appeared to be synthesizing

the necessary ribosomes, polymerases, tRNA and mRNA necessary to support the protein synthesizing system early in the cycle as they prepared for cell division. Nutrient levels were also highest early in the cycle, stimulating high cellular metabolic activity. Soon after the culture began to divide (50 minutes), the DNA concentration in the culture started to increase while the RNA levels held constant (Fig. 5.2A). Note that the range of RNA values reported as a percent of cell dry weight were lower than what is commonly reported in the literature (20.5%, [180]). Losses during the extraction and isolation are probably the cause for this result, as RNA is considerably less stable than DNA.

DNA synthesis during SCF cycles

The DNA replication shown in Fig. 5.1 was initiated after the commencement of cell division within the culture. While this can initially seem counterintuitive, this result is consistent with observations on the cell cycle. The interdivision cycle of *E. coli* is frequently modeled as discrete periods [117, 122, 184]. These include the preparation for DNA synthesis (G1), DNA replication (C-time), and the time between replication and division (D-time) [184]. Generally, the C-time is 40 minutes and the D-time is 20 minutes while G1 varies with the growth rate of the organism for an exponentially growing culture (Ingraham 1983, Cooper 1979). If the doubling time is less than 40 minutes, which is possible during balanced growth on glucose minimal medium, the G1 period no longer exists and cells undergo multiple DNA replication forks within one interdivision cycle [117, 184]. However, in the growth cycles presented here, the doubling time of the organism is well in excess of the C + D time, implying that G1, C, and D periods are all present during growth.

The period of significant DNA replication (C-time) for the *E. coli* culture grown here is shown clearly in Fig. 5.1B to have lasted from 80 minutes to 140 minutes for the late cycles. This period was shifted slightly from the period of cell division (50-120 minutes). This 20-30 minute lag likely represents a short G1 period before DNA replication begins at 80 minutes. Also, evidence suggests that cells must reach a minimum size before initiating DNA replication [125, 185-187]. In this experiment, once replication terminated, the cells were near the end of the SCF cycle as the limiting nutrient neared depletion. Biomass increase slowed significantly as shown by the trend in optical density (Fig. 5.1A) and DNA replication ceased (Fig. 5.1B). Cells prepared for maintenance growth as they started to enter stationary phase. The system was then cycled, nutrient levels replenished, and the cells initiated a flourish of metabolic activity (growth, RNA and protein synthesis) as they re-organized for cell division.

The implication stemming from the DNA concentrations shown in Fig. 5.1 coupled with the cell division data reported in earlier work [54] is that the cell would be entering the SCF cycle during the D-time, the period between DNA replication and cell division, undergo cell division, and then replicate its DNA. Therefore, each cell should contain two complete genomes at the beginning and end of the cycle.

Effect of intracellular RNA on phage productivity

The changes within the cell observed during the SCF cycle had a significant impact on the bacteriophage infective process. Phage productivity was augmented significantly, as measured by both burst size and lysis time, with increasing intracellular RNA. At the maximum specific RNA concentration, the cell burst size

reached a maximum of roughly 45 phages·cell^{-1} and the lysis time was at its lowest value of 28 minutes (Fig. 5.3). Following these optima, burst sizes decreased by over 50% towards the end of the cycle while the lysis times increased. The effect of intracellular RNA on phage infective events is apparent from the inset of Fig. 5.3A. A clear positive correlation exists (R^2 = 0.61, P=0.001) between the burst size of the cell and the specific RNA concentration of the culture while a negative correlation exists (R^2 = 0.36, P=0.051) between lysis time and intracellular RNA.

The trends in burst size and lysis time support observations reported in the literature demonstrating that the availability of the protein synthesizing system increases the efficiency of the bacteriophage infection [78, 80, 94, 181]. Replication within the host cell involves knocking out the host cell RNA polymerases and replication machinery and reprogramming them for virion production. For example, in the case of T4, the host cell polymerase is relied upon throughout the entire infection to initiate transcription of early, middle, and late phage proteins. Host cell proteins are also recruited for replication of the phage genome [50]. Higher levels of these host cell ribosomes, polymerases, and other metabolism-related molecules seem to increase the efficiency of the phage infection.

However, Fig. 5.4 demonstrates that burst size and the protein synthesizing system are not the only influential parameters to consider during phage amplification. Two important trends are apparent from the data shown in Fig. 5.4: 1) the adsorption dynamics of the system remain unchanged as established by the constant U-vales obtained for all experimental conditions and 2) the number of infected host cells (A) drastically decreases for burst size experiments initiated late in a SCF cycle.

Consequences for phage adsorption and viable infections

Importantly, the metabolic changes observed in the host cell during a SCF cycle do not appear to have important consequences for phage adsorption. Since the physical and chemical properties of the medium are roughly constant for all experiments (while the carbon source is decreasing, experiments on stationary phase cultures have shown similar adsorption kinetics to those observed in this study [164, 188]), the cell size or cell surface characteristics (i.e: receptor density) are the main factors influencing adsorption. One would also expect an increase in adsorption rate as the cell concentration increases with SCF cycle time. This would correspond to a decrease in U; however, it is not observed in the data. Perhaps it is balanced out by changes in cell size (decreasing after cell division) or changes in receptor protein surface density (decreasing due to metabolic changes). Although the scatter in the data would make these trends difficult to distinguish. On the balance, the adsorption kinetics are essentially unchanged for all burst size experiments.

While adsorption kinetics may remain unchanged by the metabolic activity of the cell cycle, the number of viable infections does vary. Burst size experiments revealed that the concentration of infected host cells A increased and then decreased significantly during a SCF cycle (Fig. 5.4B). This is most likely due, at least in part, to the changes in intracellular RNA throughout the SCF cycle. Infections started late in a cycle would also be affected by the reduction in nutrients [104]. The consequence for phage production is tremendous. The decline in viable infective centers together with the diminished burst sizes observed for infections

induced towards the end of an SCF cycle leads to an order of magnitude reduction in the number of total phages (T_F) produced.

5.6 CONCLUSION

Self-Cycling Fermentation, a semi-continuous bioprocess that induces cell synchrony, was used to study cell cycle and metabolic effects on bacteriophage production in an *Escherichia coli*- phage T4 system. Results indicated that the phage productivity is dependent on the state of the cell at the time of infection. Infections of cells with higher RNA to biomass ratios resulted in the largest cell burst sizes and the shortest lysis times, yielding the highest phage productivity per cell. In addition, the number of viable phage infections decreased significantly at slower cell growth rates and RNA to biomass ratios. This work provides valuable insight into the phage infective process and information for designing large-scale phage production systems — sufficient levels of RNA are necessary for efficient infection. More generally, this study shows how Self-Cycling Fermentation can be used to manipulate the metabolism of microorganisms for specific production needs.

5.7 ACKNOWLEDGMENTS

The authors would like to thank the National Science and Engineering Research Council of Canada as well as the Eugenie Ulmer-Lamothe Fund and Richard H. Tomlinson Doctoral Fellowship of McGill University for providing financial support for this project.

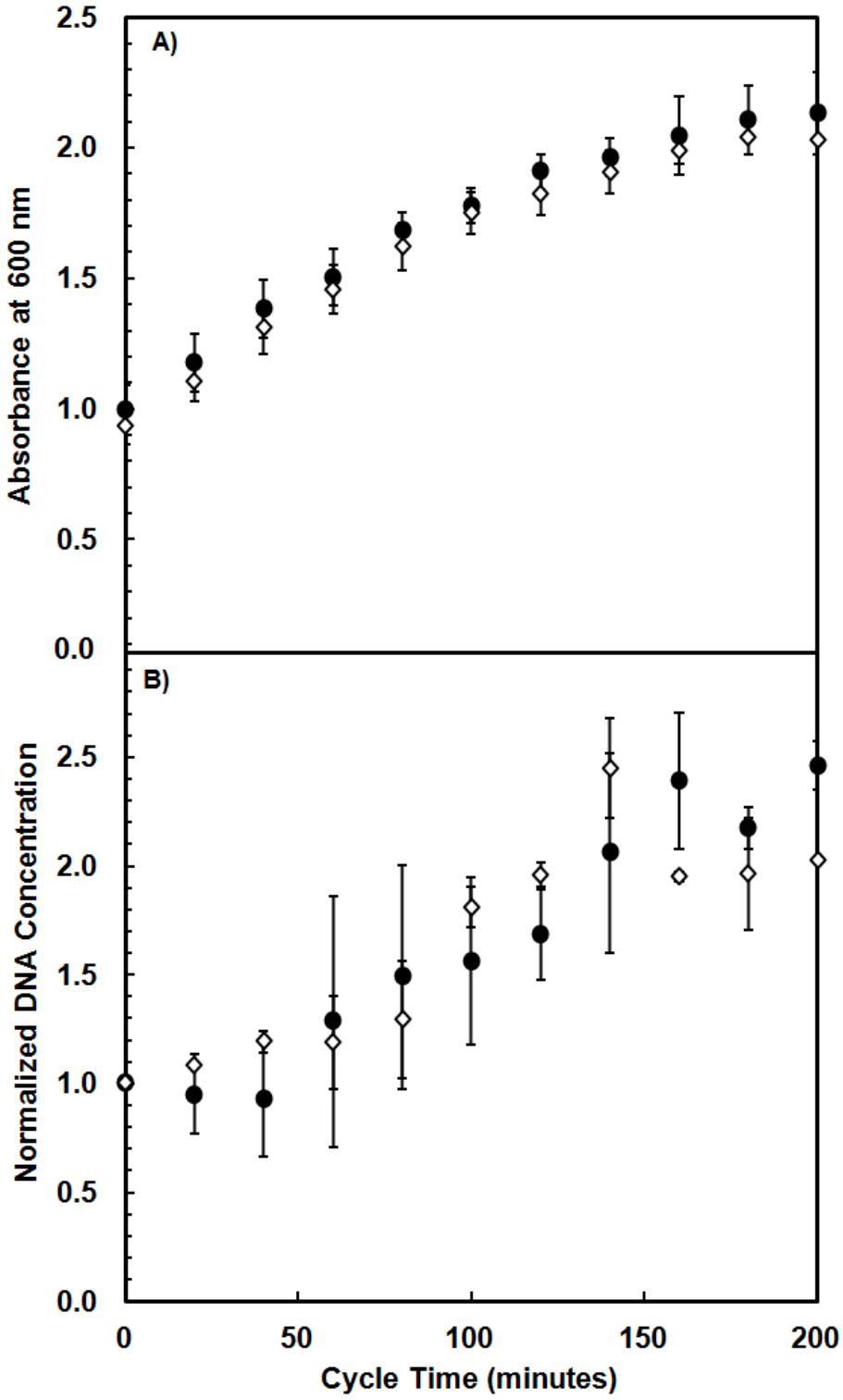

Fig. 5.1 Growth of *E. coli* ATCC 11303 during early (●) and late (◊) cycles of the SCF. The (a) culture optical density at 600 nm and (b) DNA concentration (normalized to the initial value) are shown. Error bars represent the standard deviation of replicates from three different cycles.

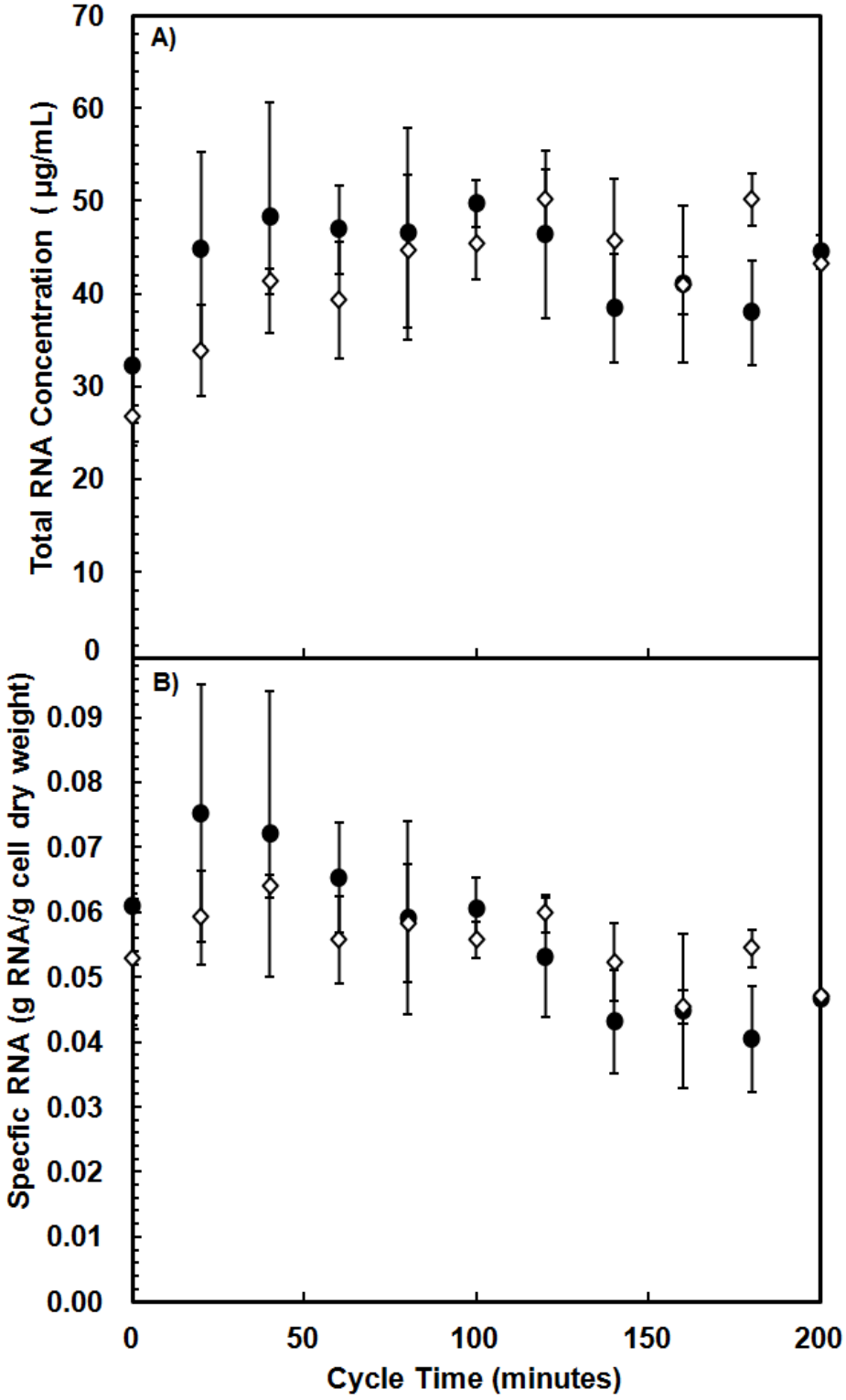

Fig. 5.2 Total RNA concentration during early (●) and late (◊) cycles of the SCF. The (a) volumetric RNA concentration and (b) specific RNA concentration defined as mass of RNA per mass cell dry weight are shown for comparison. Error bars represent the standard deviation of replicates from three different cycles.

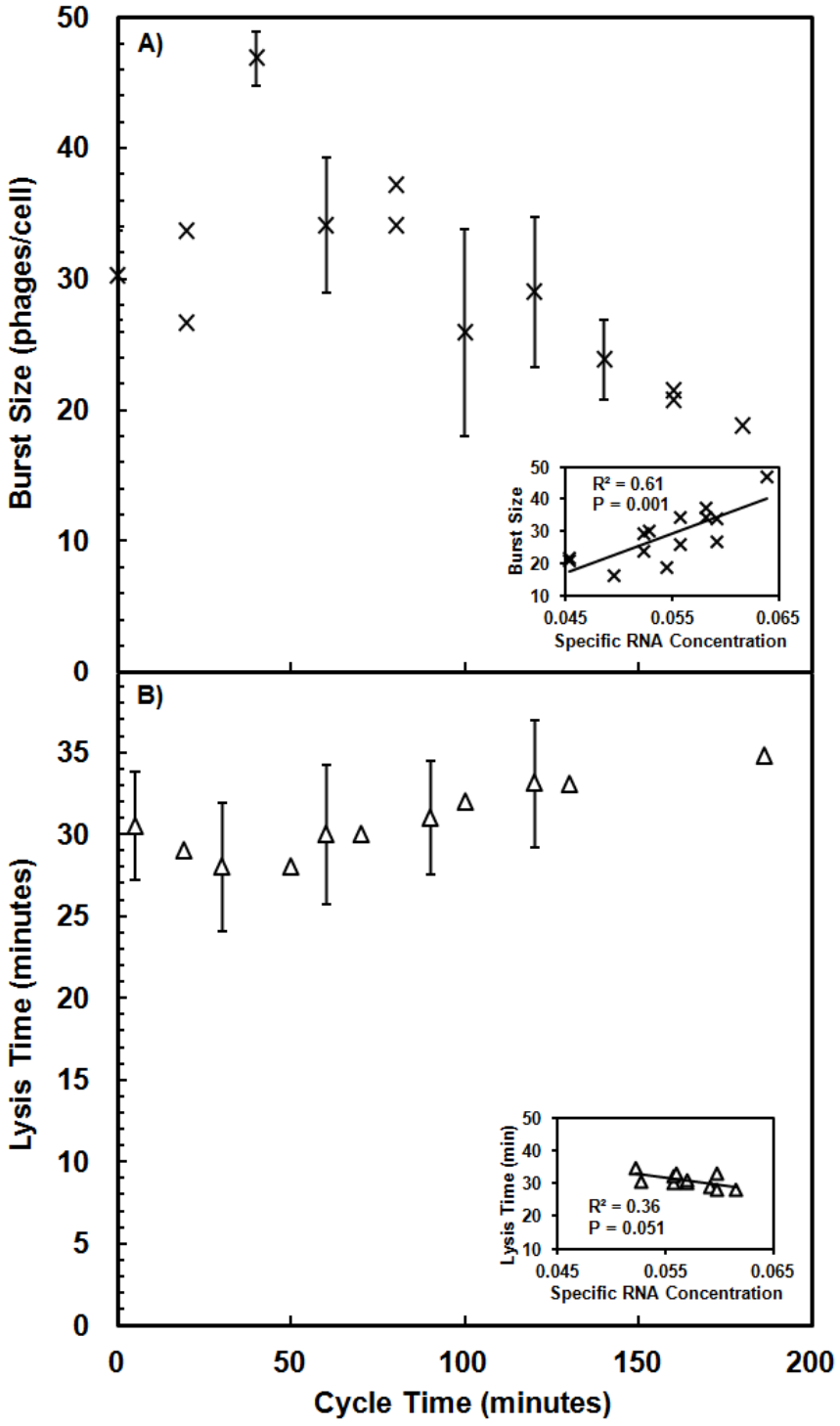

Fig. 5.3 Effect of cycle time on Burst Size (×) and Lysis Time (Δ). Experiments were initiated from growing cultures of *E. coli* ATCC 11303 sampled from the SCF at various points during a cycle. Error bars represent the standard deviation of at least 3 experiments replicated from different SCF cycles. Burst Size and Lysis Time are also plotted against the specific RNA concentration of the culture, shown in the insets of a) an b), respectively. The R^2 values were obtained from linear regression and the P-values determined from f-tests on the significance of the slope.

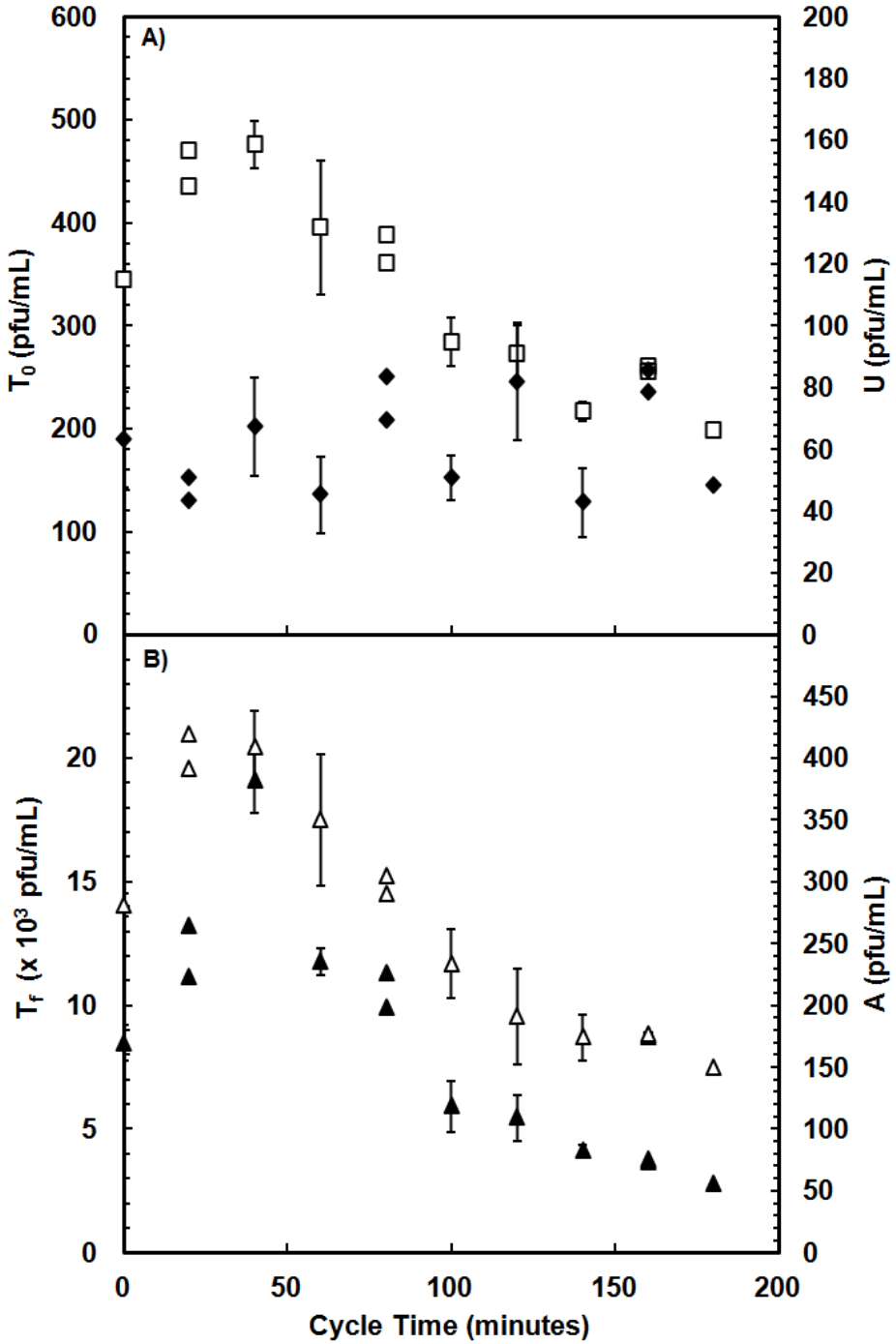

Fig. 5.4 Effect of cycle time on bacteriophage infection and production. The data was collected from burst size experiments on host cells obtained at different times in early SCF cycles. The horizontal axis represents the time at which experiments were initiated during a SCF cycle. In (a), the initial total phage titer T_0 (□) and the number of unadsorbed phages U (◆) are shown. In (b), the data shown in (a) is used to calculate the number of cells infected with viable phages (A, Δ). The final phage titer T_F (▲) is also presented. Error bars represent the standard deviation of replicates from three different SCF cycles.

SUMMARY AND CONCLUSIONS

Self-Cycling Fermentation was used as the foundation for an industrially relevant phage-based recombinant protein production scheme (Ch. 2) and as a research tool to study the cell cycle and its influence on bacteriophage productivity (Ch.5). In addition, factors influencing phage attachment to the host cell, a new model for phage adsorption, and the impact of phage adsorption efficiency on large-scale production were presented and discussed (Ch. 3 and 4).

The SCF production scheme is similar to a sequential batch procedure, achieving higher throughputs with a smaller equipment footprint while maintaining the high titers associated with batch processes and avoiding the residence time distribution problems of continuous processes. Additionally, this study has shown that host cell synchronization, a feature of SCF operation, resulted in higher cell productivities in two separate viral production systems. The operation of SCF is a fully automated process using a non-intrusive measurement for control (CER). These features make SCF an ideal fermentation strategy for use in the phage-based recombinant protein production scheme presented here and would likely make it a viable option in an industrial application.

Small-scale studies on bacteriophage adsorption revealed the importance of this infection event in phage production. A new model was proposed that simplified attachment to a single mass-action governed step but also accounted for the adsorption efficiency of the virus. The adsorption efficiency, shown to be a phenotypic trait of phage T4, depended strongly on the environmental conditions of the infection medium but was independent of MOI and temperature. The adsorption rate constant could be influenced by the growth conditions of the host.

The adsorption efficiency model was shown to perform as well or better than a common two-step model (sequential model) for T-series phages representing three tailed phage families, demonstrating the robustness of the model. Empirical results validated the assumptions inherent to the adsorption efficiency model but could not be captured by the traditional sequential model. Results suggested that the adsorption efficiency is most appropriate for tailed phages containing side-tail fibers. Finally, adsorption efficiency was negatively correlated to phage production during amplification experiments, decreasing the number of phages produced. This work demonstrates the importance of considering the adsorption efficiency in any attempt to optimize the production of bacteriophage particles in an industrial process.

Finally, SCF offers researchers a tool to study how the life cycle of a cell can influence protein expression. For example, the data presented in Chapter 2 suggests that inducing protein synthesis prior to cell division results in the highest cellular productivity. Similarly, studies on lytic phage T4 found that highest phage productivities were generated by infections of hosts preceding cell division. A correlation between intracellular RNA and phage productivity was observed, offering an explanation for the increased phage yield.

This thesis offers the coming phage-based industries insight into how phage production may be influenced by the phage infective process and the metabolic state of the host cell. It illustrates a possible phage-based recombinant protein production scheme and offers Self-Cycling Fermentation as a research tool to study the influence of the cell cycle on productivity.

FUTURE RESEARCH DIRECTIONS

The work presented in this thesis opens a number of avenues for further investigation. The results of Chapter 5 indicate that the cell cycle can significantly influence the phage infective process. That study was completed using a strictly lytic phage. Evidence in the literature suggests that the cell cycle may also influence the lysis/lysogeny decision in temperate phages [114]. It would be interesting to use Self-Cycling Fermentation to study how the cell cycle influences the lysis/lysogeny decision in phage λ. The system is essentially set-up for such an undertaking; the main hurdle would be devising a reliable protocol to differentiate between infections leading to the lytic or lysogenic life cycle.

While the adsorption efficiency was introduced as a useful modeling parameter that should be accounted for in phage amplification experiments, a rigorous study relating adsorption efficiency to phage production was not performed. A proper phage amplification model would have to account for various parameters in the infection process—adsorption kinetics, adsorption efficiency, burst size, lysis time—in order to provide a complete picture of the amplification process. It would be instructive for phage production processes and various phage applications to have a mathematical relation predicting how the adsorption efficiency in particular will influence phage amplification within a culture.

The adsorption studies of Chapters 3 and 4 largely ignored the fate of the free phage fraction F. Sometimes referred to as the residual fraction, these phages do eventually adsorb to a host, albeit at much slower rates than the efficient fraction ε. A full characterization of these phages could lead to new insight as to why some phages readily adsorb while others do not. The residual free phages may represent a specific phenotype or perhaps are

simply the result of random error in assembly of key adsorption proteins on the phage tail. If the trait is associated with a phenotype or genotype, it may be possible to select for fast-adsorbing or slow-adsorbing strains through successive rounds of adsorption and amplification experiments, a potentially useful tool in phage research.

Finally, the cell cycle analysis presented in Chapter 5 offers a very limited picture of how intracellular properties influence production processes. A complete metabolic analysis of the cell culture throughout the SCF cycle coupled with a transciptomics study to understand gene expression and regulation during the cell cycle would provide the insight needed to tailor Self-Cycling Fermentation for specific production processes.

REFERENCES

1. d'Herelle, F., (1917) *An invisible antagonist microbe of dysentery bacillus.* Comptes Rend Hebdom Des Seances De L Academie Des Science, 165: 373-375.

2. Twort, F.W., (1915) *An investigation on the nature of ultra-microscopic viruses.* Lancet, 2: 1241-1243.

3. Pirnay, J.P., et al., (2011) *The phage therapy paradigm: pret-a-porter or sur-mesure?* Pharm Res, 28(4): 934-7.

4. Sulakvelidze, A., Z. Alavidze, and J.G. Morris, (2001) *Bacteriophage therapy.* Antimicrob Agents Chemothe, 45(3): 649-659.

5. Monk, A.B., et al., (2010) *Bacteriophage applications: where are we now?* Lett Appl Microbiol, 51(4): 363-369.

6. Flemming, A., (1929) *On the antibacterial action of cultures of a penicillium, with special reference to their use in the isolation of B. influenzae.* Brit J Exp Pathol, 10: 226-236.

7. Spellberg, B., (2008) *Dr. William H. Stewart: Mistaken or maligned?* Clin Infect Dis, 47(2): 294-294.

8. Brusselaers, N., D. Vogelaers, and S. Blot, (2011) *The rising problem of antimicrobial resistance in the intensive care unit.* Ann Intensive Care, 1: 47.

9. Foxnews.com, *MRSA strikes more hospital patients, study finds*. August 13, 2012.

10. Watkins, J.L. *With increased drug resistance, health officials warn of gonorrhea*. Chicago Phoenix August 7, 2012 Available from: http://chicagophoenix.com/2012/08/20/gonorrhea-resistant-to-oral-antibiotic-treatment/.

11. Bush, K., et al., (2011) *Tackling antibiotic resistance.* Nature Rev Microbiol, 9(12): 894-896.

12. Allen, H.K., et al., (2010) *Call of the wild: antibiotic resistance genes in natural environments.* Nature Rev Microbiol, 8(4): 251-259.

13. Kummerer, K., (2004) *Resistance in the environment.* J Antimicrob Chemother, 54(2): 311-320.

14. Kummerer, K. and A. Henninger, (2003) *Promoting resistance by the emission of antibiotics from hospitals and households into effluent.* Clin Microbiol Infect, 9(12): 1203-1214.

15. Pirnay, J.P., et al., (2012) *Introducing yesterday's phage therapy in today's medicine.* Future Virol, 7(4): 379-390.

16. Spellberg, B., et al., (2008) *The epidemic of antibiotic-resistant infections: A call to action for the medical community from the Infectious Diseases Society of America.* Clin Infect Dis, 46(2): 155-164.

17. Rhoads, D.D., et al., (2009) *Bacteriophage therapy of venous leg ulcers in humans: results of a phase I safety trial.* J Wound Care, 18(6): 237-8, 240-3.

18. Wright, A., et al., (2009) *A controlled clinical trial of a therapeutic bacteriophage preparation in chronic otitis due to antibiotic-resistant Pseudomonas aeruginosa; a preliminary report of efficacy.* Clin Otolaryngol, 34(4): 349-357.

19. Budynek, P., et al., (2010) *Bacteriophages and cancer.* Arch Microbiol, 192(5): 315-20.

20. Gorski, A., et al., (2003) *New insights into the possible role of bacteriophages in host defense and disease.* Med Immunol, 2(1): 2.

21. Pal, C., et al., (2007) *Coevolution with viruses drives the evolution of bacterial mutation rates.* Nature, 450(7172): 1079-81.

22. Verbeken, G., et al., (2012) *Optimizing the European regulatory framework for sustainable bacteriophage therapy in human medicine.* Arch Immunol Ther Exp (Warsz), 60(3): 161-72.

23. Merabishvili, M., et al., (2009) *Quality-Controlled Small-Scale Production of a Well-Defined Bacteriophage Cocktail for Use in Human Clinical Trials.* PLoS One, 4(3).

24. FDA, (2006) *Food additives permitted for direct addition to food for human consumption; bacteriophage preparation.* Fed. Regist. , 71: 47729-32.

25. Loc Carrillo, C., et al., (2005) *Bacteriophage therapy to reduce Campylobacter jejuni colonization of broiler chickens.* Appl Environ Microbiol, 71(6554-6563).

26. Park, S.C. and T. Nakai, (2003) *Bacteriophage control of Pseudomonas plecoglossicida infection in ayu Plecoglossus altivelis.* Dis Aquat Organ, 53(1): 33-9.

27. Guenther, S., et al., (2012) *Biocontrol of Salmonella Typhimurium in RTE foods with the virulent bacteriophage FO1-E2.* Int J Food Microbiol, 154(1–2): 66-72.

28. Jones, J.B., et al., (2007) *Bacteriophages for plant disease control.* Annu Rev Phytopathol, 45: 245-62.

29. Schnabel, E.L. and A.L. Jones, (2001) *Isolation and characterization of five Erwinia amylovora bacteriophages and assessment of phage resistance in strains of Erwinia amylovora.* Appl Environ Microbiol, 67(1): 59-64.

30. Fox, J.L., (2000) *Phage treatments yield healthier tomato, pepper plants.* Asm News, 66(8): 455-456.

31. Fujiwara, A., et al., (2011) *Biocontrol of Ralstonia solanacearum by treatment with lytic bacteriophages.* Appl Environ Microbiol, 77(12): 4155-62.

32. Adriaenssens, E.M., et al., (2012) *T4-related bacteriophage LIMEstone isolates for the control of soft rot on potato caused by 'Dickeya solani'.* PLoS One, 7(3): e33227.

33. Guntupalli, R., et al., (2012) *Detection and identification of methicillin resistant and sensitive strains of Staphylococcus aureus using tandem measurements.* J Microbiol Methods, 90(3): 182-91.

34. Huang, S., et al., (2008) *The Effect of Salt and Phage Concentrations on the Binding Sensitivity of Magnetoelastic Biosensors for Bacillus anthracis Detection.* Biotechnol Bioeng, 101(5): 1014-1021.

35. Park, M.K., et al., (2012) *The effect of incubation time for Salmonella Typhimurium binding to phage-based magnetoelastic biosensors.* Food Control, 26(2): 539-545.

36. Tawil, N., et al., (2012) *Surface plasmon resonance detection of E. coli and methicillin-resistant S. aureus using bacteriophages.* Biosens Bioelectron, 37(1): 24-29.

37. Cardinale, D., N. Carette, and T. Michon, (2012) *Virus scaffolds as enzyme nano-carriers.* Trends in Biotechnol, 30(7): 369-376.

38. Ngweniform, P., et al., (2009) *Self-Assembly of Drug-Loaded Liposomes on Genetically Engineered Target-Recognizing M13 Phage: A Novel Nanocarrier for Targeted Drug Delivery.* Small, 5(17): 1963-1969.

39. Chen, B.Y. and H.C. Lim, (1996) *Bioreactor studies on temperature induction of the Q(-) mutant of bacteriophage lambda in Escherichia coli.* J Biotechnol, 51(1): 1-20.

40. Kim, T.S. and T.H. Park, (2000) *Optimization of bacteriophage lambda Q(-)-containing recombinant Escherichia coli fermentation process.* Bioproc Eng, 23(2): 187-190.

41. Oh, J.S., D. Cho, and T.H. Park, (2005) *Two-stage continuous operation of recombinant Escherichia coli using the bacteriophage lambda Q(-) vector.* Bioproc Biosyst Eng, 28(1): 1-7.

42. Oh, J.S., et al., (2007) *Construction of various bacteriophage lambda mutants for stable and efficient production of recombinant protein in Escherichia coli.* Proc Biochem, 42(3): 486-490.

43. Oh, J.S., H.H. Park, and T.H. Park, (2008) *Temperature management strategy for efficient gene expression in a thermally inducible Escherichia coli/bacteriophage system.* Biotechnol Bioprocess Eng, 13(4): 470-475.

44. Padukone, N., S.W. Peretti, and D.F. Ollis, (1990) *Lambda vectors for stable cloned gene-expression.* Biotechnol Prog, 6(4): 277-282.

45. Padukone, N., S.W. Peretti, and D.F. Ollis, (1992) *Characterization of the mutant lytic state in lambda expression systems.* Biotechnol Bioeng, 39(4): 369-377.

46. Park, T.H., J.H. Seo, and H.C. Lim, (1989) *Optimization of fermentation processes using recombinant Escherichia-coli with the cloned trp operon.* Biotechnol Bioeng, 34(9): 1167-1177.

47. Park, T.H., J.H. Seo, and H.C. Lim, (1991) *2-Stage fermentation with bacteriophage-lambda as an expression vector in Escherichia-coli.* Biotechnol Bioeng, 37(4): 297-302.

48. Molineux, I., *Structural insights into the initiation of phage infection using electron cryo-tomography*, in *Viruses of Microbes*. 2012: Brussels, Belgium.

49. Leiman, P.G. and M.M. Shneider, (2012) *Contractile Tail Machines of Bacteriophages.* Viral Mol Machines, 726: 93-114.

50. Roucourt, B. and R. Lavigne, (2009) *The role of interactions between phage and bacterial proteins within the infected cell: a diverse and puzzling interactome.* Environ Microbiol, 11(11): 2789-2805.

51. Goldberg, E., E. Grinius, and L. Letellier, (1994) *Attachment and Injection*, in *Molecular Biology of Bacteriophage T4*, J.D. Karam, Editor. American Society for Microbiology: Washington, DC. p. p. 347-348.

52. Sauvageau, D., B. Allain, and D.G. Cooper, (2010) *Using the rate of respiration to monitor events in the infection of Escherichia coli cultures by bacteriophage T4.* Biotechnol Prog, 26(3): 865-71.

53. Sauvageau, D. and D.G. Cooper, (2010) *Two-stage, self-cycling process for the production of bacteriophages.* Microb Cell Fact, 9: 81.

54. Sauvageau, D., Z. Storms, and D.G. Cooper, (2010) *Synchronized populations of Escherichia coli using simplified self-cycling fermentation.* J Biotechnol, 149(1-2): 67-73.

55. Abedon, S.T., (2008) *Phages, ecology, evolution*, in *Bacteriophage Ecology: Population Growth, Evolution, and Impact of Bacterial Viruses*, S. Abedon, Editor. Cambridge University Press: New York.

56. Hatfull, G.F., (2010) *Bacteriophage Research: Gateway to Learning Science* Microbe Magazine, 5 (June).

57. Abedon, S.T., (1994) *Lysis and Interaction between Free Phages and Infected Cells*, in *Molecular Biology of Bacteriphage T4*, J.D. Karam, Editor. American Society for Microbiology: Washington, D.C.

58. Sambrook, J., E.F. Fritsch, and T. Maniatis, (1989) *Molecular cloning : a laboratory manual*. 2nd ed. Cold Spring Harbor, N.Y.: Cold Spring Harbor Laboratory.

59. Stent, G.S. and E.L. Wollman, (1952) *On the two step nature of bacteriophage adsorption.* Biochim Biophys Acta, 8(3): 260-9.

60. Molineux, I.J., (2006) *Fifty-three years since Hershey and Chase; much ado about pressure but which pressure is it?* Virology, 344(1): 221-229.

61. Leiman, P.G., et al., (2007) *The structures of bacteriophages K1E and K1-5 explain processive degradation of polysaccharide capsules and evolution of new host specificities.* J Mol Biol, 371(3): 836-49.

62. Walter, M., et al., (2008) *Structure of the receptor-binding protein of bacteriophage det7: a podoviral tail spike in a myovirus.* J Virol, 82(5): 2265-73.

63. Adams, M.H., (1959) *Bacteriophages*. New York: Interscience Publishers.

64. Christensen, J.R., (1965) *The kinetics of reversible and irreversible attachment of bacteriophage T-1.* Virology, 26(4): 727-37.

65. Gamow, R.I., (1969) *Thermodynamic Treatment of Bacteriophage T4B Adsorption Kinetics.* J Virol, 4: 113-115.

66. Garen, A. and T.T. Puck, (1951) *The first two steps of the invasion of host cells by bacterial viruses. II.* J Exp Med, 94(3): 177-89.

67. Moldovan, R., E. Chapman-McQuiston, and X.L. Wu, (2007) *On kinetics of phage adsorption.* Biophys J, 93(1): 303-315.

68. Puck, T.T., (1953) *The first steps of virus invasion.* Cold Spring Harb Symp Quant Biol, 18: 149-54.

69. Puck, T.T., A. Garen, and J. Cline, (1951) *The Mechanism of Virus Attachment to Host Cells 1. The Role of Ions in the Primary Reaction.* J Exp Med, 93(1): 65-88.

70. Zonenstein, Y., et al., (2010) *The initial adsorption of T4 bacteriophages to Escherichia coli cells at equivalent concentrations: Experiments and mathematical modeling.* Biochem Eng J, 48(2): 225-229.

71. Anderson, T.F., (1945) *The Role of Tryptophane in the Adsorption of Two Bacterial Viruses on their Host, E. coli.* J Cellular Comp Physiol, 24: 17-26.

72. Hershey, A.D., G.M. Kalmanson, and J. Bronfenbrenner, (1944) *Coordinate Effects of Electrolyte and Antibody on the Infectivity of Bacteriophage.* J Immunol, 48: 221-239.

73. Stent, G.S. and E.L. Wollman, (1950) *Studies on Activation of T4 Bacteriophage by Cofactor II: The Mechanism of Activation.* Biochim Biophys Acta, 6: 307-316.

74. Stent, G.S. and E.L. Wollman, (1951) *Studies on Activation of T4 Bacteriophage by Cofactor III: Conditions Affecting the Activation Process.* Biochim Biophys Acta, 6: 374-383.

75. Tolmach, L.J. and T.T. Puck, (1952) *The Mechanism of Virus Attachment to Host cells: III.* J Am Chem Soc, 74: 5551-5553.

76. Wollman, E.L. and G.S. Stent, (1950) *Studies on Activation of T4 Bacteriophage by Cofactor I: The Degree of Activity.* Biochim Biophys Acta, 6: 292-306.

77. Wollman, E.L. and G.S. Stent, (1952) *Studies on Activation of T4 Bacteriophage by Cofactor IV: Nascent Activity.* Biochim Biophys Acta, 9: 538-550.

78. Hadas, H., et al., (1997) *Bacteriophage T4 Development depends on the Physiology of its Host Escherichia coli.* Microbiol, 143: 179-185.

79. Ellis, E.L. and M. Delbruck, (1939) *The growth of bacteriophage.* J Gen Physiol, 22(3): 365-384.

80. You, L., P.F. Suthers, and J. Yin, (2002) *Effects of Escherichia coli physiology on growth of phage T7 in vivo and in silico.* J Bacteriol, 184(7): 1888-94.

81. Shao, Y. and I.N. Wang, (2008) *Bacteriophage adsorption rate and optimal lysis time.* Genetics, 180(1): 471-82.

82. Bull, J.J., (2006) *Optimality models of phage life history and parallels in disease evolution.* J Theor Biol, 241(4): 928-938.
83. Wang, I.N., D.E. Dykhuizen, and L.B. Slobodkin, (1996) *The evolution of phage lysis timing.* Evol Ecol, 10(5): 545-558.

84. Hutchison 3rd, C.A. and R.L. Sinsheimer, (1966) *The process of infection with bacteriophage ΦX174: X. Mutations in a ΦX lysis gene.* J Mol Biol, 18(3): 429-447.

85. Josslin, R., (1970) *Lysis Mechanism of Phage T4 - Mutants Affecting Lysis.* Virology, 40(3): 719-726.

86. Wang, I.N., (2006) *Lysis timing and bacteriophage fitness.* Genetics, 172(1): 17-26.

87. Abedon, S.T., T.D. Herschler, and D. Stopar, (2001) *Bacteriophage latent-period evolution as a response to resource availability.* Appl Environ Microbiol, 67(9): 4233-4241.

88. Kerr, B., J. West, and J.M. Bohannan, (2008) *Bacteriophages: models for exploring basic principles of ecology*, in *Bacteriophage Ecology: Population Growth, Evolution and Impact of Bacterial Viruses*, S.T. Abedon, Editor. Cambridge University Press: New York.

89. Abedon, S.T., P. Hyman, and C. Thomas, (2003) *Experimental examination of bacteriophage latent-period evolution as a response to bacterial availability.* Appl Environ Microbiol, 69(12): 7499-506.

90. Heineman, R.H. and J.J. Bull, (2007) *Testing optimality with experimental evolution: lysis time in a bacteriophage.* Evolution, 61(7): 1695-1709.

91. Gallet, R., Y. Shao, and I.N. Wang, (2009) *High adsorption rate is detrimental to bacteriophage fitness in a biofilm-like environment.* BMC Evol Biol, 9: 241.

92. Gallet, R., S. Kannoly, and I.N. Wang, (2011) *Effects of bacteriophage traits on plaque formation.* BMC Microbiol, 11: 181.

93. Kutter, E., et al., (1994) *Effects of bacterial growth conditions and physiology on T4 infection.*, in *Molecular Biology of Bacteriophage T4*, J.D. Karam, Editor. ASM Press: Washington, D. C.

94. Rabinovitch, A., et al., (1999) *Model for bacteriophage T4 development in Escherichia coli.* J Bacteriol, 181(5): 1677-1683.

95. Sargeant, K. and R.G. Yeo, (1966) *Production of Bacteriophage Mu2.* Biotechnol Bioeng, 8(2): 195.

96. Sargeant, K., et al., (1968) *Production of Bacteriophage T7.* Appl Microbiol, 16(10): 1483-&.

97. Abedon, S.T., (2003) *Phage population growth: constraints, games, adaptation*, in *Bacteriophage Ecology: Population Growth, Evolution, and Impact of Bacterial Viruses*, S.T. Abedon, Editor. Cambridge University Press: New York.

98. Abelson, J. and C.A. Thomas Jr, (1966) *The anatomy of the T5 bacteriophage DNA molecule.* J Mol Biol, 18(2): 262-288.

99. Marks, T. and R. Sharp, (2000) *Bacteriophages and biotechnology: a review.* J ChemTechnol Biotechnol, 75(1): 6-17.

100. Branston, S., et al., (2012) *Precipitation of filamentous bacteriophages for their selective recovery in primary purification.* Biotechnol Prog, 28(1): 129-136.

101. Branston, S., et al., (2011) *Study of Robustness of Filamentous Bacteriophages for Industrial Applications.* Biotechnology and Bioengineering, 108(6): 1468-1472.

102. Grieco, S.H., et al., (2009) *Maximizing filamentous phage yield during computer-controlled fermentation.* Bioprocess Biosyst Eng, 32(6): 773-9.

103. Wenzel, M., et al., (2011) *Self-inducible Bacillus subtilis expression system for reliable and inexpensive protein production by high-cell-density fermentation.* Appl Environ Microbiol, 77(18): 6419-25.

104. Los, M., et al., (2007) *Effective inhibition of lytic development of bacteriophages lambda, P1 and T4 by starvation of their host, Escherichia coli.* BMC Biotechnol, 7(1): 13.

105. Park, S.H. and T.H. Park, (2000) *Analysis of two-stage continuous operation of Escherichia coli containing bacteriophage lambda vector.* Bioproc Engineer, 23(6): 557-563.

106. Buckling, A. and P.B. Rainey, (2002) *Antagonistic coevolution between a bacterium and a bacteriophage.* Proc Biol Sci, 269(1494): 931-6.

107. Mizoguchi, K., et al., (2003) *Coevolution of bacteriophage PP01 and Escherichia coli O157:H7 in continuous culture.* Appl Environ Microbiol, 69(1): 170-6.

108. Smith, H.L. and H.R. Thieme, (2012) *Persistence of bacteria and phages in a chemostat.* J Math Biol, 64(6): 951-979.

109. Weitz, J.S., H. Hartman, and S.A. Levin, (2005) *Coevolutionary arms races between bacteria and bacteriophage.* Proc Natl Acad Sci USA, 102(27): 9535-9540.

110. Hershey, A.D. and M. Chase, (1952) *Independent Functions of Viral Protein and Nucleic Acid in Growth of Bacteriophage.* Journal of General Physiology, 36(1): 39-56.

111. Ptashne, M., (2004) *A Genetic Switch: Phage Lambda Revisited.* Cold Spring Harbor, N.Y.: Cold Spring Harbor Laboratory Press.

112. Herskowitz, I. and D. Hagen, (1980) *The lysis-lysogeny decision of phage lambda: explicit programming and responsiveness.* Annu Rev Genet, 14: 399-445.

113. Lieb, M., (1953) *The establishment of lysogenicity in Escherichia coli.* J Bacteriol, 65(6): 642-51.

114. St-Pierre, F. and D. Endy, (2008) *Determination of cell fate selection during phage lambda infection.* Proc Natl Acad Sci USA, 105(52): 20705-20710.

115. Lin, C.S., et al., (1998) *Characterization of bacteriophage lambda Q(-) mutant for stable and efficient production of recombinant protein in Escherichia coli system.* Biotechnol Bioeng, 57(5): 529-535.

116. Campbell, A., (1957) *Synchronization of cell division.* Bacteriol Rev, 21(4): 263-72.

117. Ingraham, J.L., O. Maaloe, and F.C. Neidhardt, (1983) *Growth of the Bacterial Cell*. Sunderland, MA: Sinauer Associates, Inc.

118. Blumenthal, L.K. and S.A. Zahler, (1962) *Index for measurement of synchronization of cell populations.* Science, 135(3505): 724.

119. Helmstetter, C.E. and D.J. Cummings, (1963) *Bacterial synchronization by selection of cells at division.* Proc Natl Acad Sci USA, 50(4): 767.

120. Powell, E.O., (1956) *Growth rate and generation time of bacteria, with special reference to continuous culture.* J Gen Microbiol, 15(3): 492-511.

121. Shehata, T.E. and A.G. Marr, (1970) *Synchronous growth of enteric bacteria.* J Bacteriol, 103(3): 789.

122. Cooper, S. and C.E. Helmstetter, (1968) *Chromosome replication and the division cycle of Escherichia coli B/r.* J Mol Biol, 31(3): 519-40.

123. Cutler, R.G. and J.E. Evans, (1966) *Synchronization of bacteria by a stationary-phase method.* J Bacteriol, 91(2): 469-76.

124. Dawson, P.S.S., (1972) *Continuously synchronized growth.* J Appl Chem Biotechnol, 22(1): 79-103.

125. Fritsch, M., et al., (2005) *Cell cycle synchronization of Cupriavidus necator by continuous phasing measured via flow cytometry.* Biotechnol Bioeng, 92(5): 635-42.

126. Sheppard, J.D. and D.G. Cooper, (1990) *Development of computerized feedback-control for the continuous phasing of Bacillus-subtilis.* Biotechnol Bioeng, 36(5): 539-545.

127. Brown, W.A., (2001) *The self-cycling fermentor - development, applications, and future opportunities.* Rec Res Develop Biotechnol Bioeng, 4: 61-90.

128. Brown, W.A., D.G. Cooper, and S.N. Liss, (2000) *Toluene removal in an automated cyclical bioreactor.* Biotechnol Prog, 16(3): 378-384.

129. Hughes, S.M. and D.G. Cooper, (1996) *Biodegradation of phenol using the self-cycling fermentation (SCF) process.* Biotechnol Bioeng, 51(1): 112-119.

130. Sarkis, B.E. and D.G. Cooper, (1994) *Biodegradation of aromatic-compounds in a self-cycling fermenter (SCf).* Canadian J Chem Eng, 72(5): 874-880.

131. Sheppard, J.D. and D.G. Cooper, (1991) *The Response of Bacillus-subtilis ATCC-21332 to manganese during continuous-phased growth.* Appl Microbiol Biotechnol, 35(1): 72-76.

132. van Walsum, G.P. and D.G. Cooper, (1993) *Self-cycling fermentation in a stirred-tank reactor.* Biotechnol Bioeng, 42(10): 1175-1180.

133. McCaffrey, W.C. and D.G. Cooper, (1995) *Sophorolipids production by Candida-bombicola using self-cycling fermentation.* J Ferment Bioeng, 79(2): 146-151.

134. Wentworth, S.D. and D.G. Cooper, (1996) *Self-cycling fermentation of a citric acid producing strain of Candida lipolytica.* J Ferment Bioeng, 81(5): 400-405.

135. Yanofsky, C., R.L. Kelley, and V. Horn, (1984) *Repression Is relieved before attenuation in the trp aperon of Escherichia-coli as tryptophan starvation becomes increasingly severe.* J Bacteriol, 158(3): 1018-1024.

136. Miller, J.H., (1972) *Experiments in Molecular Genetics*. Cold Spring Harbor Laboratories: Cold Spring Harbor, New York.

137. Zenaitis, M.G. and D.G. Cooper, (1994) *Antibiotic production by Streptomyces-aureofaciens using self-cycling fermentation.* Biotechnol Bioeng, 44(11): 1331-1336.

138. Creanor, J. and J.M. Mitchison, (1982) *Patterns of protein-synthesis during the cell-cycle of the fission yeast Schizosaccharomyces-pombe.* J Cell Science, 58(Dec): 263-285.

139. Iba, H., A. Fukuda, and Y. Okada, (1978) *Rate of major protein-synthesis during cell-cycle of Caulobacter-crescentus.* J Bacteriol, 135(2): 647-655.

140. Mitchison, J., (1969) *Enzyme synthesis in synchronous cultures.* Science, 165(3894): 657-663.

141. Yashphe, J. and H.O. Halvorson, (1976) *Beta-D-Galactosidase activity in single yeast-cells during cell-cycle of Saccharomyces-lactis.* Science, 191(4233): 1283-1284.

142. Aucoin, M.G., et al., (2006) *Identifying conditions for inducible protein production in E. coli: combining a fed-batch and multiple induction approach.* Microb Cell Fact, 5: 27.

143. Caspeta, L., et al., (2009) *The effect of heating rate on Escherichia coli metabolism, physiological stress, transcriptional response, and production of temperature-induced recombinant protein: a scale-down study.* Biotechnol Bioeng, 102(2): 468-82.

144. Valdez-Cruz, N.A., et al., (2010) *Production of recombinant proteins in E. coli by the heat inducible expression system based on the phage lambda pL and/or pR promoters.* Microbial Cell Factories, 9: 18.

145. Brown, W.A. and D.G. Cooper, (1991) *Self-cycling fermentation applied to Acinetobacter-calcoaceticus Rag-1.* Appl Environ Microbiol, 57(10): 2901-2906.

146. Bremer, H. and P.P. Dennis, (1996) *Modulation of chemical composition and other parameters of the cell by growth rate*, in *Esherichia coli and Salmonella: Cellular and Molecular*

Biology, F.C. Neidhart, Editor. American Society for Microbiology: Washington, D. C.

147. d'Herelle F, (1926) *The bacteriophage and its behavior*. Baltimore: The Williams & Wilkins Company. xiv, 629

148. Glynn MK, et al., (1998) *Emergence of multidrug-resistant Salmonella enterica serotype typhimurium DT104 infections in the United States.* N Engl J Med, 338(19): 1333-8.

149. Hofmann J, et al., (1995) *The prevalence of drug-resistant Streptococcus pneumoniae in Atlanta.* N Engl J Med, 333(8): 481-6.

150. Panlilio AL, et al., (1992) *Methicillin-resistant Staphylococcus aureus in U.S. hospitals, 1975-1991.* Infect Control Hosp Epidemiol, 13(10): 582-6.

151. Thiel, K., (2004) *Old dogma, new tricks - 21st century phage therapy.* Nat Biotechnol, 22(1): 31-36.

152. Kellenberger, E., et al., (1965) *Functions and Properties Related to the Tail Fibers of Bacteriophage T4.* Virology, 26: 419-440.

153. Brenner S, et al., (1962) *On the Interaction of Adsorption Cofactors with Bacteriophages T2 and T4.* Virol, 17: 30-39.

154. Gamow RI and Kozloff LM, (1968) *Chemically Induced Cofactor Requirement for Bacteriophage T4D.* J Virol, 2: 480-487.

155. Anderson TF, (1948) *The Inheritance of Requirements for Adsorption Cofactors in the Bacterial Virus-T4.* J Bacteriol, 55(5): 651-658.

156. Edgar, R.S. and I. Lielausis, (1964) *Temperature-Sensitive Mutants of Bacteriophage T4d: Their Isolation and Genetic Characterization.* Genetics, 49: 649-62.

157. Galvez, A., et al., (2010) *Microbial antagonists to food-borne pathogens and biocontrol.* Curr Opin Biotechnol, 21(2): 142-148.

158. Hanlon, G.W., (2007) *Bacteriophages: an appraisal of their role in the treatment of bacterial infections.* Int J Antimicrob Agents, 30: 118-128.

159. Bradley, D.E., (1967) *Ultrastructure of bacteriophage and bacteriocins.* Bacteriol Rev, 31(4): 230-314.

160. Steven, A.C., et al., (1988) *Molecular substructure of a viral receptor-recognition protein. The gp17 tail-fiber of bacteriophage T7.* J Mol Biol, 200(2): 351-65.

161. Effantin, G., et al., (2006) *Bacteriophage T5 structure reveals similarities with HK97 and T4 suggesting evolutionary relationships.* J Mol Biol, 361(5): 993-1002.

162. Hendrix, R.W. and R.L. Duda, (1992) *Bacteriophage lambda PaPa: not the mother of all lambda phages.* Science, 258(5085): 1145-8.

163. Letellier, L., et al., (2004) *Main features on tailed phage, host recognition and DNA uptake.* Front Biosci, 9: 1228-1239.

164. Storms, Z.J., et al., (2010) *Bacteriophage adsorption efficiency and its effect on amplification.* Bioprocess Biosyst Eng, 33(7): 823-31.

165. Adam, G. and M. Delbruck, (1968) *Reduction of Dimensionality in biological diffusion processes.*, in *Structural Chemistry and Molecular Biologogy*, A. Rich and N. Davidson, Editors. W. H. Freeman & Company: San Francisco.

166. Berg, H.C. and E.M. Purcell, (1977) *Physics of Chemoreception.* Biophys. J., 20(2): 193-219.

167. Crawford, J.T. and E.B. Goldberg, (1977) *The effect of baseplate mutations on the requirement for tail-fiber binding for irreversible adsorption of bacteriophage T4.* J Mol Biol, 111(3): 305-13.

168. Heller, K. and V. Braun, (1979) *Accelerated adsorption of bacteriophage T5 to Escherichia coli F, resulting from reversible tail fiber-lipopolysaccharide binding.* J Bacteriol, 139(1): 32-8.

169. Davies, J.K. and P. Reeves, (1975) *Genetics of Resistance to Colicins in Escherichia-Coli K-12 - Cross-Resistance among Colicins of Group-B.* J Bacteriol, 123(1): 96-101.

170. Morona, R. and U. Henning, (1986) *New locus (ttr) in Escherichia coli K-12 affecting sensitivity to bacteriophage T2 and growth on oleate as the sole carbon source.* J Bacteriol, 168(2): 534-40.

171. Rakhuba, D.V., et al., (2010) *Bacteriophage receptors, mechanisms of phage adsorption and penetration into host cell.* Pol J Microbiol, 59(3): 145-55.

172. Braun, V., K. Schaller, and H. Wolff, (1973) *A common receptor protein for phage T5 and colicin M in the outer membrane of Escherichia coli B.* Biochim Biophys Acta, 323(1): 87-97.

173. Braun, V. and H. Wolff, (1973) *Characterization of the receptor protein for phage T5 and colicin M in the outer membrane of E. coli B.* FEBS Lett, 34(1): 77-80.

174. Manning, P.A. and P. Reeves, (1976) *Outer membrane of Escherichia coli K-12: tsx mutants (resistant to bacteriophage T6 and colicin K) lack an outer membrane protein.* Biochem. Biophys. Res. Com., 71(2): 466-470

175. Steven, A.C. and B.L. Trus, (1986) *The structure of bacteriophage T7*, in *Electron Microscopy of Proteins, Viral Structure, Vol 5.*, J.R. Harris and R.W. Horne, Editors. Academic Press: London.

176. Serwer, P., et al., (2008) *Evidence for bacteriophage T7 tail extension during DNA injection.* BMC Res Notes, 1: 36.

177. Brock, T.D., (1990) *The Emergence of Bacterial Genetics*. Cold Spring Harbor, N.Y.: Cold Spring Harbor Laboratory Press.

178. Stroud, R.M., P. Serwer, and M.J. Ross, (1981) *Assembly of bacteriophage T7. Dimensions of the bacteriophage and its capsids.* Biophysical Journal, 36(3): 743-57.

179. Rao, A.S., (1997) *Introduction to Microbiology*. New Delhi: Prentic-Hall of India Private Limited.

180. Neidhardt, F.C. and H.E. Umbarger, (1996) *Chemical Composition of Escherichia coli*, in *Escherichia coli and Salmonella: Cellular and Molecular Biology* F.C. Neidhardt, Editor. ASM Press: Washington, D. C.

181. Storms, Z.J., et al., (2012) *Self-cycling operation increases productivity of recombinant protein in Escherichia coli.* Biotechnol Bioeng, 109(9): 2262-70.

182. Dawson, P.S.S., (1985) *Growth, cell cultivation, cell-metabolism, and the cell-cycle of Candida utilis as explored by continuous phased culture.* Can J Microbiol, 31(3): 183-189.

183. Noack, S., W. Kloden, and T. Bley, (2008) *Modeling synchronous growth of bacterial populations in phased cultivation.* Bioprocess Biosyst Eng, 31(5): 435-43.

184. Cooper, S., (1979) *Unifying model for the G1 period in prokaryotes and eukaryotes.* Nature, 280(5717): 17-19.

185. Donachie, W.D., (1968) *Relationship between cell size and time of initiation of DNA replication.* Nature, 219(5158): 1077.

186. Donachie, W.D., (1993) *The Cell-cycle of Escherichia coli.* Ann Rev Microbiol, 47: 199-230.

187. Thomas, K.C., P.S.S. Dawson, and B.L. Gamborg, (1980) *Differential growth-rates of Candida utilis Mother and daughter cells under phased cultivation.* J Bacteriol, 141(1): 1-9.

188. Storms, Z.J., et al., (2012) *Modeling bacteriophage attachment using adsorption efficiency.* Biochemical Engineering Journal, 64: 22-29.

APPENDIX A: ELECTRONICS, HARDWARE, AND SOFTWARE

DAQ and relay boards

The data acquisition system set-up including the computer, DAQ boards and optical relays is shown in Figure A.1. There were four digital outputs associated with DAQ board 0: the heater, motor, valve 1, and valve 2. There were three analog inputs associated with DAQ board 0: CO_2 gas sensor, O_2 gas sensor, and a thermocouple. There were two digital inputs associated with DAQ board 1: level sensor 1 and level sensor 2.

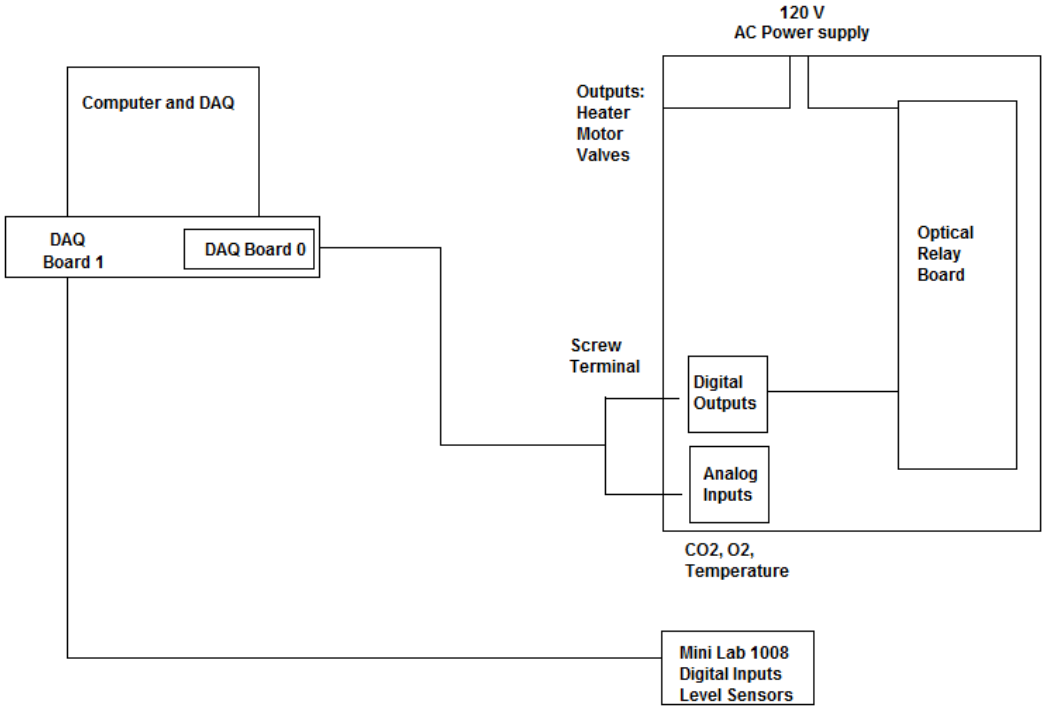

Fig. A.1 Diagram of data acquisition system set-up.

The computer used in the set-up was a Pentium IV (1.6 GHz, 128 MB SDRAM). Table A.1 lists the specifications for the two DAQ boards. The relay board consisted of 16 Opto22 OAC5 relays. The specifications for the relays are shown in Table A.2. To activate the relay, a 5 VDC signal was sent from the computer which turned on an LED in the relay. Energy from the LED

activated electrons, closing the circuit between the 120 VAC power supply and the designated output.

Table A.1 DAQ board specifications.

	DAQ Board 0	**DAQ Board 1**
Model	AMCC S5920	Minilab 1008
Channel size	32-bit	12-bit
Transfer Rate	132 MB/s	
Analog Inputs	8	8
Digital I/O	8	28
Output Voltage	$5V_{DC}$	$5V_{DC}$

Table A.2 Relay specifications.

Company	**Opto 22**
Model	OAC5
Current Rating @ 45°C	3 amps
Operating Frequency	25-65 Hz
Nominal Line Voltage	120 VAC
Nominal Logic Voltage	5 VDC

Gas sensors

Vernier gas sensors were used to monitor the carbon dioxide and oxygen concentration in the air stream leaving the reactor. Tables A.3 and A.4 list the specifications for the gas sensors. The O_2 gas sensor can measure oxygen concentrations ranging from 0 to 27% (0.0004% resolution for 16 bit channel) with an output voltage of 0 to 4.8 VDC.

The CO_2 gas sensor has two ranges of operation: 0-10,000 ppm CO_2 and 0-100,000 ppm CO_2. It was set to the lower range of operation, yielding a resolution of 0.2 ppm CO_2 for a 16 bit channel. The output signal ranges from 0 to 4 VDC. The CO_2 sensor contains an LED on one end of the chamber that emits infrared radiation (IR). A sensor on the other end of the chamber measures the amount of IR that makes it through the chamber without being absorbed by CO_2 molecules at a wavelength 4260 nm. The CO_2 sensor is sensitive to temperature changes and

therefore a heat exchanger was used to cool the air stream leaving the reactor before it reaches the sensor.

Table A.3 Oxygen gas sensor specifications.

Company	**Vernier**
Order number	O2-BTA
Range of gas sensor	0-27%
Resolution	16 bit, 0.0004%
Response Time	12 seconds to 90% of final value
Output Signal Range	0 to 4.8 VDC
Output Impedance	1 KΩ
Input voltage	5 VDC
Operating Temperature	5 to 40°C

Table A.4 Carbon Dioxide gas sensor specifications.

Company	**Vernier**
Order number	CO2-BTA
Range	0-10,000 ppm CO_2, 0-100,000 ppm CO_2
Resolution	16 bit, 0.2 ppm
Response Time	120 seconds to 95% of final value
Output Signal Range	0 to 4.0 VDC
Input Potential	5 V +/- 0.25 V
Operating Temperature	25°C (+/- 5°C)

Thermocouple

Temperature was monitored in the reactor using an OMEGA type J thermocouple. Specifications for the thermocouple are given in Table A.5. The thermocouple has linear readings between 0 and 45°C. The thermocouple was attached to a monolithic thermocouple amplifier chip to produce an output voltage of 0-1.25 V. Specifications for the amplifier chip are given in Table A.6.

Table A.5 Thermocouple specifications.

Company	**OMEGA**
Order number	GJQSS
Type	J
Alloy	Iron-Constantan
Sheath	304 Stainless Steal
Output Signal Range	0-1.25 V

Table A.6 Amplifier chip specifications.

Company	**Analog Devices**
Order number	AD594CQ
Low Impedance Voltage Output	10 mV/°C
Power Supply Range	+/- 5 V
Accuracy	1°C

Level sensors

When the reactor was cycling, exactly half the volume was removed and then fresh medium was added to the reactor to return the liquid volume to its original level. Electro-optic point level sensors (Gems Sensors, Plainfield, CT) were used to indicate once the appropriate volume of liquid had been withdrawn or added to the reactor. Specifications for the sensors are shown in Table A.7. The level sensors contain an LED and a light receiver encased within a prism. In the absence of liquid, light from the LED is reflected within the prism to the light receiver. When the prism is immersed in liquid, light refracts out from the prism, significantly reducing the amount of light reaching the receiver. Once this change is determined, the receiver actuates electronic switching within the sensor. The output signal range is 0-5 V.

Table A.7 Level sensor specifications.

Company	**Gems Sensors**
Order number	ELS-900
Housing and Prism	Polyethersulfone
Current Consumption	18 mA, approximately
Input voltage	5-12 V
Output Signal Range	0-5 V
Repeatability	+/- 1 mm

Outputs

In the reactor, a motor was used to stir the liquid volume and increase oxygen transfer. It was kept at 200 rpm during biomass production. Two fail-close solenoid valves control fluid flow into and out of the reactor. A heater was used to maintain the liquid temperature at 37°C. Specifications for the motor, valves, and heater are shown in Tables A.8, A.9 and A.10, respectively.

Table A.8 Motor specifications.

Company	**Caframo**
Order number	RZR1
Input Voltage	120 VAC
Frequency	60 Hz
Stirrer speed	35-250 rpm

Table A.9 Valve specifications.

Company	**Honeywell Skinner Valves**
Input Voltage	120 VAC
Frequency	60 Hz
Operation	Fail Close

Table A.10 Heater specifications.

Company	**Chromolax**
Order number	CIR-2040
Input Voltage	120 VAC
Frequency	60 Hz
Power	300 W

Signals and wiring

Table A.11 lists the signal specifications for the inputs to Board 0 (AMCC S5920). Figure A.2 shows the wiring of inputs to Board 0. The signal from the thermocouple was first sent to the amplifier chip before passing through a low pass filter on its way to the screw terminal. Each input had two connections to their respective screw terminal channel, the output signal and a sensor ground signal. All inputs were powered with a 5 VDC power supply.

Table A.11 Signal specifications for the inputs to Board 0.

	Voltage Range	**Resolution**
O_2 Gas Sensor	0-1.4 V	0.0004%
CO_2 Gas Sensor	0-5 V	0.2 ppm
Thermocouple	0-1.25 V	0.02 mV (0.002°C)

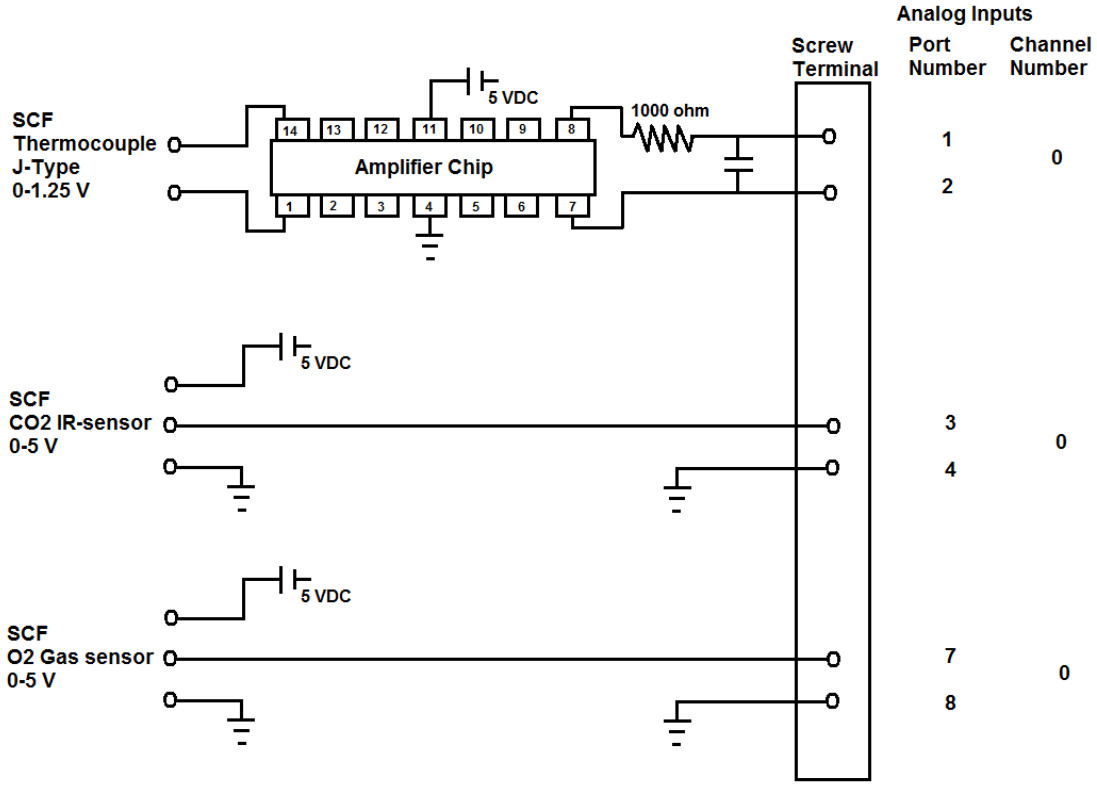

Fig. A.2 Wiring of inputs to Board 0 (AMCC S5920).

Table A.12 lists the signal specifications for the inputs to Board 1 (MiniLab 1008). Figure A.3 shows the wiring of inputs to Board 1.

Table A.12 Inputs to Board 1 (Minilab 1008).

	Voltage Range	**Resolution**
Level Sensor 1	0-5 V	1 mm
Level Sensor 2	0-5 V	1 mm

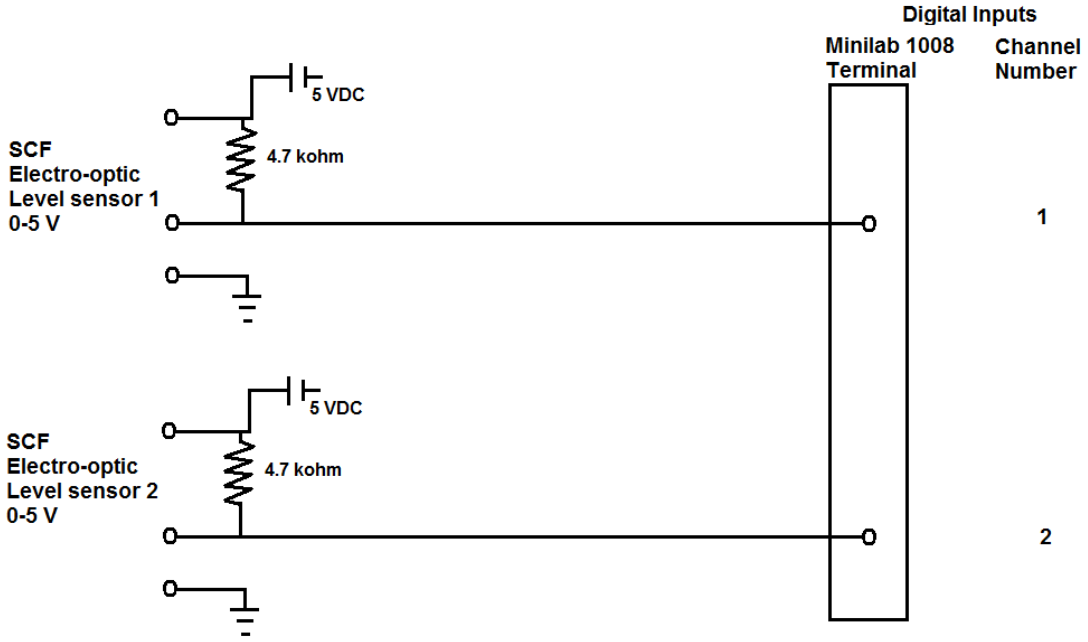

Fig. A.3 Wiring of digital inputs to Board 1 (Minilab 1008).

Table A.13 lists the outputs from Board 0 (AMCC S5920). Figure A.4 displays the wiring of the outputs. Opto22 OAC5 electro-optic relays were used to close the circuit between the outputs and the 120 VAC power source. A 5 VDC signal from the computer closed the electro-optic switches.

Table A.13 Signal specifications for Board 0 outputs.

	Voltage Range	**Frequency**
O_2 Gas Sensor	120 VAC	60 Hz
CO_2 Gas Sensor	120 VAC	60 Hz
Thermocouple	120 VAC	60 Hz

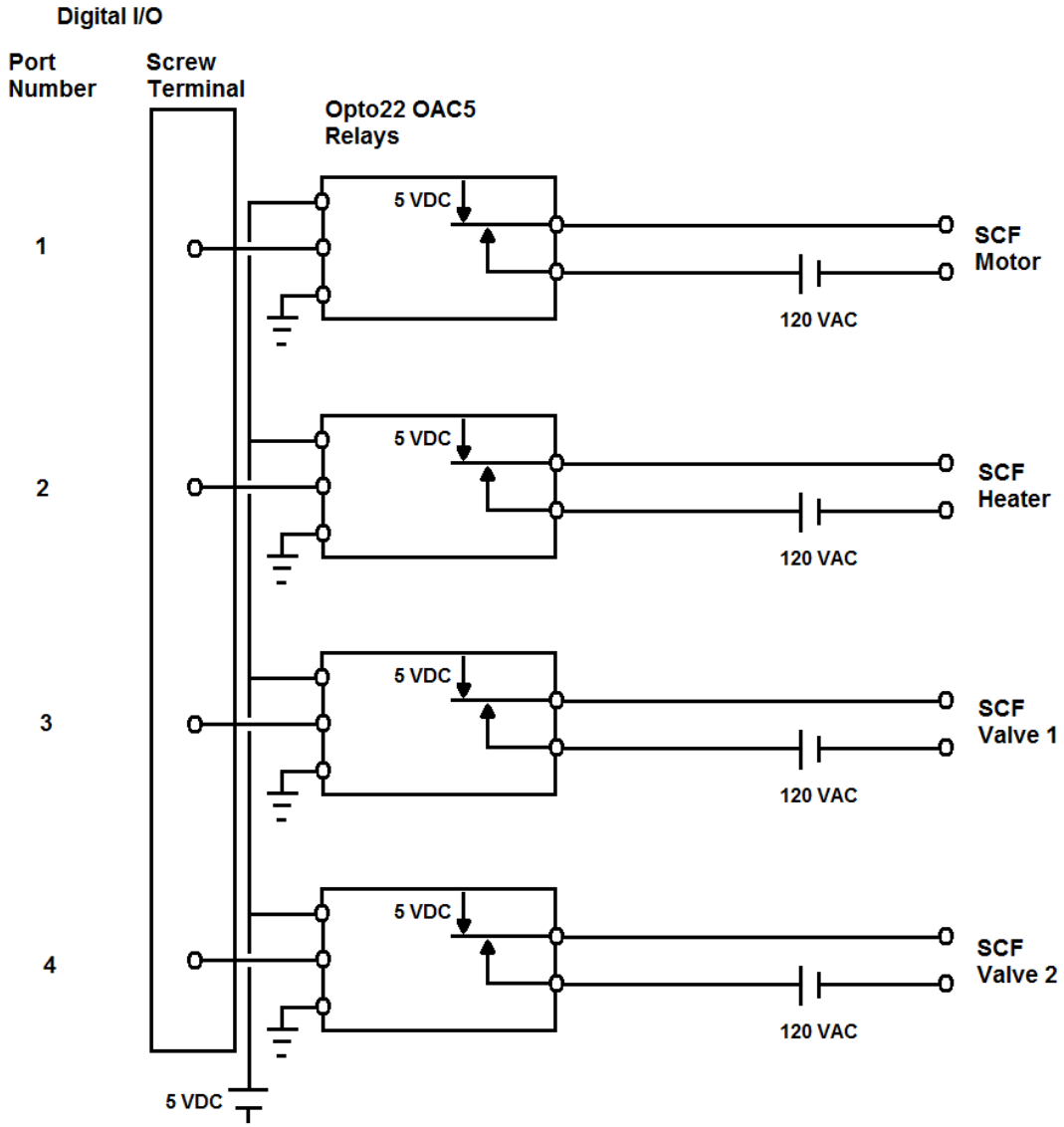

Fig. A.4 Wiring of digital outputs from Board 0 (AMCC S5920).